2-1P

X-690-70-78

PREPRINT

NASA TM X- 63887

MAGNETOMETERS FOR SPACE RESEARCH

Norman F. Ness*
CNR Laboratorio del Plasma nello Spazio
Istituto di Fisica
Citta Universita-Roma

March 1970

*On leave from NASA-Goddard Space Flight Center

TABLE OF CONTENTS

Page

1.0 Introduction

Many scientific disciplines have been remarkably stimulated by the technological developments of satellites and space probes. With these sophisticated, self-contained and automatically operating unmanned laboratories it has been possible to place sensitive instrumentation at very remote distances from the earth's surface and at unique positions within the solar system and thereby measure important physical parameters in situ. One of the more significant parameters is the magnetic field and its spatial and temporal variations, since it is the most important force field affecting the motion of charged particles and ionized gases beyond the earth's atmosphere. Because most of the matter in our universe appears to be in the form of magnetized plasmas, the magnetic field plays a fundamental role in the dynamical behavior of our astrophysical environment.

This paper presents a review of those spacecraft instruments which have provided measurements of the magnetic fields of the earth, moon, Mars, Venus and interplanetary measurements of the extended solar field obtained near the ecliptic between the orbits of Mars and Venus. A chronological summary of spacecraft to be discussed in this article is presented in Figure 1 in the form of a bar graph extending throughout the data lifetime of the magnetometer experiments. A total of 51 separate or paired spacecraft launches have occurred since 1958, each instrumented with one or more magnetometers. This graph illustrates the advances made in the technology and reliability of the lifetime of such experiments. Up until 1965 only 2 spacecraft, the USA Explorers 14 and 18, had operational

lifetimes of more than 6 months with the others restricted to weeks or even days. The increased lifetimes combined with a larger number of launches yielded a situation in which simultaneous magnetic field data from two or more spacecraft have been available since 1965. Since these spacecraft also frequently carry particle detectors and plasma probes, the chart is of general interest for such simultaneous observations.

While the exploration of space can be expected to continue, it is clear that the decade of the 1960's represented an especially vigorous and productive period for the study of magnetic field, plasmas and energetic particles whose uniqueness shall not be matched in the future. This appears certain due to the reassessments of priorities and expenditures for such activities by those nations which have thus far conducted such investigations.

A critical turning point has been reached and a review of the successful experiments at this juncture, the entry into the 1970's is timely. The fact is that, during the past 12 years since these studies began, over 50% of all of the magnetic field experiments have been conducted within the past 5 years. More relevant, however, is the situation regarding the acquisition, analysis and interpretation of these data. More than 80% of all the magnetic field data obtained has been collected during the past 4 years and of this less than 25% has yet been adequately or even partially studied. Thus, in the future, more emphasis will be placed on the evaluation of experimental data already available and less on the acquisition of as much new data. In this spirit it is hoped that this review will be most useful to provide a reference for the characteristics of each experiment.

Significant discoveries concerning the magnetic fields in space have already been made, many of them in the spirit of exploration of the unknown. The more recent experiments have been of a second or third generation, with respect to instrument development and their objectives being directed toward more specific quantitative studies elucidating a particular physical phenomena. The proper understanding of the characteristics of the instruments is necessary to an evaluation of the significance of newly found or as yet unexplained phenomena. Moreover, many studies have or will require the intercomparison and correlation of simultaneous observations of the same or complementary physical parameters from different positions in space.

This review will begin with a discussion of the fundamental principles of operation of the different types of magnetometers which have been developed for space flight, measuring the weak magnetic fields in space. A discussion of their operation on the two types of attitude stabilized spacecraft, fixed and spinning, follows. Aspects of these devices as sources of magnetic field data and the subsequent processing of this data to obtain unique information will then be given. A discussion of the most frequently used coordinate systems and the properties of vector field averages follows.

The next part of the review consists of a discussion of the specific characteristics of those instruments which have been flown in earth orbit (in Section 5) and those flown on lunar or planetary and interplanetary missions (in Section 6). The last section discusses the future programs which will be carried out in the 1970-1975 period. It should be noted

that no explicit discussion of rocket magnetometers is included except insofar as the operating principles are identical. A short survey of those studies conducted in the USA up to 1967 is given by Cahill (1967). Earlier reports including limited discussions of magnetometer instrumentation have been given by Cahill (1964b) and Cantarano and Mariani (1966). Earlier reviews of general magnetic field instrumentation techniques have been given by Fromin (1952), discussing the fluxgate magnetometer and an excellent discussion by Grivet and Malnar (1967) of the fundamental physical principles of atomic or quantum magnetometers. The USSR program up to 1965 has been briefly reviewed by Frazier (1968).

Tables I and II present a chronological listing of the 60 separate magnetic field experiments to be discussed in Sections 5 and 6, with technical performance characteristics of both the spacecraft and instruments summarized for easy comparison. The absence of specific data on certain instruments is due to lack of published or privately communicated data. In certain instances, the operational characteristics of an instrument are sufficiently complex that they cannot be properly simplified for inclusion of all of the necessary modes and details. For a correct understanding of an individual experiment, the reader should utilize the corresponding discussion in Sections 5 or 6.

The definitions of the column headings which are not clearly self-explanatory are:

P.I. Principal Investigator responsible for experiment

APO Apogee, Aposelene or Aphelion (AU) for earth, lunar or solar orbits

PERI Perigee, Periselene or Perihelion (AU) as above

INCLIN Geographic, selenographic or Heliocentric Inclination of orbit

PERIOD Orbital period in hours except for heliocentric orbits when asterisk indicates period is in days

INSTRUMENTATION F(j) = Fluxgate magnetometer with j sensor axes

SC(j)= Search coil magnetometer with j sensor axes

RB^{xx} = Rubidium vapor self-oscillating magnetometer using xx isotope

OUTPUT Basic experimental data interface with spacecraft, with D meaning digital data and A analog data

QUANTIZATION Intrinsic digitization uncertainty, in γ, associated with experiment, spacecraft telemetry system and ground data processing

S/C FIELDS Net spacecraft field at sensor position

BANDPASS Detector bandpass, before on-board processing.

SPIN PERIOD Period of rotation for spin stabilized spacecraft

AS = Attitude Stabilized with gas jets
GG = Gravity Gradient attitude stabilized
MS = Magnetically Stabilized

In all the individual entries a question mark means no data available, ST means See Text for description and bar means not relevant.

1.1 Brief Summary of Major Results

Magnetic field experiments, their data analysis and interpretations have led to a considerably revised view of the field structure of the distant geomagnetic field and in interplanetary space than prevailed before space studies began. A primary phenomena of special interest connecting these two regions is the supersonic flow of the solar wind plasma, the expansion of

the solar corona into interplanetary space, carrying with it magnetic fields of solar origin, as shown in Figure 2a. The structure of the interplanetary medium itself has thus far been most clearly revealed in studies of the magnetic structure of interplanetary space with the classification of significant features shown in Figure 2b.

The interaction of the solar wind plasma with the earth's magnetic field confines it to a region of space called the magnetosphere and also forms the geomagnetic tail, as shown in Figure 3a. The existence of the detached collisionless bow shock wave and the geomagnetic tail were two of the important discoveries of the past decade of magnetic field studies. The interaction of the solar wind with the essentially unmagnetized and atmosphere-free moon leads to a completely different set of flow characteristics. As shown in Figure 3b, the creation of a plasma wake and umbra behind the moon occurs as a result of the absorption of solar particles by the lunar surface and leads to the absence of a shock wave or sheath region surrounding the moon. The solar wind interactions with the planets Mars and Venus, although poorly studied, appear to be intermediate between the earth and the moon. It is not known if a Martian magnetic field exists which is sufficiently strong to deflect the solar wind flow. In the case of Venus, it is clearly the ionosphere which deflects the flow and causes the development of a detached bow shock wave.

The above remarks are sufficient for our purposes here in establishing the general nature of the phenomena which the experiments to be discussed have revealed. There are several review papers dealing with the topic of the solar wind (Hundhausen, 1968; Parker, 1965) the interplanetary

magnetic field (Dessler, 1967; Ness, 1969 ; Wilcox, 1968), the geomagnetosphere field (Fairfield, 1968) and tail (Ness, 1969) and the solar wind flow past the moon (Ness, 1970), which should be consulted for additional details. No effort has been made to include a complete bibliography of all published papers which have results from the data obtained by each experiment. However, references to the more important papers discussing the instruments, data analysis procedures and interpretations will be given.

2.0 Magnetometer Fundamentals

The measurement of the interplanetary magnetic field, the fields of the moon and planets and the distant geomagnetic field has required the development of highly sensitive and accurate instruments which function over a wide dynamic range, from fractions of a γ ($1\gamma = 10^{-5}$ Gauss) to 0.7 Gauss. In addition, stringent requirements for extremely low weight, low power and small volume necessitated the redesign or imaginative adaptation of classically used techniques in order to measure magnetic fields in space from a totally new kind of laboratory bench, the spacecraft.

The advent of solid state devices in electronics such as transistors and more recently large scale integrated circuits using MOSFET's has permitted the technology of magnetometers to rapidly advance and satisfy the unique needs for space applications. Indeed, the present state of the art is such that the principal limitations of precise magnetic field measurements of high accuracy are due to the magnetic noise generated by the spacecraft and not the basic instruments themselves. It is also true that frequently insufficient telemetry bandwidth for communication of data restricts the time resolution of the data well below the capability of the instruments.

This section will discuss the five basic types of magnetometers which have been developed and used for space measurements; they are:

2.1 Induction or search coil,

2.2 Fluxgate or saturable core,

2.3 Proton precession,

2.4 Alkali vapor self-oscillating, and

2.5 Helium vapor low-field

The order of their presentation reflects the historical sequence of their development and use as well as an increasing complexity in their principles of operation. It should be noted that of these instruments only the Rubidium vapor and the proton precession instruments are absolute in their measurements since their calibration depends upon fundamental atomic constants. The other devices are all relative, requiring a calibration of their performance in a facility established especially for that purpose.

An effort is made to include a discussion of possible error sources in each type of magnetometer and both the advantages and unique merits as well as disadvantages of each. Specific applications to space studies on spacecraft, presented in Sections 5 and 6, also includes discussions of the possible error sources of each experiment.

All magnetometer experiments can be analyzed in terms of the block diagram shown in Figure 4 for a universal spacecraft instrument. The basic detector system consists of a sensor, and possibly a calibration subsystem, with the necessary electronics to present the information on the magnetic field as a voltage, current, or frequency modulated signal. Subsequently this analog signal is processed, either by the instrument or the spacecraft electronics, to prepare it for data transmission. This may also include analog or digital operations which perform mathematical computations on the data because of experiment design or because of spacecraft imposed conditions. Following the transmission and reception of these data, the telemetry signal is decoded and ground data processing occurs to convert the information into the necessary format for data analysis.

In this section we are concerned only with the operation of the sensor, primary electronics and the calibration subsystem. The last item will also be discussed in Section 3 on the operation of experiments on the two types of spacecraft which carry such instruments.

2.1 Induction or Search Coil

Conceptually, the simplest type of instrumentation for measuring the magnetic field is the induction magnetometer. The basic principle of its operation is Faraday's Law of magnetic induction, which states that a time varying magnetic field $\vec{B}(t)$ generates an electric field, $\vec{E}$:

$$\nabla \times \vec{E} = - \frac{d\vec{B}}{dt} \qquad 2.1.1$$

With a loop of wire describing a closed path in space, the time rate of change of total magnetic flux threading the loop area, $\vec{A}$, can be determined from the integrated electric field along the loop as:

$$\oint \vec{E} \cdot d\vec{s} = \iint \nabla \times \vec{E} \cdot d\vec{A} = - \iint \frac{d\vec{B}}{dt} \cdot d\vec{A} \qquad 2.1.2$$

Generally a solenoidal coil of N turns is used enclosing a ferromagnetic core which increases the magnetic flux threading the coil. The integrated electric field, the output voltage V, is then given by:

$$V = \oint \vec{E} \cdot d\vec{s} = - AN\mu' \frac{dB_{\perp}}{dt} * 10^{-8} \text{ volts/Gauss/cm}^2 \qquad 2.1.3$$

where A is measured in cm^2, μ' represents the effective magnetic permeability of the core material, and $B_{\perp}$ represents the field component perpendicular to the coil area A or equivalently parallel to the solenoid's magnetic axis.

It is clear from this equation that the induction magnetometer does not respond to a steady or time stationary magnetic field, and may be insensitive to slowly fluctuating fields. The frequency response characteristics are represented by the transfer function

$$V = -\omega A N \mu' B_o \times 10^{-8} \quad V/\Gamma/cm^2 \qquad 2.1.4$$

where B_o is the amplitude of a magnetic signal varying sinusoidally with time at a frequency $f = \omega/2\pi$. Thus it is seen that the induction magnetometer sensitivity increases linearly with frequency and this indicates why this type of instrument is generally employed for measuring fluctuating fields and only rarely, and in special circumstances, for the measurement of steady fields. Note also that it is sensitive only to the component of the field variations parallel to the magnetic axis of the coil+core.

The analysis of the signal generated by such an instrument is derived using Figure 5a, in which $\vec{S}_i$ represents the axis of a mono-axial sensor and $\vec{F}$ the magnetic field. The coordinate system in this figure is called "payload" and assumes that the sensor position relative to the set of X_p- Y_p-Z_p coordinates is known at all times. For the case of spin stabilized spacecraft, the Z_p axis is normally selected to be coincident with the instantaneous spin axis while the X_p-Y_p plane includes a vector from the spacecraft to the sun. This diagram will be generally useful for the discussions of all magnetometers and their data analysis since it forms a natural reference system for directional measurements on spacecraft.

The component of the magnetic field which induces a signal in the coil is $\vec{F} \cdot \vec{S}$ so that equation 2.1.3 becomes, with the gain factor K defined as $N A \mu' 10^{-8}$:

$$V = -K \frac{d}{dt} [\vec{F} \cdot \vec{S}] = -K [\vec{F} \cdot \frac{\partial \vec{S}}{\partial t} + \vec{S} \cdot \frac{\partial \vec{F}}{\partial t} + (\vec{v} \cdot \vec{\nabla} \vec{F} \cdot \vec{S})] \qquad 2.1.4$$

Here the complex signal output from an induction magnetometer is revealed with the three terms in brackets representing contributions due to, respectively:

1) Motion of the coil, about its center, in the stationary field $\vec{F}$,

2) Explicit time variations of $\vec{F}$, and

3) Implicit time variations of $\vec{F}$ due to displacement or convective motion of the coil with the velocity $\vec{v}$ relative to the magnetic field $\vec{F}$.

Note that the terms 1) and 3) are not equivalent since there is no net displacement of the coil in 1) but only a time varying aspect of the coil geometry with respect to the field $\vec{F}$.

No technique exists which can uniquely separate or identify the relative contributions of these three terms by analysis of the output signal. However, depending upon the characteristics of the spacecraft and the spectrum of the magnetic field, it is possible to make certain plausible assumptions regarding the relative significance of each term. In practice usually only one or at most two of the terms must be considered as contributing significantly to the signal and on this basis two versions of this type of magnetometer have been developed. Rather than to postpone the specific description of these separate versions to Section 3, they shall be discussed in the following paragraphs.

The first use of an induction magnetometer for space magnetic field measurements was on the spin stabilized spacecraft Pioneer 1 (Sonett et al.,

1960) to measure the ambient magnetic field in space, undistorted by the magnetic field of the spacecraft. In this application the sensor, a coil wound on a core, was fixed rigidly to the spacecraft perpendicular to the nominal spin axis and rotated with the spacecraft at a rate ω_{sc} so that the three components of $\vec{S}_1$ become $(\cos\omega_{sc}t, \sin\omega_{sc}t, 0)$. Thus Equation 2.1.4 is given by:

$$V = K\omega_s F \cos\alpha \sin(\omega_{sc}t - \varphi_F) - K[\vec{S} \cdot \frac{\partial \vec{F}}{\partial t} + \vec{v} \cdot \nabla\vec{F} \cdot \vec{S}] \qquad 2.1.4$$

Through use of a bandpass filter centered at the nominal spin frequency and telemetry of the output waveform, the signal thus detected can be inspected and the spin modulation readily verified with amplitude proportional to $F\cos\alpha$ and phase, φ_F measuring the direction of the magnetic field component transverse to the spin axis. A portion of the block diagram in Figure 6 represents this version of the induction magnetometer.

However, if the field $\vec{F}$ itself varies at frequencies within the bandpass or related to the spin rate and axis in a unique way, the output waveform may be severely distorted from its nominally sinusoidal variation. Both amplitude and phase modulation occur in a manner which cannot be uniquely separated from that due to the rotation of the spacecraft. Considerable complexity and ambiguity can also occur if the spacecraft is not simply spinning but is also precessing and nutating. The magnetic field, as represented in Figure 5, will then include variations dependent upon the exact motion of the spacecraft as it affects the direction angles α and φ_F. An analysis of the output signal under such conditions has been given by Sonett (1963).

Because of its inherent increasing sensitivity as the frequency of the magnetic field fluctuations increases, the induction magnetometer has been most frequently employed to study the explicit time variations of the magnetic fields in space. This is especially true for those spacecraft of fixed or slowly changing attitude, or even spin stabilized spacecraft when the spin rate is much lower than the frequency range of interest.

Under these conditions, this version of the induction magnetometer is normally employed with three orthogonal sensors and identical electronics for each axis. A block diagram illustrating the design of this version for a single axis is shown in Figure 6. (The presence of a reject filter may be necessary because of spacecraft generated fields). The on-board processing of the signal may include a series of overlapping bandpass filters, whose outputs are sampled at relatively low rates to yield average, peak or mean square estimates of the signal strength in each frequency band. A correct power spectrum is obtained only if the signal is rectified, squared and then averaged.

The low pass channel output permits the reconstruction of the actual output waveform on the ground and subsequent studies of the characteristics of the fluctuations such as polarization and the orientation of the normal to the plane of polarization. This information is of much more value in ascertaining the type of fluctuation studied with respect to wave mode than if only the spectrum is available. This depends to some degree upon the nature of the medium in which the fluctuations are observed and the time-frequency structure of the spectrum. The use of the bandpass filters and spectral analyzers is necessitated by the insufficient telemetry data bandwidth to transmit all the data in the low pass channel mode.

The design and fabrication considerations for optimum performance of the induction magnetometer detector are of specific interest for its overall performance. The geometry of the coil is clearly selected to be circular for a maximum ratio of coil area to circumference, which is a measure of the ratio of the gain of the coil to its weight. In order to reduce weight, the detector sensitivity can be increased considerably by the use of a ferromagnetic core and fortunately not in proportion to the increase in weight. Both the geometry and the permeability of the core material, μ_c, determine the effective permeability of the core, μ'. The geometry affects it because of the variable demagnetizing factor $\mathcal{L}$, as:

$$\mu' = \left[\frac{\mu_c}{\mu_o - (\mu_c - \mu_o)\mathcal{L}}\right] \mu_o \qquad 2.1.6$$

The factor, L, has been tabulated for a number of geometries by Bozorth (1951). It is found that μ' increases significantly with length to diameter ratio, L/D. For moderate values of L/D between 5-50 and very high permeabilities of core material, $\sim 1\text{-}2\times10^3\ \mu_o$, then μ' is between $20\text{-}500\mu_o$.

The design of the coil is not based only on the total mass available for the detector system and consideration of the effective μ' for various core designs. Two other factors affect the coil parameters:

1) the intrinsic thermal noise (Johnson noise) which depends upon the real part of the coil impedance, and
2) the natural resonances of the coil+core system itself.

The latter phenomenon automatically limits the spectral response of

induction magnetometers essentially to the range below and up to the resonance frequency. Above this, the gain of the coil is no longer dependent upon the frequency as in Equation 2.1.4 but instead decreases rapidly at a rate dependent upon the exact equivalent circuit for the coil+core system. The resonance occurs because of the capacitance which is formed between the successive windings and between the coil and the core. This problem can be alleviated somewhat but not eliminated by the forming of the coil into several separate coils (on spools or bobbins) and spacing them on the order of the width of the coils.

The thermal noise problem forces the use of less than the maximum number of turns that would be possible if a fixed weight of wire were capable of being fabricated with the smallest diameter wire that could be mechanically handled. The root-mean-square noise voltage is given by:

$$V_{rms} = \sqrt{4KRT\Delta f} \qquad 2.1.7$$

where K is Boltzman's constant, R the real part of the impedance of the coil+core detector system, T, the temperature and Δf the width of frequency pass band. Normally the design strategy is to equate this noise power to the minimum detectable signal which it is desired to measure and then determine the corresponding physical parameters for the coil+core. Due consideration must also be given to the noise and impedance characteristics of the instrument pre-amplifier. A method for systematically designing an optimumly sensitive monoaxial induction magnetometer taking these several factors into account has been given by Inouye and Judge (1964).

In those cases where only the spectral power levels in various frequency bands are desired, Cantarano and Pallottino (1968) have studied the use of two parallel induction magnetometers with a cross-correlation of their separate outputs after bandpass filtering. This powerful technique, developed in statistical communication theory, yields an estimate of the power for each band of the spectrum that is independent of the noise characteristics of the individual detectors. Hence it permits the design of an experiment with an improved signal-to-noise ratio. By the use of substantially smaller cores and coils, leading to much higher resonance frequencies, the net performance of the detector system is substantially improved over that of a single sensor design by factors up to 50, as measured by signal to noise ratio. Equivalent noise power spectral densities of $10^{-4}/f^2$ γ^2/Hz are achieved by this technique, with resonance frequencies of 12KHz.

In certain regions of space, such as the magnetosheath and the interplanetary medium, the motion of the magnetized plasma past the spacecraft occurs at velocities of 200-800 km/sec. This is many times larger than the propagation velocity of waves and disturbances, which is normally on the order of 50 to 100 km/sec. Thus, in these regions of space, the signal output consists of a contribution due to the third term in Equation 2.1.4 which cannot be readily assessed as to its relative importance but is probably the dominant term. The velocity of the spacecraft, here and in other regions of space, is sufficiently low, that only during perigee passes or flyby trajectories is it potentially high enough to be important in the interpretation of the data. Thus the

induction magnetometer signal output can be generally considered to be rather complex and only in the magnetosphere is its interpretation relatively straightforward.

2.2 Fluxgate or Saturable Core

The fluxgate magnetometer is conceptually the next most simple instrument for the measurement of magnetic fields and the one which has been most frequently used. It is based upon the non-linear characteristics of a magnetically saturable reactor or saturable transformer, which is used as the sensing element (Geyger, 1964). In the fluxgate magnetometer, the measurement of the second harmonic of the input frequency becomes a direct measure of the external magnetic field in which the sensor, a saturable transformer, is placed. The word "Fluxgate" refers to the gating of magnetic flux in the detecting element and the nature of its origin will become evident after a discussion of its operating principles.

The analysis of the fluxgate magnetometer operation is frequently carried out by means of a diagram similar to that shown in Figure 7. The non-linear or hysteresis characteristics of the core material for the saturable transformer are assumed to be combinations of simple linear segments in the B-H plane. A triangular drive waveform of frequency 1/T is used as the input signal with amplitude H_D, and is applied through a primary coil winding on the core. The core material saturates when H reaches $\pm H_C$, when the magnetic induction is $\pm B_S$. The triangular waveform possesses only odd harmonics and although in practice a sinusoidal drive waveform is employed, the use of this simplified triangular waveform will not invalidate the principles upon which the instrument is based. It is

assumed that an ambient external magnetic field, of intensity $+\Delta H$, has biased the drive field intensity in the core as shown.

The resultant magnetic flux linking a secondary sensing coil, operating on Faraday's law of magnetic induction, is then obtained by following along the B-H hysteresis curve to obtain B_R, as shown. The output signal induced in the coil is proportional to the time rate of change of the "flux" which is alternately switched or "gated" to plus and minus saturation. It is seen to consist of an interlaced train of identical positive and negative pulses of width αT which are non-uniformly spaced in time. Successive pulses are separated by either βT or $(1-\beta)\ T$. It is this alternating saturation of the core in opposite directions which "gates the flux" in the sensing coil in the time sequence shown. The gating occurs as the result of driving the core into the flux saturation condition, which then leads to a complete circuit of the hysteresis curve.

A Fourier analysis of the output waveform of $\frac{dB_r}{dt}$ yields the formula shown in Figure 7, with the indicated values for α and β. Note that α is independent of ΔH and that β depends only upon the ratio of $\Delta H/H_D$. In the absence of an external magnetic field, i.e., $\Delta H=0$, the bracketed term becomes

$$[1 - \cos(k\pi)] = \begin{cases} +2 & k = 1,3,\ldots \text{ odd} \\ 0 & k = 0,2,\ldots \text{ even} \end{cases} \qquad 2.2.1$$

This means that even harmonics of the primary frequency occur only in the presence of an external magnetic field, $\Delta H \neq 0$. Since the amplitude of the harmonics decreases with their order, k, it is clear that the best one to use is the second harmonic because it leads to a maximum signal at least twice as large as the next even harmonic.

The amplitude and phase of the second harmonic are important in quantifying the magnitude and direction of the ambient magnetic field. In order to study this relationship, the ratio of the second to the first harmonic is formed:

$$r = \left[\frac{1-e^{-i\pi(1-\Delta H/H_D)2}}{1-e^{-i\pi(1-\Delta H/H_D)}}\right] X \left[\frac{\sin 2\pi\alpha}{2\sin\pi\alpha}\right] \qquad 2.2.2$$

Assume that the field to be measured, ΔH, is much smaller than that of the drive field, H_D and the drive field H_D is much larger than the coercive force H_C required to drive the core into saturation so that $\alpha \ll 1$. This equation becomes:

$$r = \frac{1-1+i\sin(2\pi\Delta H/H_D)}{1+1-i\sin(\pi\Delta H/H_D)} = \pm i\frac{\Delta H}{H_D}\pi \qquad 2.2.3$$

This states that the second harmonic is $\pm 90^{\circ}$ out of phase with the primary, with the sign indicating the sense of the field ΔH relative to the core axis, and the amplitude is linearly dependent upon the value of $\Delta H/H_D$. This summarizes the operating principle of the fluxgate magnetometer: the instrument is a device which measures the magnetic field component parallel to the core axis. The frequency response characteristics depend upon the drive frequency and amplifier electronics and the desired noise level in a complex manner. As with the induction magnetometer, the design of an optimum instrument includes a consideration of not only the sensor but also the electronics.

A block diagram of a simplified fluxgate magnetometer is shown in Figure 8. Here a primary frequency is first generated and then doubled

for comparison with the filtered and amplified second harmonic. In other designs, the primary drive frequency is obtained by a divide-by-two operation from a reference oscillator that is run at essentially the second harmonic. The use of a narrow bandpass filter and a very stable oscillator are essential so that the response of the instrument over the operating range is a fixed linear function of the input and to reduce the noise level at the output. In order to improve on the stability of the magnetometer, a magnetic feedback loop is often employed as shown in addition to purely electronic feedback used for amplifier gain stability. The detected output is then low pass filtered to provide a voltage which is proportional to the magnetic field. In order to verify the sensitivity of the instrument, that is, the change in field ΔB required for a certain change in the output, ΔV, it is possible to add a known field to the sensor and measure the change in the output, $\frac{\Delta B}{\Delta V}$ (gammas/volt).

The foregoing simplified analysis has assumed a parallelogram hysteresis curve for the B-H saturable core characteristics and used a triangular waveform for the primary frequency. Neither of these assumptions nor the neglect of eddy currents induced in the core material, however, negate the operating principles. See Williams and Noble (1950) for a discussion of the analysis using a sine wave drive. In practice a more serious problem arises since the measurement of weak magnetic field means that the magnitude of the second harmonic is only $10^{-6 \pm 2}$ of the primary. The accurate measurement of such small signals is not easily accomplished with the use of a simple bandpass filter especially under the limitations on weight, power and volume imposed on space applications.

A solution to the problem of detection of a small second harmonic signal is to configure the core and the primary and secondary coils so that the secondary coil is insensitive to the primary signal. This can be accomplished in several ways, as shown in Figure 9. The geometry shown in 9b illustrates the use of two cores, side by side, around which a common secondary responds only to even harmonics because the primary coil is wound in series opposition on the cores. This introduces a 180° phase shift in the contributions of the primary frequency to the induced voltages from the two separate cores. The degree to which exact cancelling of the primary signal occurs depends upon the two cores being magnetically identical to each other and wound in the same fashion. By careful treating of core material and precise quality control selecting matched pairs, in addition to using a variable number of windings on each core to trim the sensor system to precise equality, the ideal situation is approximated. Typical drive frequencies of 1-2 KHz are used in this type of fluxgate sensor.

Another approach to the problem of primary-secondary decoupling by core and coil geometry is the "Heliflux" sensor shown in Figure 9c. Here the two coils are wound orthogonal to each other around a helical core which is overlapped on itself as shown. This geometry has additional advantages because the thickness of the core material, which is a tape wound on a ceramic tube, can be made very thin. This reduces the amount of drive current necessary to switch the core material from positive to negative saturation, lowering the hysteresis loop losses, as well as the eddy current losses.

This Heliflux geometry also permits the use of higher operating frequencies, as opposed to the twin core geometry, since in order to switch all the material in the core, eddy current losses prevent full penetration to the center of the core. The use of higher operating frequencies will intrinsically increase both these losses but may permit lighter weight components in the electronics and permit higher operating efficiency in the electronics. This geometry of the fluxgate magnetometer sensor is the one which has been most widely used by the USA and ESRO. It is a patented design of the E. O. Schonstedt Instrument Company of Reston, Virginia (Schonstedt, 1959; 1961). Typical drive frequencies of 5-20 KHz are used in these sensors.

An alternative closed magnetic flux loop geometry, called the Ring Core (Gordon et al., 1968), has recently been developed and is shown in Figure 9d. A toroidal core of permeable material, which can be a very thin tape, is wound with a concentric circular solenoidal primary winding while the secondary is wound as a linear solenoid around the entire core+primary coil system. The directional characteristics of the sensor depend on the geometrical axis of the secondary since the primary coil and core have no directional sense except with respect to the external magnetic field. This geometry offers the possibility of a two component magnetometer on a single core, as well as the advantages of thin core material discussed previously. This type of core geometry has yet to be used in space magnetometers.

Regardless of the various geometries as described above, there are a number of problems intrinsic to fluxgate magnetometers which arise from several sources. Firstly, it is absolutely essential that the primary

waveform be free of second harmonic distortion. Otherwise the output will contain a spurious second harmonic content. Most important, however, is the need for full saturation of all of the core material in opposite polarities on each half cycle so that any residual magnetism of the core is fully removed, or "shaken out" as it is frequently described. Failure to utilize a core with zero residual magnetism will lead to a second harmonic signal that is legitimately due to a magnetic field, but unfortunately is that due to the permanent internal magnetism of the core itself. These "Magnetic memory" effects, or "zero level" offsets, can arise from a number of sources among which primarily are variability of material properties, mechanical or thermally induced stress and incomplete saturation. The latter occurs because not all the magnetic domains in the core are periodically reversed as the flux is gated in the core.

There is no way to eliminate permanently the possibility of memory effects. This is true regardless of the mechanical, electrical and magnetic flux path of the sensor. While in practice, it is now possible to consider the stability of zero levels of some fluxgate magnetometers to be better than 1-3 gammas over periods of many months, these are not adequate for many studies in space. The only way to determine the amount of zero level offset uniquely is to physically reverse the sensor by exactly 180° in the magnetic field being measured. This must be done with respect to its magnetic axis and not the geometrical axis since the two may not be colinear or even parallel. By averaging the two values of the measurements thus obtained, taking into account correctly the reversed directional sense of the detector, the zero level offset, δV, is obtained:

$$\delta V = \tfrac{1}{2} [(V+\delta V) - (V-\delta V)] \qquad 2.2.4$$

The measurement of the vector magnetic field requires the use of three monoaxial fluxgate magnetometers. Since the sensors are of modest but finite size, roughly that of a short pencil, they cannot all be located at the same point with a common magnetic center. The spatial gradient of the field to be measured is such that generally a separation of the three sensors by several cm. is unimportant. They are then mounted in a geometry as to minimize the electrical and magnetic cross coupling between separate sensors. The mechanical adjustment of such units is conducted on a hunt-and-try basis. Some designs, particularly in the USSR programs, have found it necessary to use separate drive frequencies for each axis to eliminate cross-coupling although this requires more weight, volume and power in the electronics since a common primary frequency cannot be used.

Presently the state of the art of fluxgate magnetometry is such that intrinsic noise levels, due to thermal and magnetic material sources, yield field equivalent RMS deviations of 0.1 gamma or less for pass bands of 0-10 Hz. The dynamic range of such instruments can be several hundred gamma to several thousand gamma and techniques exist for extending the ranges beyond this (see Section 4.0). The spectral noise characteristics over the frequency range zero to several Hz is known to be a steeply falling function of frequency. By careful selection of the individual sensor cores and their coil windings, it is possible now to achieve sensitivities of 0.02 to 0.03 gamma RMS noise equivalent.

The advantages of these instruments for the measurement of magnetic fields is multifold: precise continuous vector data with passbands up to several 10's of Hz, lightweight, rugged and low power. The one disadvantage, the zero level uncertainty associated with memory effects, can be overcome on spin stabilized spacecraft automatically for two axes and for the third with a flipper, to be described in section 3.2. When compared with the induction magnetometer, the fluxgate noise figures are such that they possess superior performance up to about 10 Hz. Beyond this range the intrinsic increasing gain of the induction magnetometer makes it the superior device.

2.3 Proton Precession Magnetometer

This instrument was the first of several "quantum" or absolute magnetometers which were adapted from terrestrial models and developed explicitly for space applications. Its operation is based upon the magnetic properties of the fundamental atomic particle, the proton, the nucleus of the hydrogen atom. The measurements made with such an instrument are referred to as absolute because the calibration of these instruments is universal, depending only upon the fundamental atomic constant, the gyromagnetic ratio for the proton.

The operation of the instrument can be described in either quantum mechanical or classical mechanical terms. Both shall be used since a quantum-mechanical description will be necessary in the analysis of the operation of the alkali vapor and helium vapor magnetometers. The classical description shall be given first as it has given the name to this type of magnetometer.

The sensing element is a sample of hydrogeneous liquid material such as water, alcohol or n-heptane. Because of the magnetic moment of the hydrogen nucleus, the sample can be magnetically polarized, albeit quite weakly even if a strong field, H_p, of several hundred Gauss is used. The sample volume V will become magnetized with the magnetic moment $\vec{M}$ given by:

$$\vec{M} = \frac{\mu^2}{kT} n V \vec{H}_p \qquad 2.3.1$$

where n is the concentration of hydrogen nuclei, μ is the nuclear magnetic moment (Bloch, 1946).

Following the removal of the polarizing field, this net magnetic moment will be forced to move in a precessional motion about the ambient magnetic field because the force exerted on it is a torque given by $\vec{M} \times \vec{H}$ where $\vec{H}$ is the external magnetic field. The motion is governed by the equation:

$$\frac{d\vec{M}}{dt} = (\vec{M} \times \vec{H})\, \gamma_p \qquad 2.3.2$$

where γ_p is the gyromagnetic ratio, a measure of the proportionality between the magnetic moment and the angular momentum of the proton.

The processional motion around the ambient field occurs at the frequency given by $\gamma_p |\vec{H}|$ and it is this frequency which is the parameter to be measured to yield information on the scalar magnitude of the magnetic field. Since the frequency depends linearly upon the field magnitude and the gyromagnetic ratio, which is the same for all hydrogen nuclei, this instrument is absolute insofar as γ_p is a parameter which represents a fundamental property of nature. For the proton, the value of γ_p is

$(2.67519 \pm 0.00002) \times 10^{4}$ sec/Gauss so that the precession frequency, f_p, is determined by the field intensity F as

$$f_p = 4257.7 \text{ F (Hz/Gauss)} \qquad 2.3.3$$

For the relatively strong fields of the earth, approximately 0.3 to 0.7 Gauss, the frequency ranges from 1.2 to 2.9 KHz. However in the much weaker fields in interplanetary space the frequency is less than 1 Hz. This is so low as to be difficult to instrument appropriately and too low to accurately measure a varying magnetic field. As a result, these instruments have been used primarily in studies of near earth magnetic fields.

The alternative quantum mechanical analysis follows and the discussion of the actual instrumentation to measure the precession frequency shall be given at the end of this section. The proton is a two-level quantum system in the presence of a magnetic field because it possesses a magnetic moment which is aligned parallel to its angular momentum associated with the spin of the proton. In an external magnetic field there are two possible equilibrium positions for this magnetic moment: aligned parallel (minimum energy) or antiparallel (maximum energy) to the magnetic field. In a state of thermal equilibrium, the relative population of these two states, or energy sublevels N_p and N_a, is given by statistical mechanics as:

$$\frac{N_P}{N_a} = e^{-2\mu H/KT} \qquad 2.3.4$$

where K is Boltzman's constant and the other parameters are as defined before. This separation or splitting of the energy states into sublevels in the presence of an external magnetic field is an effect known as Zeeman splitting.

In order to measure the magnetic field strength, a means must be found for either determining the relative populations of N_p/N_a or for measuring the change in energy as they move from one state to the other. The proton magnetometer is based upon measuring the energy change associated with the transitions from one sublevel to the other. This is accomplished by application of a strong polarizing field which changes the population so that mainly one sublevel is occupied. By observing the relaxation of this modified distribution to a final equilibrium state in the magnetic field, H, the energy separation can be measured by observing the emission of energy.

This corresponds to measuring the frequency, ν, of the emitted quantized radiation, which is related to the magnetic field by:

$$\nu = \frac{\gamma_p}{2\pi} |\vec{H}| \qquad 2.3.4$$

Thus this measurement of the energy difference between the two possible energy sublevels of the proton is exactly equivalent to the measurement of the precession frequency of the macroscopic magnetic moment of the polarized sample.

In practice, the thermal energy and interactions between the nuclear moments lead to a decay of the net magnetic moment, as the protons begin to incoherently precess, at a rate determined by the transverse relaxation time, T_2. That is, $\vec{M}$ effectively decays as:

$$|\vec{M}| \propto e^{-t/T_2} \qquad 2.3.5$$

where T_2 ranges from approximately 1-10 seconds. A measurable precession signal is available for only a limited time which depends upon the specific properties of the sample used and its temperature.

A simplified block diagram of a proton precession magnetometer is given in Figure 10b. A solenoidal coil is employed with its axis colinear with the X axis as shown in Figure 10a. A polarizing field is applied for a time long compared to the thermal relaxation time, T_1, for the particular sample material. A switch then connects the coil to a sensitive amplifier, which may be followed by a frequency meter to determine the precession frequency. The precession frequency is detected by Faraday's law of induction as discussed in Section 2.1 for the induction magnetometer in the case where the magnetic field is changing periodically with the precession frequency. The simplicity, ruggedness and absolute calibration of the data obtained from this type of instrument make it valuable for those applications where only the magnitude of the field is required and not the direction. If the field is varying, then an average field will be measured since any frequency meter will count the average period over the counting interval.

One problem which arises in the use of this instrument is due to the variable signal to noise ratio due to the variation of the angle between the coil axis, $\vec{s}$, and the unknown field, $\vec{F}$. Although the frequency of precession is independent of this angle, the net detected signal is not, varying as $\sin^2 \theta$ where θ is the angle between the two directions, $\vec{s}$ and $\vec{F}$. Null zones exist in which the instrument cannot produce measurable precession signals. These problems can be overcome if the spacecraft is slowly rotating and tumbling in space so that the relative orientation of the field and coil axis are changed. If this is done too fast, however, it induces another signal in the coil whose contribution can

distort the pure precession signal. The most common solution is the use of two proton magnetometers with their coil axes oriented at 90° to each other so that regardless of the direction of the field at least one of the magnetometers has a favorable signal to noise ratio.

The problems which this instrument presents for space applications are:

1) Discontinuous measurements of the field, the interval between measurements being required for the polarize+readout cycle. This is a minimum of about 5 seconds.

2) Relatively large current requirements, albeit intermittently, for the polarization current. These are on the order of 5-20 amps. The decay of the polarizing current must be fast, on the order of a few μ seconds in order to avoid an adiabatic relaxation of $\vec{M}$ after which no precession would occur.

3) A spatially homogeneous magnetic field must be present at the sample or the relaxation time T_2 will be significantly decreased to a value less than 0.1 second. This may be an insufficient time to perform a precise measurement of the frequency.

4) The rotation of the spacecraft introduces an error in the resonant frequency of amplitude proportional to the ratio of the spin rate to the gyromagnetic ratio. This can thus approach 1γ for 1 RPM in the geomagnetic field at the earth's surface.

5) Design of high gain, low noise, broad band amplifier and possibly a frequency meter for counting the precession frequency signal.

However, in certain applications these disadvantages are outweighed by the unique advantages of the absolute measurement of the field magnitude. And

indeed the development of lightweight low-power versions for rockets and spacecraft have made this instrument a utilitarian device for certain space studies.

2.4 Alkali Vapor Self-Oscillating

The alkali vapor magnetometers are quantum devices which, like the proton magnetometer, depend upon the intrinsic magnetic properties of the fundamental particles in the atom (Bloom, 1962). But here the magnetic properties are those of the electrons and the quantum characteristics of the electron spin systems. The sensing element in the instruments is a glass cell containing a vapor phase of the corresponding alkali metal, among which Rubidium and Cesium have thus far been used. The Zeeman splitting of the energy states of the atom is dependent upon the magnetic field strength but in a rather complicated way because of the complex nature of the electron spin systems. The process of modifying the relative populations of the various sublevels is accomplished in a different fashion as is the detection of the energy changes between the split sublevels, when compared to the proton magnetometer.

The operating principles can be illustrated with the aid of a diagram for the hyperfine energy level structure for the Rb^{85} isotope shown in Figure 11. The principles for Rb^{87} and Cs^{133} are the same although there are differences in the exact structure of the sublevels and corresponding differences in the numerical parameters relating field and frequency. The important feature of the diagram is that in the ground state ($5\ ^2S_{\frac{1}{2}}$) and the first excited state ($5\ ^2P_{\frac{1}{2}}$), the possible configuration of the energy structure is separated or split into 7 sublevels for F=3 and

5 sublevels for F=2. The energy differential separating these sublevels from each other is dependent nonlinearly upon the magnetic field intensity. The deviation from linearity becomes important at the large fields near the earth's surface.

By use of a process called "optical pumping" first demonstrated by Dehmelt (1957), the state of the atoms in the sensing element can be altered so that upon relaxation they become preferentially distributed into only one of the possible ground states. This is accomplished by illuminating the vapor in the gas cell with photons (of the correct quanta) to raise them to the first excited state. In this process the atoms in the gas cell absorb energy from the incident light beam and because circularly polarized light is used, the excited states can be reached only with a change in the magnetic quantum sublevel of $\Delta m = +1$ (or -1) depending upon the sense of the polarization relative to the direction of the beam or the optical axis of the exciting lamp-gas cell system (see Figures 11b and 12a).

After excitation, the atoms will spontaneously decay to their ground states by the emission of energy but because of the mixing among the excited phases which takes place, the decay occurs with equal probability for $\Delta m = 0, +1$ or -1. Thus the final state of the absorption gas cell is that all the atoms become trapped in the m=+3(or-3) sublevel, since they are not able to make the transition to the excited state from that sublevel (see Figure 11). In this case the atoms are said to be "pumped" into a preferred metastable state where they can no longer absorb energy.

The magnetic field is measured by determining the energy difference between the sublevels and this can be accomplished by forcing a redistribution

of the atoms by the application of energy with the correct quanta to disturb the metastable equilibrium. In fact, this turns out to be an RF electromagnetic field at the correct frequency and subsequent to its application, the gas cell once more becomes capable of absorbing energy.

A block diagram of a simplified alkali vapor magnetometer is shown in Figure 12a. Here resonance radiation light from a Rb^{85} lamp is obtained by means of an RF electrodeless discharge using a small glass bulb containing the Rb metal. The light is optically collimated and passed through an interference filter that removes light at a wavelength λ=7800 A^{o} which would cause redistribution of the atoms in the ground state and preclude achieving a non-uniform distribution of the atoms in the ground state. A circular polarizer then leads to the quantum selection rule favoring one or the other extreme sublevel in the split ground states. Finally the light is passed through the gas cell where the vapor absorbs some of the incident energy until it becomes preferentially pumped. With the use of a collimating optical system and a photo-cell detector sensitive to light of the wavelength in the incident beam, the output can measure the optical transparency of, or transmission of light through, the gas cell.

When the cell is first illuminated it becomes transparent shortly after first being somewhat opaque as energy is absorbed by the gas cell. If now an external RF magnetic field is applied at right angles to the optical axis (assumed parallel to the external field), the atoms will be redistributed to the various sublevels and the opacity of the cell will increase. If the frequency of the RF field is made to sweep across the

spectrum a decrease in light transmission on the order of 10-20% will be observed at that frequency corresponding to the splitting of the energy sub-levels.

This in fact is the Larmor frequency of the electron spin system in the classical mechanical analysis of nuclear resonance. However, this method is no better than the proton magnetometer since there is still not a continuous measure of the magnetic field unless a servo-controlled sweep oscillator is used to maintain the transparency of the cell at a minimum and the frequency monitored.

By suitably modifying the system, as shown in Figure 12b, the modulation of the transmitted light itself can be effected at the Larmor frequency. This is accomplished by using a feedback loop with the appropriate phase shift and loop gain which then creates a magnetometer which spontaneously self-oscillates at the Larmor frequency. The condition for resonance requires that in this system, with the optical and RF axes colinear, a 90° phase shift be used to compensate for the -90° phase shift which occurs between the RF field and light modulation. The 0 to 180° phase shift selector is required to choose the proper phase since the direction of the field may change relative to the optical axis of the system and the sense of the circular polarizer is fixed. By measuring the frequency of the feedback loop a measure of the intensity of the magnetic field is achieved.

Two problems arise in the accurate and continuous measurement of a magnetic field by such instruments. As is the case with the proton magnetometer, the signal amplitude and thus the signal to noise ratio of

the sensing element is dependent upon the orientation of the field relative to the optical axis as sin 2θ. Thus three null zones exist, two near the poles, as with the proton magnetometer, and also a large zone near the equator, for $\theta = 90^{o} \pm 11^{o}$.

A much more serious problem, however, is that of the slight but increasingly important dependency of the resonant frequency on the magnitude and direction of the magnetic field. This is because the frequency corresponding to the Zeeman splitting of the energy levels is a nonlinear function of the field intensity, and is not the same between adjacent energy levels. For a magnetometer this means that a resonance condition exists over a finite and variable band of frequencies related to the magnetic field in a complex manner. Thus the frequency will change as the orientation of the field changes. For the Rb^{85} diagram shown in Figure 11 the 6 frequencies for the transitions between sublevels m = +3 to -3 are given by the Breit-Rabi formulae as (Farthing and Folz, 1967).

$$\left.\begin{aligned} f_{\pm 3} &= \pm 359\,B^{2} \\ f_{\pm 2} &= 4.66737B + \{ \pm 215\,B^{2} \\ f_{\pm 1} &= \pm 72\,B^{2} \end{aligned}\right\} \qquad 2.4.1$$

where f_i = the frequency (Hz) for the transition between the m and [m-sgn(i)] sublevel. This means that the resonance frequency of the single gas cell system is biased higher or lower than the center frequency by a non-negligible amount in strong fields, that is greater than 10^{4} gammas. This is because the resonant feedback loop cannot resolve the 6 very closely spaced lines and instead operates on an effectively "smeared" line width composed of the

6 lines. The maximum heading error for Rb^{85} in a field of 0.5 Gauss is thus 186γ, for Rb^{87} it is 82γ while for Cs^{133} it is only 6γ. In practice the heading errors are less than these values and thus a Cesium magnetometer is the most accurate single gas cell alkali vapor instrument.

An elegant solution to this "heading error" problem for the Rb^{85} and Rb^{87} isotopes (Ruddock, 1961) which consisted of using two cross-coupled self-oscillating magnetometers is shown in Figure 13. Here the photo-cell amplifier output of one gas cell is used as the input to the RF coil of the other. With this design, there is complete symmetry of the response characteristics of the magnetometer for variable field orientations and except for the same signal-to noise-ratio problem which remains, the resonant frequency will be independent of the orientation. This occurs because when one gas cell is being pumped into the m=+3 state, it implies that the other is being pumped into the m=-3 state. The transfer function of the feedback loop depends upon the product of the individual lines and so with the complete symmetry of the instrument response to an external field the smeared resonance line width is made symmetrical and the loop operates at the center frequency of the 6 lines or at

$$f = 466737\ B \qquad 2.4.2$$

The problem of the null zones can only be solved by reorienting the magnetometer continuously in order to maintain an adequate signal-to-noise ratio or to use a pair of magnetometers, as done with the proton precession system. However, since the signal-to-noise ratio is dependent upon sin 2θ this means that the optimum angle between the two axes is 45°. In practice an angle of 55° has been used, leaving only two small null zones, elliptical

regions of approximately 20° by 10° in size. The outputs from the two units are then mixed before subsequent processing.

Other problems exist than the theoretically based ones just discussed in connection with the actual fabrication and operation of such devices. The temperature of the resonance excitation lamp and the gas absorption cell must be independently controlled and confined with limits of approximately 2-5 $^{\circ}C$ in order to maintain adequate signal strength. The temperature controls the pressure in the gas cell and this in turn controls the rate at which collisions of the atoms with the walls of the cell occur. The collisions result in enhancing the relaxation process so that unless limited by either the use of special coatings on the walls and/or the use of a buffer gas, the atoms cannot be pumped. The pumping must occur faster than the natural depumping for the magnetometer to self-oscillate. Such temperature control is achieved through the use of additional power to actively thermostat the units. Of course extreme care must be taken in the winding of these heating coils to avoid generating magnetic fields which would be sensed by the magnetometer.

Within the electronics system, all sources of phase shift spurious to those required must be eliminated, whether they be temperature or frequency dependent. This becomes extremely difficult when considering the wide range over which an electronic system must operate to cover the range of field strengths to be measured in space. Going from 0.5 Gauss to 0.5 gamma spans 5 decades and this is simply not feasible with a single low noise high gain amplification system. Normally a much smaller range is selected as the objective, and frequency ranges up to the order of 3.5 decades can be built. The instruments which have been employed in space

studies have either been able to provide measurements of relatively low field strengths or high.

For the other alkali vapor systems which have been developed and used on spacecraft the resonance frequency is different. For the Rb^{87} isotope the resonance frequency is 6.99632 Hz/gamma while for the Cs^{133} isotope it is 3.49869 Hz/gamma. Of these three, the first two have been used on satellites while the last one has been only used in rockets (Cloutier and Haymes, 1968), although a satellite version has been developed (Dolginov et al., 1969). The selection of which of these shall be used depends upon several considerations, among which are

1) Resonance frequency and range of operation

2) Width of resonance line

3) Temperature range of gas cell and lamp

4) Power required (~3 watts per lamp and 0.5 watts per gas cell).

In all of these self-oscillating magnetometers, the units provide continuous absolute measurements of the intensity of the magnetic field. The power required for these instruments varies among designers but ranges between 3 to 10 watts continuous plus 1-5 watts for heater power.

A problem common to all of these magnetometers is the width and asymmetry of the resonance line, which is dependent upon the nonlinear Zeeman splitting, the Doppler broadening associated with collisions of the atoms in the gas cell with its walls and the intensity of the pumping light. This broadened and possibly asymmetric resonance line leads to three problems:

1) Accuracy of measurements which is limited by the resolution and heading errors (if present)

2) Low field response limited by resonance line width which means that fields $<3\gamma$ cannot be measured.

3) Response to fluctuations limited to being less than resonance line width ($<$ 20-50 Hz), and

4) Intrinsic noise level proportional to resonance bandwidth

These factors combine in magnetometers built for space applications so that absolute accuracies of better than 0.1γ with sensitivities of 0.01γ in fields of $50\text{-}100\gamma$ are possible. The Larmor frequency is so high that these quantum magnetometers can be used to measure the weak fields in the distant magnetosphere and in interplanetary space.

2.5 Helium Vapor Magnetometer

The vector low field Helium vapor magnetometer is another "quantum" instrument whose operation depends upon the magnetic properties of the two electrons in the Helium atom. There is no direct determination of the Zeeman splitting of the energy levels of the electron spin system, however, as in the alkali vapor self-oscillating instruments discussed in Section 2.4, and the device does not oscillate at the Larmor frequency. The operation is somewhat analogous to that of a fluxgate magnetometer, in that:

1) a primary sweep frequency is the means whereby information on the magnetic field at the sensor is obtained,

2) the instrument measures the components of the magnetic field, and

3) it is not an absolute instrument because its calibration is not dependent upon fundamental atomic constants.

The original instrumentation development has been discussed by Slocum and Reilly (1963). A brief summary of its operating principles shall be given here, depending heavily upon the description of the optical pumping and optical transmission properties of the alkali vapor absorption cell given in Section 2.4. As in those devices, the basic sensor is an absorption cell whose light transmission characteristics are detected to determine information about the external magnetic field.

The energy level diagram for ^4He is shown in Figure 14 for those levels involved in the optical pumping process. Helium can exist in two states, para-and ortho-, but transitions between them which produce optical radiation are forbidden. The instrument uses the optical pumping process to create an unequal distribution over the magnetic sub-states of metastable ortho-helium, which cannot spontaneously decay by any radiative process. The absorption of pumping light from an RF electrodeless discharge effectively transfers the atoms from the $^1S_0$ parahelium ground state to a non-uniform distribution in the $^2S_1$ metastable level, which is the ground state for orthohelium.

The Helium atoms are "pumped" when the parahelium atoms, excited to the $2\ ^3P_{0,1,2}$ levels by absorption of energy at frequencies corresponding to the transitions D_0, D_1 and D_2, spontaneously decay to the $2\ ^3S_1$ level but with a net change in their magnetic sublevels of either $\Delta m = +1$ (or -1). An unequal distribution of sub-levels results with the use of circularly polarized light, which is selectively absorbed by the Helium vapor as the electron spin systems become oriented, that is polarized by the light.

The information on the external magnetic field is obtained by disturbing the "pumped" state and detecting it as a modulation of the

pumping light beam. This occurs because the pumped gas is more transparent than the unpumped gas. Unlike the self-resonance magnetometers of Section 2.4, however, the method of orientation detection and disturbing is not based on the absorption of RF energy whose frequency is the Larmor frequency. Rather the variation of the status of the atoms in the absorption cell is observed by detecting the variation in the transparency of the cell as it is exposed to a known magnetic field of variable orientation.

The optical pumping process depends upon the sense of polarization of the pumping light and the angle θ between the magnetic field and the optical axis of the instrument. For circularly polarized light, the sub-levels will have a non-uniform population, all atoms in either the +1 or -1 sublevels depending upon the sense of the external magnetic field component parallel to the optical axis. In the absence of such a component the populations of all three sublevels will be the same.

By systematically varying the direction of the magnetic field at the cell, the transparency can be systematically modified and detected in the modulation of the transmitted light, which will vary as $\cos^2\theta$. Thus with an external magnetic field sweeping in a plane, as shown in Figure 15, the transparency of the cell will be varied as the atoms change from the +1 population to the -1 population. The frequency spectrum of the amplitude variations of the modulated light reflects the status of the net magnetic field at the absorption cell. In the absence of an external magnetic field, the frequency content of the output signal will consist of a second harmonic of the sweep frequency. However, if a steady external magnetic field is present at the absorption cell then there will be a fundamental frequency component whose magnitude and phase are related to the external field component in the sweep plane.

With reference to Figure 15, the ambient field to be measured is H_A while the sweep field H_S has components in the X-Z plane given by ($H_S \sin \omega t$, $H_S \cos \omega t$). The relative transparency, δT, of the cell is given by:

$$\delta T = H_R \cos^2 \theta \qquad 2.5.1$$

which is:

$$\delta T = \frac{(H_{AZ} + H_S \cos \omega t)^2}{[(H_{AZ} + H_S \cos \omega t)^2 + (H_{AX} + H_S \sin \omega t)^2]^{\frac{1}{2}}} \qquad 2.5.2$$

Assuming that $H_A << H_S$, valid for the null detector manner in which the device will be operated yields

$$\delta T = H_S \cos 2\omega t + \frac{5}{2} H_{AZ} \cos \omega t - \tfrac{1}{2} H_{AX} \sin \omega t + \ldots \qquad 2.5.3$$

Thus the operation is rather different from a fluxgate in that the presence of a second harmonic does not carry the information but rather it is the fundamental frequency which does. The functional dependence of the light transmission properties of the absorption cell is the source of this characteristic behavior.

The addition of a feedback loop which generates a steady magnetic field at the cell to exactly cancel the external magnetic field and reduce the first harmonic to zero then leads to a magnetometer which measures two components of the magnetic field. By use of a sweep vector in a second plane orthogonal to the first, a three component measurement can be performed by switching the system repeatedly between the two planes. The

magnitude and phase of the fundamental harmonic carries the information about the two components in each plane and by monitoring the current required in the feedback coils to reduce the first harmonic to zero a measurement of the magnetic field is made. A simplified block diagram of a Helium vapor magnetometer of the type just discussed is shown in Figure 15, with an IR detector shown since the resonant radiation to excite the atoms has the wavelength of approximately 1.08 A^{o}. A phase sensitive detector is used to measure the fundamental frequency component and drives the feedback coils which cancels the external field.

These instruments are thus relative devices which depend upon calibration of the external magnetic field to current relationship existing between the absorption cell+feedback coil system. The use of a Helium vapor cell which must be stimulated by an external magnetic field sweep is somewhat like the fluxgate sensor since it is the magnetic state of the sensor which leads to the eventual field measurement. One advantage of this device is that there is no phenomenon analogous to magnetic memory effects in the sensor and only the stability of the electronics is a source of error. These devices use calibration systems similar to fluxgates for their sensitivity but there is no way to verify the zero level of the electronics.

These devices use on the order of 5 watts power mainly because of the RF spectral lamp but are not as temperature sensitive as the Rubidium and Cesium systems. The dynamic range depends upon the electronics design and the noise level upon the electronics feedback loop. The RMS equivalent noise in a 1 Hz bandpass is 0.2γ and the magnitude of the field in the sweep vector is 50-200γ. The frequency of the sweep vector, on the order of 100-200 Hz, limits the response characteristics to less than 10 Hz.

2.6 Instrument Testing and Calibration

One of the most time consuming but absolutely essential parts of the fabrication of spacecraft instrumentation is that of test and calibration of the performance of every flight unit under environmental conditions expected to occur during launch and operation. This proves to be an extremely difficult task for magnetic field experiments since special facilities are required to simulate the physical conditions in space and at the same time to be capable of reducing the ambient magnetic field in the test environment to the very weak values to be subsequently measured.

The tests that must be performed are:

1) Zero-level stability, long term;
2) Sensitivity or noise spectral density;
3) Frequency response characteristics;
4) Variation of the above with temperature and pressure; and
5) Stability of the above following environmental changes and launch simulation

The use of large coil systems which cancel the geomagnetic field has become a standard method to simulate the weak fields in space as well as the use of specially constructed non-magnetic thermal simulators adapted to operations within such coil systems. Frequently, it is possible to measure only the operation of the instrument without the presence of the spacecraft in such facilities and this precludes a complete end-to-end test of the entire instrument. This becomes a possible error source if the instrument utilizes long booms and associated cabling to place the sensors at remote distances from the main electronics assemblies.

Typical operating ranges for the main electronics units on spacecraft are -10 to +50 °C while maintaining calibration to that nominally desired in the original instrument design. The sensors, being placed at more remote positions must withstand temperatures from -75 °C to +75°C and this may require additional power to provide thermostatic control under adverse conditions. Since the temperature variations are not precisely predictable in advance, the prudent instrument designer also includes a temperature monitor within the sensor and perhaps also within the electronics to provide in-flight data.

The long-term testing of the relative instruments such as the fluxgate, the search coil and the helium vapor devices, requires a servo-controlled feedback system to maintain the field in the test coil facility steady within the variation desired. In the absence of such a system, there can only be a verification of the zero levels of the fluxgate by reversing the sensor in a fixed field. This calibration will not work for either of the other two devices and another magnetometer must be employed, such as a proton or Rb vapor absolute instrument. In this case, the sensitivity of the units can be calibrated but they cannot be operated at extremely small fields with any confidence.

The determination of the sensitivity or noise characteristics of the sensors is made difficult by the ambient fluctuations of the earth's magnetic field. This requires that an especially quiet period be chosen or that during such tests the sensor be placed within a magnetic shield to attenuate the fluctuations. This of course must also be done within a coil facility so that the instrument is operating in a linear portion of its operational range.

In the previous sections descriptions of the five basic types of instruments which have been or are being used for space magnetic field investigations have been presented. The specific configuration and selection of anyone of the basic types to be used on a particular spacecraft depends primarily upon the philosophy of the principal investigator, the objectives of the study and the characteristics of the spacecraft.

3.0 Response on Spacecraft

The instruments discussed in Sections 2.1-2.5 have been employed on different spacecraft in a number of distinct configurations. The primary concern in the selection of both instrument and experimental system design, is whether the spacecraft is attitude stabilized by an active control system using gas jets or a passive system using magnetic torques or gravity gradient torques of the earth's fiel^s, or gyroscopically by spin stabilization. The majority of spacecraft which have included magnetometers have been spin stabilized, which offers a number of advantages for these experiments and also for other experiments such as particle and plasma detectors. The principal advantage gained and common to all experiments is an intrinsic directional scan of the angular acceptance aperture of the instrument over a much larger region of space than on an attitude stabilized spacecraft. In the case of magnetic field experiments this means determining separately the effects of the magnetic field of the spacecraft and hence the accuracy of the measurements, for the field components perpendicular to the spin axis (see section 3.2). In the following sections, the mathematical analyses of the several versions of magnetometers, as adapted to flight on the two types of spacecraft will be presented.

3.1 Response on Fixed-Attitude Spacecraft

The use of induction magnetometers on these spacecraft is generally limited to those experiments which have as their objective the detection of explicit time variations of the magnetic field and may include 1-3

detectors. The use of a triaxial set of fluxgate magnetometer sensors permits the direct determination of the vector magnetic field within the accuracy limited by the stability of the zero levels and the magnitude of the spacecraft field's contributions to each component value.

The use of any of the "atomic" magnetometers permits only a determination of the magnitude of the total magnetic field, and not its vector direction, unless additional electronics are included. The purpose of these units is to provide the capability for the addition of a sequence of accurately known bias magnetic fields. With a properly selected series of such bias fields it becomes possible to convert the magnitude data into component measurements.

Consider the unknown external field F with components F_x, F_y and F_z. If a bias field (B_i) can be added (and subtracted) for a pair of data points then the component of the field F_i can be determined. This is derived for the x component, B_x, as follows: let $R_\pm$ be the resultant field including the bias field ($\pm$), then

$$(R_\pm)^2 = F^2 \pm 2 F_x B_x + B_x^2 \qquad 3.1$$

Now, the value of F_x is obtained from the separate measurements R_+ and R_- as:

$$F_x = \frac{1}{4} \left[\frac{R_+^2 - R_-^2}{B_x} \right]. \qquad 3.2$$

The time required to obtain a complete vector measurement is then 6 times the interval required for making one measurement and may become long if the field is weak and a high degree of precision is desired. It also requires that the field be constant over the measuring interval.

This technique is of limited value unless the bias field value can be varied, even if the vector field to be measured is constant over the measurement time. This is because the error in determining a component from a pair of biased measurements depends upon the ratio of the field to the bias value. This can be seen in the following development. Let δ represent a small variation in the parameters F_x, R_+, R_- .

$$\delta F_x = \frac{1}{2} \left[\frac{R_+ \delta R_+ - R_- \delta R_-}{B_x} \right] \qquad 3.3$$

If R_+ and R_- can be determined to 0.1%, a reasonable value, so that

$$| \delta R_\pm | \leq 10^{-3} R_\pm$$

then

$$\left| \frac{\delta F_x}{F} \right| \leq 10^{-3} \left[\frac{F}{|B_x|} + \frac{|B_x|}{F} \right] \qquad 3.4$$

Hence regardless of whether the ratio B_x/F is large or small, the fractional error in determining the x component of F may become very large. In order to cover a wide range of field magnitudes with a uniform accuracy, the magnitude of the bias fields must be varied. Thus far, only fixed magnitude bias fields have been used on spacecraft which have carried these absolute magnetometers.

3.2 Response on Spin Stabilized Spacecraft.

The analysis of the output of a mono-axial detector, such as a fluxgate sensor or a search coil detector, on a spinning spacecraft is straight forward if there is no precession or nutation of the instantaneous spin

axis. The following development will assume a payload coordinate system fixed in inertial space with the Z_p axis parallel to the spin axis ($\vec{\omega}_{SC}$) and the X_p - Z_p plane selected to include the spacecraft-sun line (see Figure 5). The detector system will be assumed to be fixed rigidly to the structure, which is spinning at a constant rate, ω_{SC}. Let the magnetic field $\vec{F}$ be represented by a vector at the polar angle α and the azimuthal angle φ_F, while the ith component sensor is represented by a unit vector $\vec{S}_i$ in the direction (θ_i, φ_{si}). Thus the orthogonal components of $\vec{F}$ and $\vec{S}$ are:

$$\vec{F} = (F \sin\alpha \cos\varphi_F,\ F \sin\alpha \sin\varphi_F,\ F \cos\alpha)$$
$$S_i = (\sin\theta_i \cos(\omega_{SC}t+\varphi_{si}-\varphi_{ei}),\ \sin\theta_i \sin(\omega_{sc}t+\varphi_{si}-\varphi_{ei}),\ \cos\theta_i) \qquad 3.2.1$$

The parameter φ_{ei} represents the electronic circuit delay or phase shift at frequency ω_{sc} and φ_{si} the angular offset of the sensor from the spacecraft reference meridian plane, the plane defined at t=0.

The instantaneous output of the sensor is then

$$G_i\ [\vec{F}\cdot\vec{S} + Z_i] = \text{Output} = D_i \qquad 3.2.2$$

where Z_i represents the deviation from absolute zero of the apparent zero level of the sensor plus the component of the magnetic field of the spacecraft parallel to the sensor axis. G_i is the functional gain of the sensor which relates its output (normally in volts) to its input (normally in γ). There may be a nonlinear relationship between input and output although in this analysis we shall assume that G_i is a linear multiplicative factor (volts/γ). Substituting 3.2.2 into 3.2.1 and collecting terms, we obtain

$$D_i = G_i[F\cos\alpha\cos\theta_i + \sin\alpha\sin\theta_i\cos(\omega_{sc}t+\varphi_{si}-\varphi_{ei}-\varphi_F)+Z_i] \qquad 3.2.3$$

It is seen that this consists of:

(1) a steady component depending upon the amplitude of the external field parallel to the spin axis plus spacecraft field and the inaccuracy of the sensor, and

(2) a component varying at the spin rate which is proportional to the component of the external magnetic field perpendicular to the spin axis.

Thus, even for those experiments in which the spacecraft field is non-negligible and the accuracy of the sensor unknown, ($Z_i \neq 0$), it is possible to determine the field transverse to the spin axis within the uncertainty of the sensitivity or gain factor (G_i) of the sensor. This is because the amplitude of the spin modulated signal is independent of Z_i and depends only upon F sin α sinθ_i. That is

$$\max[D_i(t)]-\min[D_i(t)] = 2\ F\ G_i\ \sin\alpha\ \sin\theta_i \qquad 3.2.4$$

In a sense, the use of a spin stabilized spacecraft introduces a signal at a carrier frequency whose amplitude and phase is modulated by the external field component transverse to the spin axis. There is no manner in which the external field component parallel to the spin axis can be uniquely determined however. Hence the necessity for long booms to put the sensor at a remote distance from the contaminating field of the spacecraft is necessary. On an attitude stabilized spacecraft it is

impossible accurately determine the field within the uncertainty placed by the spacecraft field itself, regardless of instrumental accuracy.

Assuming the existence of a sufficiently long boom to eliminate the spacecraft field as a source of error, there still remains the uncertainty in the accuracy of the absolute zero level of the sensor system. This can be determined for those sensors which are mounted perpendicular to the spin axis ($\theta_i = 90^o$) since data obtained at intervals of one-half a rotation ($\Delta t = \pi/\omega_{sc}$) can be used to determine Z_i. That is

$$\tfrac{1}{2}\left[D_i(t) + D_i\left(t+\pi/\omega_{sc}\right)\right] = Z_i G_i \qquad 3.2.5$$

This then suggests that if a means for reorienting the sensors while in flight exists so that periodically each one is perpendicular to the spin axis, their zero level can be monitored. In the event of variations, these can be incorporated into the analyses to yield more accurate data than would be available without this reorientation. The development of lightweight non-magnetic mechanical devices for reorienting sensors in-flight has progressed rapidly since the first such unit was flown on Pioneer 6 in 1965 (Bauernschub, 1967). Normally these devices reorient a sensor (or triaxial sensor set) by 180^o (or 90^o) about an axis perpendicular to the spacecraft spin axis.

For instantaneous accurate measurements of the vector magnetic field in space, it is necessary to have a triaxial sensor set which measures three orthogonal components in a time interval short compared to the time constant corresponding to the instrument passband and the most rapid fluctuations of the ambient field expected. In order that the spin

modulation by the external field be detected with little distortion, this requires that the passband of the sensor system extend to $\omega \gg \omega_{sc}$. The sampling rate of the sensor system, and problems related to the presence of fluctuations of relatively significant amplitude for $\omega \geq \omega_{sc}$ does not affect the determination of the instantaneous magnetic field. However, determining uniquely the relationship of successive vector measurements may be impossible and this problem shall be discussed in Section 4.1.

In determining the vector magnetic field, it is necessary to determine the effects of errors in the numerical values of the parameters ω_{sc}, θ_i, φ_{si}, φ_{ei} and Z_i. Assume that a triaxial sensor system is placed on a spin stabilized spacecraft with sensor orientation as shown in Figure 5b. From the above discussion, it is clear that an optimum orientation for the three orthogonal sensors is to have 2 of them transverse to the spin axis while the third is parallel to it. Then, through use of a single reorientation device, with its axis transverse to the spin axis, the sensor parallel to $\vec{\omega}_{sc}$ can be exchanged with one of the transverse sensors, as shown in Figure 5b and 5c. This permits the determination of all three sensors' zero levels and by periodically alternating the sensor set between the two positions shown in Figure 5b a continuous monitoring of the zero levels can be maintained. Note that if the spacecraft field transverse to the spin axis is non-negligible at the sensor position, then it is impossible to determine the zero level for the array sensor parallel to the spin axis. This is because Z_i may include different contributions from the spacecraft field in the two positions shown in 5b and 5c.

For purposes of the error analysis in this section, it will be assumed that $Z_i \neq 0$. To convert the triaxial measurements made on the rotating spacecraft to the non-rotating payload system as a function of time, it is necessary to know the relative orientation of the sensor system as a function of time. Normally this is accomplished with knowledge of the sampling time of the sensors (t_i) relative to the time at which an aspect sensor "looks" in a particular direction. Most commonly, a "sun-sensor" is employed which produces a signal pulse at that moment (t_{sun}) that the sun illuminates a photosensitive-diode whose viewing aperture is restricted to a meridian plane containing the spin axis. With knowledge of the relative geometry of the magnetometer sensor system and the "sun-sensor", only the time difference between the sample time and the sun pulse as well as the spin period is required.

The position of the spin axis in inertial coordinates is established by use of one (or preferably) two other aspect sensors. One sensor measures the polar angle of the sun and this limits the position of the spin axis to lying on a conical surface centered on the spacecraft sun line. Another independent measurement is necessary and can be provided by a third aspect sensor which utilizes the lunar or terrestrial albedo to yield another conical surface on which the spin axis may lie. (See Albus and Schaeffer (1963) for a discussion of such support instrumentation used in the Explorer and IMP series of spacecraft). The intersection of these two surfaces has one (or two) solutions, and usually vehicle launch dynamics selects the correct solution. It is also possible to use the directional characteristics of the spacecraft antenna to establish

the size and position of the second conical surface, as was done in the Pioneer 6-9 program.

If the spin period is incorrectly known, by an amount $\delta\omega_{sc}$, this will introduce an apparent phase distortion which is linearly dependent upon the time difference $(t_i - t_{sun})$ and the error in the spin rate. That is

$$\epsilon(\varphi_F) = (t_i - t_{sun})\delta\omega_{sc} \qquad 3.2.6$$

Problems of this nature are generally restricted to sporadic erroneous data transmissions of spin period data. However, a very unique example of this type of problem occurred on Lunar Explorer 35 when the optical shadowing of the spacecraft by the moon eliminated the solar illumination and thermal input for a sufficiently long period (up to 1 hour) so that the lowered temperatures led to a contraction of the structure. The concomitant decrease in angular moment of inertia led to an increased spin rate in order that angular momentum be conserved. While the change in spin rate in the lunar shadow was only 0.1% under full solar illumination, the spacecraft completed up to 10^3 rotations in shadow. This led to phase errors of up to more than 360^o using the pre-shadow or post-shadow spin rate data. The necessary mathematical analysis to reconstruct the variable spin rate from data taken by this spacecraft both pre-and post-shadow has been presented by Taylor (1968).

Assuming the spin period is accurately known, however, there remains the task to determine the effects of errors in the other parameters. Such errors can arise from a number of physical sources:

1. Non-orthogonality of the triaxial sensor axes (internally):

$$\vec{S}_i \cdot \vec{S}_j \neq 0; \; i \neq j)$$

2. Non-orthogonality of triaxial sensor axes (externally)

$$(\vec{S}_1 \cdot \vec{\omega}_{sc} \neq 0, \; \vec{S}_2 \cdot \vec{\omega}_{sc} \neq 0, \; \vec{S}_3 \times \vec{\omega}_{sc} \neq 0)$$

3. Inaccurate geometry of sensor set relative to sun-sensor ($\delta\varphi_{si}$)
4. Timing errors: in sampling S_i or sun-sensor (δt_i, δt_{sun})
5. Electronic phase shift errors ($\delta\varphi_{ei}$)
6. Gain errors (δG_i)

Items 1-3 are mechanical in origin and may vary depending upon which of the two possible positions the sensor is in as shown in Figure 5b and 5c. Items 4-6 are electronic in origin and are sensitive to both spin rate and temperature variations.

With values of t_i, t_{sun} and ω_{sc}, the components in payload coordinates (P_i) are determined from the triaxial sensor set output (D_j) as

$$P_i = \sum_{j=1}^{3} R_{ij} D_j \qquad 3.2.7$$

where R_{ij} represents the direction cosine between the ith payload axis and the jth detector axis. The instantaneous position of each of the detector axes can be computed and the rotation matrix R_{ij} takes the familiar form:

$$R_{ij} = \begin{bmatrix} +\cos A_1 & +\cos A_2 & 0 \\ +\sin A_1 & +\sin A_2 & 0 \\ 0 & 0 & 1 \end{bmatrix}$$

where $A_i = \omega_{sc} t + \varphi_{si} - \varphi_{ei}$ 3.2.8

After substitution of 3.2.3 and 3.2.8 into 3.2.7 we obtained, after some algebraic manipulations, for the transverse components:

$$X_p = \sum_{i=1}^{2} \{FG_i \sin\alpha \sin\theta_i [\tfrac{1}{2}\cos\varphi_F(1+\cos 2A_i) + \tfrac{1}{2}\sin\varphi_F \sin 2A_i] + G_i(F\cos\alpha\cos\theta_i + Z_i)\cos A_i\} \qquad 3.2.9$$

A similar expression is derived for Y_p,

$$Y_p = \sum_{i=1}^{2} \{FG_i \sin\alpha \sin\theta_i [\tfrac{1}{2}\sin\varphi_F(1-\cos 2A_i) + \tfrac{1}{2}\cos\varphi_F \sin 2A_i] + G_i(F\cos\alpha\cos\theta_i + Z_i)\cos A_i\} \qquad 3.2.10$$

The component parallel to the spin axis, Z_p, is given essentially by equation 3.2.3 with i = 3.

The effects of errors in the determination of X_p and Y_p are evaluated from

$$\delta X_p = \sum_{n=1}^{5} \frac{\partial X_p}{\partial a_n} \delta a_n \qquad 3.2.11$$

where a_n represents the parameters θ_i, G_i, φ_{si}, φ_{ei} and Z_i which is evaluated at the nominal values $\theta_1 = \theta_2 = 90^o$; $\varphi_{s2} - \varphi_{e2} = \varphi_{s1} - \varphi_{e1} + 90^o$, $Z_i = 0$, $G_2 = G_1 = 1$.

For the X_p component, the result is,

$$\delta X_p = F \sum_{i=1}^{2} \{\cos(\ A_i\ )[\delta Z_i - \sin\alpha\ \delta\theta_i] - \sin(2\omega_{sc}t + 2\varphi_i - \varphi_F)\sin\alpha\ \delta\varphi_i + \tfrac{1}{2}[\cos\varphi_F + \sin(2\omega_{sc}t + 2\varphi_i + \varphi_F)]\sin\alpha\ \delta G_i\} \qquad 3.2.12$$

where $\varphi_i = \varphi_{si} - \varphi_{ei}$ and $\delta\varphi_i = \delta\varphi_{si} - \delta\varphi_{ei}$. A similar expression can be derived for δY_p. It is seen that errors in the angle, $\delta\theta_i$, and zero level accuracy, δZ_i, introduce variations in the transverse components at the spin rate, ω_{sc}. Uncertainties in the gain functions, G_i, will introduce errors both steady state and at a second harmonic of the spin rate. Uncertainties in either the position or the phase delay, $\delta\varphi_i$, will introduce both first and second harmonics of the spin rate.

The significance of these errors in experiments performed thus far has varied widely. In cases where the spacecraft has been magnetically contaminated and/or the zero level has changed, the presence of a harmonic at the spin rate has permitted the determination of the error from inflight measurements. The very interesting feature of a second harmonic of the spin rate associated with both phase and gain errors has also been observed. Impossible to identify uniquely are those errors in the steady value of the component due to the gain errors, δG_i. Errors in the parameters for the Z_p component introduce errors both steady state and at the spin frequency but not at twice the spin frequency.

Generally, the experimental results have been analyzed and interpreted in the time domain, i.e., a chronological data plot is constructed and inspected. If the errors due to parameter uncertainties are sufficiently large relative to the quantization uncertainty, then they can readily be seen as sinusoidal variations. When small, however, then it is only in the frequency domain, when the spectra of the time series is obtained, that the presence of spectral lines corresponding to the spin frequency (and its second harmonic) are observed.

Rather then reconstruct post-flight the measured vector magnetic field in payload coordinates, triaxial fluxgate magnetometer experiments on Explorers 33, 35 (and Pioneer 9) have used an on-board analog (digital) spin demodulation system. The electronic unit essentially generates sine and cosine time functions synchronous in phase with the rotation of the spacecraft and then multiplies the detector 1 and 2 outputs by these continuous values. Subsequent low pass filtering performs an integration of these products and yields, upon summation, the component output. The mathematical description is similar to that given in this section.

This method requires additional complex electronics, and restricts the output bandpass of the detected signal to be well below the spin frequency of the satellite. This constraint is independent of the telemetry sampling rate. Because of the errors discussed in this section, unless an independent test of the accuracy and sensitivity of the sensor system is performed, the data may be subject to errors in the steady state values due to gain shifts of the electronics which go undetected because there is no method to determine if harmonics of the spin frequency are present.

Actually there is no reason why a triaxial sensor set is required if this method of on-board spin demodulation is used. All that is necessary is to employ a tilted single sensor and through use of filters, separate the steady value which is due to the field component parallel to the spin axis from the modulated value which measures the field perpendicular to the spin axis. This version of a spin demodulator has yet to be flown.

However, in the Explorer 10, 18, 21 and 28 experiments, single fluxgate sensors were employed which yielded complete vector measurements in post-flight data analysis.

Other techniques exist to measure the vector magnetic field but using less than three sensors and special on-board processing. One is to employ a single detector mounted at a suitably chosen orientation to the spin axis. On the Pioneer 6, 7 and 8 space probes the sensor was oriented with $\theta_1 = 54^\circ\ 45'$ for which the cosine $\theta_1 = \sqrt{3}/3$ or $\tan \theta_1 = \sqrt{2}$. Thus if $t_2 = t_{i-1} + \frac{2\pi}{3\omega_{sc}}$, yields

$$\vec{S}(t_i) \cdot \vec{S}(t_{i-1}) = \vec{S}(t_i) \cdot \vec{S}(t_{i-2}) = 0 \qquad 3.2.13$$

For this orientation, the sampling of the sensor at intervals of 1/3 the spin period leads to an orthogonal set of measurements. The only problem is that the 3 components are not sampled simultaneously and hence if relatively large field fluctuations occur near or above the spin frequency, then the field vector reconstructed may be in error.

Another technique, implemented on the ATS-1 satellite, uses two sensors mounted in a common meridian plane of the spacecraft but on opposite sides of the spin axis and at angles of 45° to the spin axis. ($\theta_1 = \theta_2 = 45^\circ$, $\varphi_{s2} = \varphi_{s1} + 180^\circ$) Through the use of simple differencing and summing electronics, the value of the field component perpendicular to the spin axis and in the plane of the sensor set is measured. The reconstruction of a vector field requires data measurements obtained over $(\omega t_i - \varphi_{si}) = 0$ to 360° in order to determine the maximum and

minimum values of the difference signal. Another two sensor detector system was used on Explorers 15 and 26, with $\theta_1 = 0^\circ$, $\theta_2 = 90^\circ$ and the sinusoidally varying signal from detector 2 used to determine the vector component of the field transverse to the spin axis. This also requires data obtained over 360°.

With due regard for the errors involved, it appears that the use of a triaxial fluxgate sensor and a simple reorientation device coupled with the intrinsic spin of a rotating spacecraft offers the best opportunity to provide accurate measurements of the vector magnetic fields in space. This is because of the numerous self-consistency checks in the data set obtained, which permit the verification of performance inflight. The problem of rapid fluctuations affecting the reconstruction of an instantaneous vector magnetic field is independent of telemetry rate and depends only upon the time interval between sampling the three orthogonal components. Use of less than three sensors can lead to situations in which these fluctuations affect the reconstruction of a vector field.

3.3 Spacecraft Magnetic Interference

The accurate measurement of the very weak magnetic fields and their fluctuations in space places severe requirements on limiting the magnetic fields which originate from the spacecraft structure, electronic subsystems, power sources and other experiment instrumentation. The goal of all magnetic experiments is to have these noise sources contribute a signal less than the intrinsic noise sensitivity of the sensor (or quantization

uncertainty) at the sensor position and over the pass band of the sensor. Almost all materials are magnetic and possibly ferromagnetic to some degree and this is especially time for electronic components. It is obvious that a non-magnetic boom must be used to place the sensors at a sufficiently remote distance from the spacecraft so that the design goal can be met. In realizing this objective technically, care must also be exercised in designing the electrical power system so that circulating currents do not generate large and variable magnetic fields.

The design goals of reducing spacecraft fields to less than 1 γ between 0-1 Hz at the sensor position have been achieved on spacecraft in the HEOS, IMP and Pioneer series. The verification of these levels is based upon extensive ground testing since there exist no methods to provide certification of the spacecraft flight interference except on the basis of the data self-consistency. This section shall briefly discuss the methods for building a minimally magnetic spacecraft, the test program followed through spacecraft integration and finally the effects of the measurements and interpretations of non-negligible spacecraft fields. The test program for the IMP-1 (Explorer 18) spacecraft has been summarized in detail by Parsons and Harris (1966).

In the structural design of the spacecraft, due consideration must be given to the use of minimally magnetic materials such as aluminium, magnesium and certain kinds of fiberglass and stainless steel. Some man-made materials utilize "filler" substances which in fact are ferromagnetic and should be avoided. The electrical design of subsystems and experiments should use non-magnetic electrical circuit equivalents where

possible and all interconnections should also be of non-magnetic material. Certain devices, such as traveling-wave tubes, relays, motors and particle detectors may be based upon the use of magnets in various geometries and strengths. The leakage flux from such units should be and can be reduced by proper design modifications without adversely affecting the device performance. In some cases this consists of using trimming magnets to cancel the intrinsic external magnetic fields of some devices.

The spacecraft power systems generally use solar cell panels and batteries and in the future RTG (Radioisotope Thermo-electric Generators) devices. For all electrical current flow, the best guiding principle, and one that has worked very successfully is that of self-compensation. In this approach all current flow, be it in solar panels, sub-systems or power distribution systems, employs return current paths which are in as close geometrical proximity to each source current as possible. The use of twisted-pair cables and either wires or current sheets flowing immediately behind each solar subarray are used, as well as arranging the various subarrays in an alternating pattern of their electrical geometry.

One of the most important aspects of the electrical power system is to use two wire distribution to each of the subsystems and instruments and a floating ground between spacecraft structure and each subsystem except at one point. The purpose of this is to eliminate large and variable ground loops. It should be noted that these self-compensation methods are also very helpful for reducing generalized EM interference and as such represent good engineering practice. The methods discussed in

this section have been used in USA and ESRO spacecraft. It is known that USSR spacecraft frequently use a compensation system employing permanent magnets to reduce spacecraft fields.

3.4 Spacecraft Magnetic Testing

Because of the two types of magnetic interference encountered, steady and fluctuating, the testing of spacecraft magnetically has been conducted in two separate ways. All terrestrial tests require the use of a large coil facility which eliminates the earth's field so that the measurement of weak fields can be carried out successfully with high accuracy. In normal order of testing, the sequence is:

1. Static field. (as received at facility),
2. Static field, after exposure to a strong steady field of 20-50 Gauss,
3. Static field, after "deperming"
4. Static field, induced by geomagnetic field,
5. Dynamic field, all subsystems operating in various modes and
6. Solar cell array field.

The measurements themselves have as a goal obtaining an equivalent magnetic field mapping of the spacecraft field near the sensor position. Since the normal fluctuation of the geomagnetic field is on the order of 1 γ or more it is common practice to perform measurements at distances much closer to the spacecraft than the sensor will be in flight and to extrapolate these measurements to the sensor position to obtain its accurate determination. The extrapolation usually assumes a dipolar behavior for the field along the boom axis, but this is also measured during the test program.

The purpose of the exposure and deperming actions is to reveal the amount of the relatively "soft" permeable material in the spacecraft, as well as to subsequently reduce the residual magnetic moment as much as possible. This is usually quite effective, although there were early concerns over the effects of the deperming operation, because it is accomplished by placing the spacecraft in a rapidly oscillating field of decreasing amplitude. The concern was based on the induction of significant and deleterious currents in either the electrical or mechanical systems in response to the changing magnetic flux. No known failures of spacecraft have been attributed to these magnetic test procedures. While it would be desirable to use deperm field magnitudes much larger than those employed and in some cases this has been done (Fiel, 1968), experience has shown that adequate demagnetization occurs with the values quoted. They were selected on the basis of field strengths to which the spacecraft were exposed during launch simulation testing. There was also early concern that during launch the spacecraft would be magnetized by the earth's magnetic field but ground tests simulating launch conditions indicated this does not occur.

The final test in the sequence is that of exercising the spacecraft electrically to measure fluctuating and steady magnetic fields. Frequently it is not possible to simultaneously illuminate the solar arrays, which are mounted on "paddles" exterior to the spacecraft or attached rigidly to the body of spacecraft. Under these circumstances, separate tests must be conducted. Normally tests 1-5 are conducted several times before and after environmental tests, after final calibration and before shipping to the launch site.

It should be noted here that the tests discussed above indicated performance only on the assembled spacecraft. In the HEOS, IMP, OGO and Pioneer programs, however, these tests were begun at subsystem level and continued from prototype through to flight instrumentation. The rationale was to identify the possible sources of large magnetic fields sufficiently early in the spacecraft program so that modifications could be made to reduce their effects.

This section has discussed those procedures developed for magnetic testing of USA and ESRO spacecraft. The author is not familiar with the procedures followed in the USSR to map the magnetic fields of spacecraft. From the published reports of problems with spacecraft magnetic fields, it appears plausible that no special efforts to design and fabricate magnetically clean spacecraft have yet occurred. The solution has been to use booms and compensating magnets as effectively as possible.

4.0 Data Processing

The primary purpose of the measurements obtained by magnetometers is to reveal information about the characteristics of the magnetic field in space. One of the most important serial elements in these experiments is the communication of the measurements via the spacecraft telemetry transmission channel. The overall design of the experiment includes a consideration of the properties of the telemetry system since they can directly affect the quality of the results even if all other aspects of the instrument design have been optimized. This section will discuss those considerations which have influenced the conceptional design and technical implementation of magnetic field experiments. The block diagram of Figure 4 will be referenced in this discussion.

The output signal from the various types of magnetometers present their information either as a variable voltage ranging between some fixed limts, or as a variable frequency signal. The signal in this form is referred to as being an analog signal and the magnetometer instrumentation itself may perform no additional processing of the data. The spacecraft telemetry encoder is then required to transform the signal into a form appropriate for the telemetry transmitter. For some spacecraft systems, the encoder includes a VCO (Voltage Controlled Oscillator) whose output, a variable frequency signal, is used to directly modulate the telemetry transmitter carrier. On the ground after reception and recording, a means of measuring the frequency, either from the VCO or the instrument itself must be devised.

A problem for the continued and generalized use of the analog on-board information encoding approach is that of limited time access to the telemetry communication channel. In almost all spacecraft there exists only one channel for information transmission so that all experiments must time share the available capacity. This means that if a multiple axis sensor is to be employed, there cannot be simultaneous transmission of all axes but rather that this must occur in time sequence. If the time interval between successive samplings of the three axes is large, then it may not be possible to accurately determine the vector magnetic field.

A solution to this problem is to employ a temporary analog memory, such as a set of capacitors, which can "store" the multiple sensor data set obtained for subsequent "read-out" by the telemetry system. While this approach is valid but difficult to accurately implement for voltage signals, it fails with the quantum magnetometers.

The need for improved precision, larger dynamic range, simultaneous component measurements and the varying capabilities of telemetry encoders, led to the on-board digitization of magnetometer data. Digital memories of tens of bits are easily implemented without magnetic core devices. In such instances the instrument must then include an analog-digital converter with word sizes typically of 8-10 bits indicating quantization uncertainties of 1 part in 256 to 1024 of the total dynamic range. The choice of logical word size is influenced by the physical word size of the spacecraft telemetry system.

The choice of the quantization step size is based on combined considerations of desired dynamic range and intrinsic noise level of the

sensors. Assuming a normal distribution of detector noise, then the peak-peak noise limits are approximately 5 times the RMS value, ϵ_{RMS}. Hence, if sensitive and advanced methods of data analysis such as power spectral studies are to be used in studying fluctuations, then it is reasonable to choose the quantization step size equal to ϵ_{RMS}. An even better technique is to utilize the power spectral noise density characteristics of the instrument, and not the RMS noise level which integrates the noise spectrum. This may indicate that quantization to fractions of ϵ_{RMS} are reasonable for the study of fluctuations in certain frequency bands. With the intrinsic RMS noise levels of sensors being 0.05-0.1γ, dynamic ranges of 50 to 100 gamma are possible with 10 bit converters.

Clearly for studies of the fields in space, such ranges are insufficient and means of range extension must be employed. In practice, this problem has been approached by two methods, see Figure 16:

(1) Use of <u>multiple ranges</u>, which are selected either by ground command or self-contained electronics. The leads to a fixed <u>relative</u> precision, given as a percentage of the dynamic range.

(2) to include separate bias fields of fixed magnitude in order to compensate for the field variability and <u>offset</u> the operating point of the sensor. This leads to a fixed absolute precision.

The second method permits compensating spacecraft fields and with the use of variable offset field magnitudes, a very wide operating range with fixed precision is made possible. The selection of appropriate levels can be effected either by ground command or on-board electronics.

Of these two methods of range extension, that of multiple ranges can be used on either spin stabilized or fixed attitude spacecraft. The offset bias field can be efficiently used only on those with fixed attitude, although, in the presence of a large fixed spacecraft field on a spin stabilized spacecraft, this offset field capability is also of great value.

4.1 Discrete Sampling and Aliasing

As a result of the time sharing of the communication channel, the magnetic field becomes discretely sampled, usually at uniform time intervals, which are dependent upon the telemetry format repetition rate. If the data signal is basically a variable frequency, then the value obtained after digitization in fact represents a time average over the digitization time interval Δt_d.

$$< X_i > = \frac{1}{\Delta t_d} \int_{t-\Delta t_d/2}^{t+\Delta t_d/2} X_i(\xi) d\xi \qquad 4.1.1$$

This time averaging is equivalent to a low pass filter operation on the frequency spectrum of the field fluctuations. The filter's amplitude characteristic is the familiar diffraction function:

$$\text{Amplitude} = \left[\frac{\sin \pi f/f_d}{\pi f/f_d}\right] \quad \text{where } f_d = \frac{1}{2\Delta t_d}$$

Thus high frequency fluctuations, $f > \frac{1}{2\Delta t_d}$, to which the sensor may respond are strong attenuated.

The data sampling rate, Δt, may be many times larger than Δt_d and under these circumstances the possibility exists for aliasing or spectral ambiguity of the fluctuations to occur. This phenomena is illustrated in Figure 17, where a frequency higher than the critical cut off, f_c, or Nyquist frequency (determined by the sample rate) appears equivalent to a much lower frequency. There is no way of determining which is the true frequency after the data has been discretely sampled. This means that successive data points cannot be uniquely related to each other with respect to the history of the field variations in between the sample points.

A solution to this aliasing problem is to include in the instrument in advance of the telemetry, a low pass filter with suitably chosen pass band. However, for very low sampling rates, another problem arises and that is that such individual measurements of the vector magnetic field may be quite different from the real instantaneous values. If one is concerned primarily with an accurate measurement of the field vector at each given instant, then one may have to accept the possibility of aliasing and be careful in the interpretation of the field fluctuations, as measured in spectral analyses. This is accomplished by choosing a moderate bandpass of the instrument, sufficient to respond rapidly enough to the fluctuations, so that each measurement includes the major fraction of the spectral energy.

Early experiments which were conducted violated this Nyquist criteria and only recently have sufficiently high telemetry data transmission rates been available to permit giving full consideration to this problem. For the most part, however, it has not been a problem which has

led to misinterpretation of data since throughout the space environment studied the naturally occurring fluctuations have an amplitude spectrum which falls off at least as fast as the frequency increases. Under this condition, the amount of energy which is aliased is a small part of the primary energy present in the fundamental frequency band.

A more common type of aliasing which does occur is when there is a spectral peak at $f>f_c$, which then appears as a much lower frequency. Under these circumstances, as long as the investigator is aware of the phenomenon of aliasing, he will not attempt to make unique interpretations of such data. In practice significant spectral peaks are generally observed only in the case where spacecraft noise exists due to various sub-systems or on a spin stabilized spacecraft due to the types of errors discussed in Section 3.2. For certain experiments, the design of an aliased data system was a planned act which permitted exploring the field fluctuations at frequencies greater than those limited by the Nyquist criteria as determined by the telemetry system. An example is the detection of rapid fluctuations in the geo-magnetosheath and the stimulated waves from the lunar wake.

The telemetry format for magnetic field sampling may be such that although the data sampling rate is uniform, there are also periodic gaps which occur due to other constraints. In this case the treatment of the aliasing problem becomes more involved but no additional subleties must be considered. The intrinsic features of aliasing in such an interlaced data stream, which is non-uniformly sampled, is the presence of a hierarchy of Nyquist frequencies.

4.2 On-board Computers

The major fraction of experiments which have been conducted have essentially been composed of a detector system with processing of the signal on the spacecraft only to prepare it for transfer to the telemetry data system. In most instances the on-board processing was that of signal conditioning and more related to matching of electrical interfaces and sampling times, as for example by using an analog or digital "buffer" memory to temporarily place the detected signals in storage until subsequently transmitted. This section shall be concerned with describing certain experiments which have included electronic subsystems which perform analyses described by mathematical formulae which usually were conducted on the ground as part of the post-flight data analysis. While a very limited number of such subsystems have been developed and flown, they already form the basis of what can be expected in future experiments.

The first computer employed in magnetic field measurements was the Time Average Unit (TAU) of Pioneer 6. As the distance from the earth increased, the spacecraft telemetry rate was reduced by up to a factor of 64. In addition during frequent telemetry "black-out" periods, the Pioneer 6 instruments were sampled at a very low rate over a time interval extending up to 17 hours in length. These data were stored in an on-board memory system for subsequent readout when ground antenna facilities became available. The instrument sampling rate changed from once every 1.5 seconds to once every 15 minutes, a factor of 600 to 1.

Over time intervals of this length, the use of a single sample to represent the magnetic field may be a poor approximation due to its intrinsic fluctuations. The TAU was designed to provide the time average of the

orthogonal components of the magnetic field for variable time intervals. That is, the computed output was

$$< X_i(t) > = \frac{1}{N} \sum_{j=1}^{N} X_i\ (t+j\Delta t) \qquad 4.3.1$$

where X_i represents the ith component of the field at the jth instant. For ease of implementation the choice of N was not variable but was fixed to an integer power of 2, $N = 2^K$, the value of the exponent, K, being selected on the basis of the real time bit rate or the length of time between successive samples in the black-out mode. The averaging operation in 4.3.1 was accomplished by shifting the binary point in an extended range accumulator. In the cases of Pioneers 6, 7 and 8, K could take on the value 2-4 or 6-8 so that up to 256 samples of data were averaged in the longest time interval.

The next computer to be flown was a spin demodulator on Explorers 33 and 35, an analog data processor, whose mathematical analysis has already been given in Section 3.2. The objective was to eliminate possible data aliasing, as discussed in Section 4.1, due to the low instrument sampling rate. A digital form of spin demodulator was used on Pioneer 9.

The most advanced computer flown to date has been the autocorrelation computer of Explorers 34 and 41. The device computed sums of the time lagged products which form the autocorrelation function.

The autocorrelation function for discrete data is defined as:

$$< X_i(t)X_i(t+\tau) > = \frac{1}{N-L} \left\{ \sum_{i=1}^{N-L} X_i(t+j\Delta t)X_i(t+(j+L)\Delta t) \right\} - \frac{1}{(N-L)^2} \left[\sum_{j=1}^{N-L} X_i(t+j\Delta t) \right] \left[\sum_{j=1}^{N-L} X_i(t+(j+L)\Delta t) \right] \qquad 4.3.2$$

where $\tau = L\Delta t$. From the autocorrelation function, the power spectrum of the fluctuations can be determined post-flight from the Fourier transform of 4.3.2. as

$$S(f) = 2 \int_0^\infty < X_i(t) X_i(t+\tau) > \cos 2\pi f\tau \, d\tau \qquad 4.3.3$$

In practice, only the first 8 raw lagged products (the term in brackets {} in 4.3.2) were computed from 256 data points and transmitted, with the necessary normalizations obtained on the ground. The lagged products were computed once every 20.46 seconds and the data transmitted from a buffer during the subsequent 20.46 second intervals. This also permitted an effective data compaction of 16:1, evaluated as:

$$\frac{(8 \text{ bits/sample}) \times 256 \text{ samples}}{(16 \text{ bits/lagged product}) \times 8 \text{ lagged product}} = 16:1$$

if all the original data have transmitted. Since relative phase information does not influence the power spectrum (or autocorrelation function), some loss of information has occurred. This is generally true for all schemes which compress data by various techniques.

It should be noted that transmitting only the first raw lagged product gives statistical information on the root mean square deviation of the signal, if the average is available, since RMS deviation =

$$\sqrt{\frac{1}{N}\sum_{i=1}^{N} (X_i - \langle X_i \rangle)^2} = \sqrt{\frac{1}{N}\sum_{i=1}^{N} X_i^2 - \langle X_i \rangle^2} \qquad 4.3.4$$

By Parseval's Theorem in Fourier Transform theory this is also a measure of the total energy in the magnetic field fluctuation spectrum.

4.3 Special Coordinate Systems and Field Averages

In the interpretation of vector magnetic field measurements in space, several different coordinate systems have been employed. The

natural extension of the traditional geomagnetic coordinates using local horizontal (H), vertical (Z) and declination (D) from the nominal magnetic North-South direction has been employed in some studies. However, this system fails to permit an organization of data obtained in widely separated places at different times as the sensor is carried along by the spacecraft. More importantly, other phenomena than the internal geomagnetic field dominate these new regions of space and new coordinates were developed specifically with these facts in mind.

The study of the interplanetary magnetic field has been carried out using two similar cartesian systems. The solar wind flows approximately radially outward from the sun and so one of the axes of these two systems is colinear with to this direction. In the solar ecliptic system shown in Figure 18a, the $\vec{X}_{SE}$ axis is directed from the place of observation to the sun. For satellites in earth or moon orbit this means essentially parallel to the earth sun line. The $\vec{Z}_{SE}$ axis is chosen to be normal to the ecliptic plane pointing northward and Y_{SE} forms the 3rd axis coordinate system.

The rotational axis of the sun is not normal to the ecliptic, and so the heliocentric system shown in Figure 18b was introduced to take this into account and chooses the axis for $\vec{N}$ to be parallel to the solar rotation axis, $\vec{\Omega}$. The difference between these systems is equal to the 7^{o} difference of the solar rotation axis from being perpendicular to the ecliptic. In view of the variability of the interplanetary field, this small difference not yet proved significant and interpretations of data in either system are equivalent. The $\vec{R}$ axis is directed parallel to the ideal solar wind flow direction and $\vec{T}$ completes the right-handed coordinate system.

The obliquity of the terrestrial rotation axis to the ecliptic is 23.4° and the non-axial dipole axis, $\vec{M}$, of the geomagnetic field is inclined at 11.7° to the rotation axis. In the study of the solar wind interaction with the earth, it was found useful to take this into account and use the solar magnetosphere coordinate system. The X_{SM}-Z_{SM} plane of the system is selected to include the dipole axis of the geomagnetic field so there is a daily oscillation of this plane by $\pm 11.7^{\circ}$ superimposed on an annual variation of $\pm 23.4^{\circ}$. The X_{SM} axis is selected to be parallel to the X_{SE} axis. The maximum deviation of the $\vec{Z}_{SM}$ axis from the $\vec{Z}_{SE}$ axis, is $\pm 35.1^{\circ}$. Solar magnetospheric coordinates have been useful also in studies of the geomagnetic tail. However, since the origin of the tail occurs at approximately 10 R_E on the geomagnetic equator, a seasonal variation by $\pm 10 \sin 35.4^{\circ} = \pm 5.8$ R_E of the field reversal region is observed parallel to the Z_{SE} axis.

The latest system introduced to study the deformed geomagnetic field is that using solar magnetic coordinates. This system uses a $\vec{Z}$ axis parallel to $\vec{M}$, and chooses $\vec{Y} \equiv \vec{Y}_{SM}$ so that it is related to the SM coordinates by a rotation by χ_{ss} about the $\vec{Y}_{SM}$ axis. Here, χ_{ss} represents the geomagnetic latitude of the sub-solar point.

In the representation of the magnetic field, a vector representation of a magnitude and two angles is frequently desired in polar coordinates. When the sampling rate is higher than desired for certain large time scale studies an average vector is needed. A method of averaging the field is used which best represents the nature of the field. Starting from component averages and RMS deviations:

$$< X_i > = \frac{1}{N} \sum_{j=1}^{N} X_i \ (t+j\Delta t)$$

$$\delta X_i = \{ \frac{1}{N} \Sigma \ (X_i - < X_i >)^2 \}^{\frac{1}{2}} \qquad 4.4.1$$

the average field magnitude and the angles are computed from the component averages as:

$$F_2 = \overline{F} = \sqrt{\sum_{i=1}^{3} < X_i >^2} \ ; \ \cos \varphi_i = \frac{< X_i >}{\overline{F}} \qquad 4.4.2$$

Another magnitude average is give by:

$$F_1 = < F > = \frac{1}{N} \sum_{j=1}^{N} [\sum_{i=1}^{3} X_i^2]^{\frac{1}{2}} = \frac{1}{N} \sum_{j=1}^{N} F(t+j\Delta t) \qquad 4.4.3$$

It is a simple task to show that $F_1 \geq F_2$. For variations of the three components, the Pythagorean mean

$$\delta C = \sqrt{\sum_{i=1}^{3} \delta X_i^2} \qquad 4.4.4.$$

can be shown to be independent of the coordinate system used. For the cases in which a sudden 180° reversal of the field occurs, the $< X_1 > \approx < X_2> \approx < X_3 > \approx 0$ and $F_2 \approx 0$ but $F_1 = F$. Here the simultaneous display of F_1 and F_2 on data plots can clearly indicate the nature of the fluctuations within the averaged period. The closer F_2 is to F_1, then the more steady the field has been during that time interval. Since averaging is an

operation equivalent to a low pass filter operation, then amplitudes computed over longer time intervals may be less than over shorter time intervals. It should be remembered that averaging is a process useful both for eliminating the effects of noise as well as satisfying the requirement for data compression when details are not essential to the study being conducted.

5.0 Earth Orbit Magnetometers

Satellites in orbit about the Earth have contributed most importantly to our knowledge of magnetic fields in space, due to the large number of separate experiments which have been performed (greater than 40) and the relative case, technically, of maintaining continuous telemetry coverage of such satellites' data transmissions. The following sections describe those instruments which have yielded results from such experiments while those to the planets, the moon and interplanetary space are presented in Section 6.

5.1 USSR Instrumentation

The USSR was the first nation to conduct magnetic field measurements from a satellite with the successful launch of Sputnik III in 1958. The experiment was conducted under the direction of N. V. Pushkov and Sh. Sh. Dolginov of the Institute for Terrestrial Magnetism, Ionosphere and Radio Propagation (IZMIRAN) located near Moscow. Since that time, all the space magnetic field experiments conducted by the Soviet Union either in earth orbit or to the planets has been implemented by the group working at IZMIRAN. The order of the presentation of these studies is chronological and by those satellites which have formed part of a series of spacecraft.

5.1.1 Sputnik III

The Sputnik III satellite, launched 15 May 1958 carried into space a self-orienting triaxial fluxgate magnetometer. Its operation

is identical in concept to those used in airborne magnetic surveys of the terrestrial field for geological studies, mineral and petroleum exploration and anti-submarine warfare. A comprehensive description of the instrument has been given by Dolginov et al. (1960).

The three axes of the sensor were mounted orthogonally in a two axis-gimballed support which was mechanically reoriented continuously in-flight to maintain one axis of the system parallel to the instantaneous magnetic field in space. This was accomplished by using the outputs of the two transverse sensors as "error" signal inputs to a servo-mechanism which then reoriented the sensor assembly until their two outputs were zero. The maximum rate of reorientation was 45°/second. The third axis of the sensor set, maintained parallel to the field to be measured, yielded the scalar magnitude of the magnetic field.

By measuring the position of the servo controlled support system relative to the spacecraft it was possible to determine the spacecraft orientation in space by comparison with the theoretical direction of the geomagnetic field (Beletskii and Zonov, 1961). This attitude determination technique has been used extensively in other USSR spacecraft programs such as the Proton Series (Sudorov and Prokhorenko, 1968). This is a moderately effective method for spacecraft orientation determinations at altitudes less than 4 R_E, where the geomagnetic field is known sufficiently accurately and the temporal variations are not significant.

The Sputnik III sensor unit was located forward of the spacecraft main body to reduce the spacecraft magnetic field contribution to the

measurements. However, the reduction was sufficient to only reduce the field to about 3000γ, as determined from both in-flight measurements and from terrestrial calibrations. No in-flight sensitivity calibrations were performed. Since the altitude range of the spacecraft corresponded to a range of the geomagnetic field of 30000-50000γ, it was only at the highest altitudes that the spacecraft field would be an important source to consider in the evaluation of the experimental results. Here the maximum attitude deviation would be on the order of 5° which leads to an error of the magnitude which is a minimum, of only 0.8%. The motion of the spacecraft consisted of a spin about the principal axis at 0.001 Hz and a precessional motion about the axis transverse to this with a period of 136 seconds (Dolginov et al., 1959).

The dynamic range of the instrument was 40000 $\pm$ 16000γ, the sensor using a digital range switch and offset field generator to partially compensate the field and thus to cover this wide range with uniform precision. The fixed offset was 3000γ for each step and the telemetry system transmitted the uncompensated residual difference signal in the range $\pm$2400γ with a sensitivity of 380γ/volt. Two analog outputs were used for fields of positive and negative polarity. Assuming that the quantization uncertainty was based upon the use of a 5 bit equivalent telemetry channel, as in all other USSR space magnetic field experiments, yields a resolution of $\pm$40γ. No information on the sampling rate has been given for this experiment.

The data from Sputnik III consisted mainly of measurements taken over the Soviet land mass during a 22 day interval ending 5 June 1958.

The interpretation of the scalar field intensity in terms of the deviations from that predicted by extrapolation of earth based measurements in the same region has been given in Dolginov et al. (1962). An agreement to within 1% was found and this was consistent with the uncertainties in the spherical harmonic coefficients determined from terrestrial surveys.

5.1.2 Electron Series

The Electron series, two sets of paired satellites, were launched on 30 January and 11 July 1964 to study the radiation belts and magnetosphere of the earth out to 11 R_E. The Electrons 2 and 4 were each placed into moderately eccentric orbits and both spacecraft included two triaxial fluxgate magnetometers with different sensitivities. A comprehensive description of the magnetometer systems has been given by Aleksanyan et al (1966).

The sensors were mounted on a special non-magnetic boom with the more sensitive unit most remote from the spacecraft, at 2.5 meters, the other at 2.1 meters, with the three axes of the separate sensors oriented parallel to each other. The dynamic ranges of the instruments on Electron 2 were $\pm 120\gamma$ and $\pm 1200\gamma$ while those on Electron 4 were $\pm 240\gamma$ and $\pm 1200\gamma$. Two telemetry outputs for each sensor axis, digitized as in Sputnik III, yielded quantization uncertainties of $\pm 2\gamma$ and $\pm 4\gamma$ for the more sensitive units and $\pm 20\gamma$ for the in-sensitive units. The sampling rates varied from one vector measurement with both sensors every 2 minutes to one every 8 minutes. The sensitivity was calibrated by addition of known fields to the sensors.

The spacecraft rotation was used to check the zero levels of the sensor and the spacecraft fields at the sensor positions. Yeroshenko (1966) has reported that from these data the drift of the zero level of the more sensitive magnetometer was less than 5-6γ on Electron 2. The spacecraft fields at the sensors position were measured on the earth's surface to be less than the sensitivity of each magnetometer, that is: 2γ and 20γ for Electron 2.

The data from these satellites has been analyzed mainly in terms of the difference in magnitude between the observed field and the predicted field extrapolated from spherical harmonic representations. As in other satellite programs, the magnetic field component measurements were used to establish the spin axis orientation and direction for other instruments on the same spacecraft. Studies of both the steady state and storm time deviations of the measured field have been presented by Dolginov et al (1966) and Yeroshenko (1966 , 1968).

A single axis induction magnetometer is also reported to have been included in the instrumentation of Electron 3, launched with Electron 4, to study the pulsations of the geomagnetic field at low altitudes. This device was sensitive to fluctuating fields with amplitudes greater than 25γ for frequencies within the two passbands 1-10 Hz and 3-300 Hz (Vernov et al., 1965). No results are published from these data.

5.1.3 COSMOS Series

The spacecraft COSMOS 26 and 49 represented the USSR contribution to the IQSY World Magnetic Survey and the bilateral agreement between the USA and the USSR on the peaceful uses of outer space. These spacecraft,

launched into 49° inclination orbits on 18 March and 24 October 1964, each carried two proton precessional magnetometers providing scalar measurements of the intensity of the geomagnetic field at altitudes between 270 and 500 Km throughout their entire orbit. A description of the instrument has been given in Dolginov et al. (1969b).

The two detectors were placed at the end of a boom 3.3 meters in length with the axes of their polarize-sense coils oriented at an angle of 90° to each other. A frequency meter covering the range 800-2000 Hz utilized a series of 11 adjacent frequency bands, each with its own narrow band amplifier, to increase the signal to noise ratio for the precession signal for subsequent on-board digitization.

Digitizing was accomplished by measuring the number of cycles of a 100 KHz reference frequency derived from a quartz oscillator which occurred during 512 cycles of the precession signal. The system was preceded by a searching counter which scanned across the 11 separate sub-channels until it found one in which a count of 32 could be obtained and this channel's signal was then diverted to the digitizer for counting. At the beginning of the next measurement cycle, the search began at the previous sub-channel in which the count was performed to minimize the search time: the minimum being 0.2 seconds, the maximum 0.6 seconds.

The two instruments were cyclically sampled at the rate of one data point each 32.76 seconds and the data stored in an on-board memory system for subsequent readout when the spacecraft was over a telemetry ground station. The spacecraft field at the sensor's position was not negligible and a compensating magnet in the spacecraft was used to

cancel the fields to a quoted accuracy of 2γ. The accuracy of the counting procedure to determine N was limited mainly by the signal to noise ratio of the proton precession signal and the stability of the reference oscillator.

The interpretation of these data has been based upon a comparison with the theoretical predictions and the spherical harmonic coefficients readjusted to yield a better fit (Tyurmina, 1968). The uncertainty of the satellite position is generally a source of larger errors than either the precision of the measurement or the accuracy due to the spacecraft fields. A special study of the Brazilian anomaly has also been reported (Konovalova and Nalivayko, 1967).

5.2 USA Instrumentation

Several groups and laboratories in the USA have conducted spacecraft experiments to study the magnetic fields in space. Frequently the payload assignments for such studies included several launches with identical or similar instrumentation. The following sections present technical summaries of the instrument characteristics, the grouping of descriptions being predicated upon similar objectives or in some cases the same group of experimenters. Generally the chronological sequence of the missions has been used to order the presentations.

5.2.1 Pioneers I, V and Explorer VI

Pioneer I was launched 11 October 1958 and carried the first USA magnetic field experiment on a spacecraft (Sonett et al. 1960). The mission objective, to orbit the moon, was not achieved and instead

the spacecraft reached an apogee of 93,000 Km before returning to earth impact. Transmission of data for approximately one day was not continuous but covered the two spatial regions 3.7-7.0 and 12.3-14.8 R_E. Explorer VI was launched 8 July, 1959 into an orbit with apogee 7.4 R_E an measured the distant geomagnetic field for 8 weeks. Pioneer V was placed into a heliocentric orbit on 11 March 1960 and measured the interplanetary magnetic field for 7 weeks.

The instrumentation on these three spin-stabilized spacecraft were nearly identical (Judge et al. 1960) and consisted of an induction magnetometer which measured the field component perpendicular to the spin axis. While only the magnitude of the field was measured on Pioneer I, both Explorer VI and Pioneer V carried an aspect indicator to measure the angle of the field component relative to the spacecraft sun-line. Explorer VI also carried a fluxgate magnetometer to measure the component of the field parallel to the spin axis, but no data were obtained since it failed to operate as planned. The sensors were all located within the main body of the spacecraft.

The detector consisted of a coil of 30,000 turns of number 40 copper wire wound on an iron-nickel alloy core. A band-pass filter with half-power width = 1.0 Hz centered at 2.0 Hz, the nominal spin rate, was used to limit the spectral sensitivity of the instrument. However, as Sonett (1963a) has shown, ambiguous spectral inversion or folding can occur in such experiments and the output can be a mixture of fluctuations at frequencies within the pass-band, 1.5-2.5 Hz and low frequency modulations near f=0. A photograph of the instrument is shown in Figure 19.

A non-linear amplifier was used with automatic-gain-control to extend the amplitude response characteristics to three decades, from 0.6 to 1.2 x $10^3\gamma$. The 15 second rise and 75 second fall time constants of the AGC circuit were highly asymmetric and influenced the response to transients. The amplifier output, 0-5 volts, was used to both directly modulate a subcarrier oscillator, and also to provide input to a digital telemetry system. There were no in-flight sensitivity calibrations. The received data was demodulated, digitized and then computer processed to yield amplitude and phase information. A sampling rate of approximately 600 Hz was employed and digital filters used to computer analyze the data. Results from these experiments have a special interest historically in magnetometer studies in space. Investigations of the interplanetary magnetic field were discussed by Coleman et al. (1960), and Greenstadt (1966). The extraterrestrial ring current was studied by Smith et al (1960). The nature of the termination of the geomagnetic field was presented in Sonett (1963b) and Sonett and Abrams (1963).

5.2.2 Vanguard III and Explorer X

The Vanguard III satellite was the third successful launch of the original USA-IGY satellite program. On 18 September 1959 it was placed into a close earth orbit with the primary purpose being to determine if an extraterrestrial ring current existed during the main phase of world-wide magnetic storms. The instrumentation consisted of a proton-precession magnetometer which operated by ground command and provided

more than 4000 measurements of the geomagnetic field intensity in the vicinity of 6 telemetry ground stations of the NRL-NASA minitrack network (Heppner et al. 1960; Cain et al. 1962).

The detector was a single cell of normal hexane, 1 inch in diameter and 4 inches long, wound with 600 turns of No. 15 Heavy Formuvlar aluminum wire. The sample was located at the end of a short boom approximately 0.5 meters long. A description of the instrument is given by Mansir (1960). A current of 7 amps for 2.2 seconds was used to polarize the sample following receipt of ground command. Subsequently the coil was connected to an amplifier whose output was used to modulate the telemetry carrier for 4.5 seconds. The amplifier pass band was from approximately 350 Hz to 4000 Hz covering field strengths from 0.1 to 0.9 Gauss. The data were transmitted, tape recorded and subsequently digitized. The battery power supply supported the operation of the instrument to the planned life time of the experiment, 90 days.

Since a coherent proton precession signal lasted only about 2 seconds, the coil+amplifier acted as a sensitive magnetic antenna and was responsive to electromagnetic fluctuations occurring naturally in the geomagnetic field. An analysis of the whistlers thus detected, an unanticipated feature of the experiment, has been given (Cain et al. 1961). Because the instrument is absolute, there was no necessity to include a calibration system, although when the signal was recorded at the telemetry ground stations, a reference 100 KC signal of high precision was recorded in parallel and used in the digitizing process.

Accuracy of the measurements was limited by spacecraft magnetic fields and the induced precession due to satellite rotation, and noise in the received signal. A consideration of all these sources led to error estimates with an RMS deviation of 3γ. A more serious problem in the interpretation of data was due to uncertainties in the satellite spatial position. This satellite data provided accurate tests of the spherical harmonic representation of the geomagnetic field (Cain and Hendricks, 1964).

The Explorer X spin stabilized space probe was launched 25 March 1961 into a highly elliptical orbit with apogee = 46.7 R_E at an angle of $\phi_{SE} = 140^\circ$ to the earth-sun line. Because it was battery powered, it provided data only for the first out bound pass through the magnetosheath (Heppner et al. 1963). The magnetic field instrumentation consisted of a dual gas cell Rb^{87} alkali vapor instrument (see Figure 21) and two monoaxial fluxgate magnetometers oriented at an angle of 57° 45' to the spin axis. All three sensing elements were placed on the ends of booms to reduce the possibility of spacecraft magnetic field contamination to less than 1γ.

The performance of all instruments was successful up to 18 R_E when the higher than optimum temperatures of the Rb^{87} absorption cell led to intermittent operation. This was caused by degradation of passive thermal control surfaces on the sphere which supported the single bias coil to convert the scalar instrument into a vector sensitive device. Fortunately there were simultaneous data from the fluxgates, whose dynamic ranges were limited to ±30γ, so that a

verification of their zero levels was possible. A sensitivity calibration was accomplished by periodically adding a known field parallel to the sensors' axis.

The Rb^{87} signal was employed to directly phase modulate the telemetry carrier while the fluxgate signal was used to provide input to a voltage-controlled-oscillator (VCO) which also modulated the transmitter. Intermittent bursts of fluxgate data for 2 seconds followed the long transmissions (137 seconds) of the Rb data. Following ground station recording, the data were digitized separately: the Rb^{87} data by a special purpose system similar to Vanguard III which yielded discrete samples every 0.010 seconds and the fluxgate data by a bank of comb-filters providing a digitization with 1% precision every 0.040 seconds. As shown in Section 3.2, the spin-modulated output of a monoaxial fluxgate sensor can be used to obtain the vector magnetic field. This was accomplished in two ways, by picking the maximum, minimum and associated times from a graphical display of the data and by computer-processing the digitized signal with numerical filters to yield the instantaneous value, and the 1st and 2nd time derivatives. Either of these three parameter data sets determine the vector field.

The results from these data were employed in assessing the nature of the distant geomagnetic and the possibility of a permanent ring current. Although trajectory uncertainties precluded absolute conclusions regarding the later feature, the data did help to clarify earlier satellite results (Smith, 1962). Of special interest was the

correlation of the magnetic field data with that of a plasma detector (Bonetti et al., 1963) revealing the presence of the magnetosheath inner boundary.

5.2.3 Explorers 12, 14, 15 and 26

These four spin-stabilized spacecraft represented the successful series of Energetic Particles Explorers which were launched into moderately eccentric orbits on 15 August 1961, 20 October 1962, 27 October 1962 and 21 December 1964. Explorer 15 was launched into a tighter orbit to study the artificial radiation belts which were created by the explosion of the USA Hydrogen bomb (Starfish) over Johnston Island in the Pacific Ocean on 9 July 1962. Only 5 hours after its launching, the USSR exploded their second high-altitude nuclear weapon of 1962 and Explorer 15 obtained a complete history of this event as well as the subsequent third USSR nuclear explosion on 1 November 1962. On all of these, fluxgate magnetometers were used, although the instrument was changed from a triaxial detector on Explorers 12 and 14 to a biaxial version on Explorers 15 and 26 in order to provide telemetry for an additional energetic particle detector to study the artificial radiation belts.

The detector assembly on all of these was mounted at the end of boom, paralleling the nominal spin axis, and at approximately 0.9 meters from the spacecraft main body. The triaxial sensor set was oriented with one axis parallel to the center tube and the other two transverse to it, with the biaxial version using only one transverse

axis. These spacecraft were solar-array powered and transmitted useful scientific data for long intervals with Explorer 14 being the first spacecraft with a magnetometer to operate for approximately one year. This was significant for it meant that the seasonal variation of the line of apsides of the satellite, relative to the earth-sun line, swept out more than 360^{o} and thus mapped the entire region of space surrounding the earth out to satellite apogee, 15 R_E.

The dynamic range of the instruments changed as more knowledge concerning the magnetosphere was acquired and as different nominal apogee distances were selected. The ranges chosen for these four missions were $\pm$1000γ, $\pm$500γ, $\pm$2000γ and $\pm$2000γ for each axis so that only data beyond 1.7 R_E or greater was obtained. The analog voltage output from each axis was 0-5 volts and used to control the output frequency of a VCO between 5-15 KHz which then modulated the transmitter. The entire spacecraft data output was formatted into a 16 frame x 16 channel matrix or sequence of discrete frequencies in a PFM encoding scheme (Rochelle, 1966) which repeated every 5.12 seconds. The magnetometer outputs were sampled in either 3 (or 2) adjacent channels every frame so that a triaxial (or biaxial) data set was obtained every 0.320 seconds. The time interval between successive axes being sampled was 0.020 milliseconds. For Explorers 15 and 26 a series of measurements was necessary to determine the transverse component from the single sensor data by best fitting an assumed sinusoidal modulation of variable amplitude and phase. The accuracy of the measurements was limited by the quantization uncertainties, which were larger than the

spacecraft fields, assuming that the zero level errors of the sensors were also small.

Following transmission, reception and recording, the data were digitized by a comb-filter bank with a precision of 1% (Explorers 12 and 14) or 0.1% (Explorers 15 and 26). This led to quantization uncertainties of $\pm 10\gamma$, $\pm 5\gamma$, $\pm 2\gamma$ and $\pm 2\gamma$ respectively. The increased precision was a result of an improved signal to noise ratio possible with the lower apogee orbits.

The spin rate of Explorer 12 was initially 27.8 RPM but increased to a 32.6 RPM maximum due to solar radiation pressure. The spin axis remained close to its initial injection position. The spin rate of Explorer 14 was initially 9.7 RPM, increasing to 12.2 RPM by 30 November 1962. The precession of the spin-axis was initially 15° half angle, decreasing to 3° but then increasing to 72° by 30 November. This large excursion continued for many months and considerably complicated the analysis of data from directionally sensitive detectors. The spin rate and orientation history of Explorers 15 and 26 were similar (Bracken et al., 1969).

The results from the Explorer XII experiment provided the first multiple measurements of the dayside boundary to the magnetosphere (Cahill and Amazeen, 1963; Cahill and Patel, 1967) and measurements of the distorted nightside magnetosphere in the near earth regions ($<12\ R_E$, Cahill, 1964a). In addition the measurement of the temporary inflation of the magnetosphere during geomagnetic storms has been reported and used in correlative studies with energetic particle flux measurements (Cahill, 1966; Hoffman and Cahill, 1968).

5.2.4 Explorers 18, 21 and 28: IMP Series

These three spin stabilized spacecraft represented the first three successful IMP (Interplanetary Monitoring Probe) satellites launched on 23 November 1963, 4 October 1964 and 29 May 1965 into highly eccentric orbits with periods of several days. These spacecraft have also been referred to in the literature as IMPS A, B and C (normally used internal to the project pre-launch) and as IMP'S 1, 2 and 3 (normally referring to post-launch spacecraft). The experiment design, telemetry data allocation, readout and processing were all identical. The instrumentation consisted of a single cell Rb^{87} self-oscillating magnetometer and two monoaxial fluxgate magnetometers oriented at angles of 30° and 60° to the spin axis (Ness et al., 1964). The sensing elements were located 1.0 and 1.5 meters from the body of the spacecraft respectively and extreme care was exercised in the design, construction and cabling so that a magnetically clean spacecraft resulted (Parsons and Harris, 1965). These magnetic fields were less than 0.5γ at the sensor positions.

The scientific objectives of these magnetic field experiments were primarily to measure the interplanetary magnetic field; the region of termination of the geomagnetic field and the distant geomagnetic field. The dynamic range of the instruments was consequently chosen to be 3-500γ for the Rb^{87} instrument and ±40γ for each of the fluxgates. The data were transmitted in a hybrid PFM format based upon that used by Explorer 12 but modified to take into account the much higher apogee by reducing the VCO bandwidth by a factor of 16. A sequence was

lengthened to 81.9 seconds, however, so the bandwidth time product remained constant, thereby assuring a similar S/N ratio to that of the EPE series. The precision of the digitization remained at 1%. Ground data processing was improved since it was possible to achieve throughput at a much higher rate. This was accomplished by recording data at the field stations at 1-7/8 ips and playing it back at 32 ips in the special purpose IMP Information Processing System.

The magnetic field data consisted of 1 sequence of Rb^{87} data every 4 sequences, with discrete samples at intervals of 320 milliseconds. The fluxgate data was digitized with a precision of $\pm 0.4\gamma$ at intervals of 160 milliseconds during every fourth frame during the 3 non-Rb^{87} sequences. These data were analyzed by linear digital filters, in a manner similar to that used for Explorer X, to yield a vector measurement of the field every 20.46 seconds. These fluxgate measurements were subsequently averaged every 4 sequences to provide the 5.4 minute averages which were most widely used in the data interpretations.

The performance of these experiments was quite successful although one of the fluxgate sensors on Explorer 28 failed during spin-up and boom erection shortly after launch. Also the performance of the Rb^{87} magnetometers was not as successful for most of the lifetime because of the very weak magnetic fields in interplanetary space, the correspondingly very low Larmor frequencies and the inferior performance characteristics of a single cell system. However, the presence of a bias coil both raised the operating frequency as well as permitted vector comparisons to calibrate the zero levels of the fluxgate sensors. A sensitivity calibration of the fluxgates was applied periodically.

The in-orbit lifetimes of these spacecraft ranged from 4 months for Explorer 21 and 6 months for Explorer 18 to 2 years for Explorer 28. Although the apogee of Explorer 21 was lower than nominal, and the spin rate was higher, the spin axis orientation in space for all 3 spacecraft changed only slowly and there was negligible precession. A photograph of the IMP spacecraft with the three magnetometer booms clearly evident is shown in Figure 22. The accuracy of the measurements was limited by the spacecraft fields and the accuracy of the vector determination of the sensors results. The fields were estimated as accurate to $\pm 0.25\gamma$ and the directions to $\pm 5^{\circ}$. In a region of rapidly fluctuating magnetic fields, such as the magnetosheath, Fredericks et al., (1967) have pointed out that the combination of the monoaxial detector system and the assumptions in the analysis procedures might lead to larger errors depending upon the frequency characteristics of the fluctuations. They suggested that these causes could explain some of the differences between the results of Explorer 18 with other satellites. Ness (1967b) showed that the differences were more apparent than real.

The results from the experiment on Explorer 18 provided the first and repeated measurements of the earth's bow shock wave (Ness et al. 1964), the first accurate measurements of the interplanetary magnetic field and its solar origin (Ness and Wilcox, 1964), the sectoring of the interplanetary medium (Wilcox and Ness, 1965), and provided a definitive mapping of the geomagnetic tail and its imbedded field reversal region, the neutral sheet (Ness, 1965 ; Speiser and Ness, 1967).

Results from Explorer 21 confirmed the quasi-stationary sectoring of the interplanetary medium and provided a definitive mapping of the distorted outer geomagnetic field (Fairfield and Ness, 1967) and the ordered field of the magnetosheath (Fairfield, 1967). The long life of Explorer 28 has provided measurements of the dynamics of the interplanetary sector structure during the rising portion of the solar activity cycle (Ness and Wilcox, 1967) and the characteristics of interplanetary shock waves (Taylor, 1969).

5.2.5 1963-38C, 1964-83C and DODGE

The US Navy satellite designated 1963-38C was launched on 28 September 1963 into a low altitude, approximately 1100 km, polar orbit. The spacecraft was magnetically stabilized with a large permanent magnet ($M=7 \times 10^4$ Gauss-cm^3) and achieved an alignment within $\pm 6^\circ$ of the local magnetic field direction throughout its orbit. A triaxial fluxgate magnetometer was included in the instrumentation complement although there was no boom to place the sensors at a remote distance from the spacecraft to reduce magnetic field contamination.

One axis of the sensor set was aligned parallel to the magnet axis and the other two orthogonal to it so that they responded to transverse fluctuations of the local magnetic field. The nominal oscillation frequency of the spacecraft about the magnetic field was approximately 100 seconds. The range of these two sensors was $\pm$ 2500γ and the analog output of the instrument was digitized on the ground with a resolution of $\pm 15\gamma$. The data sampling rate varied from essentially continuous, when in sight

of a telemetry ground station and real time transmission was possible, for one of the three sensors to a vector sample once every 22 seconds when the spacecraft was storing data in its on-board memory. The results from this experiment have been used to study the transverse fluctuations of the magnetic field in the auroral oval (Zmuda et al. 1966).

The US Navy satellite designated 1964-83C was launched 13 December 1964 into a polar orbit at approximately 1000 Km altitude. The magnetic field experiment consisted of a single cell Rb^{85} self-oscillating magnetometer and a complex system of a reversible moment ($M_c = 7 \times 10^3$ Gauss cm^3) permanent magnet to calibrate the large spacecraft generated field. This is due to the presence of a much larger permanent magnet ($M = 1.5 \times 10^5$ Gauss-cm^3) which was used to stabilize the spacecraft with magnetic torques. The orientation of the optical axis of the sensor unit was 45^o to the magnetic axis of the spacecraft, and the sensor was located at the end of an extendable boom nominally 4.9 meters in length.

There was no positive indication of the full extension of the boom but with the consistency of the calibration results it was assumed that the boom was in a rigid configuration. These data yielded estimates of the spacecraft field of 201 $\pm$18γ for one polarization of M_c and 183 $\pm$ 18γ for the opposite. The uncertainty of 18γ is a measure of the accuracy of the scalar measurements, which ranged between 15000 to 31000γ. An on-board counter measured the resonance frequency of the magnetometer every 0.65 seconds with a precision of 0.01% or better.

The data, in the form of a digital number, were transmitted, recorded and converted to field magnitude.

The experimental results were analyzed by comparison with a theoretical field model and interpretation of residual magnitude differences, which contain unknown errors due to trajectory uncertainties. The data mapped covered the region of the South Atlantic anomaly and showed that during one geomagnetic storm the perturbations at satellite altitude was comparable in intensity to that observed on the earth's surface (Zmuda et al., 1968).

The US Navy satellite DODGE, representing the Department of Defense Gravity Gradient Experiment, was launched 1 July 1967 into an approximately synchronous orbit with period 22 hours. The spacecraft included a triaxial fluxgate magnetometer with a range of ±250γ mounted at the end of a boom 1.7 meters in length. The sampling rate of the instrument was 0.8 Hz and the instrument passband from 0.5 to 10 Hz. No results have been been published from this experiment.

5.2.6 OGO Series

The Orbiting Geophysical Observatory series of spacecraft consisted of 6 very large spacecraft placed into earth orbits of two different types (Ludwig, 1963). The OGO's 1, 3 and 5 (also known pre-launch as OGO's A, C, and E) were designed to measure mainly the magnetosphere, radiation belts, magnetosheath and interplanetary medium from highly Eccentric Orbits and are referred to as the EOGO spacecraft. The OGO's 2, 4 and 6 (or B, D and F) were designed to study mainly the atmosphere and lower ionosphere of the Earth from Polar or high

inclination, low altitude orbits and were referred to as the POGO spacecraft. These spacecraft were launched one each year over a period of 6 years beginning in 1964, as shown below, with the two sub-series alternating in sequence.

Spacecraft	E/P	Launch Date
OGO - 1	E	5 September 1964
2	P	14 October 1965
3	E	7 June 1966
4	P	28 July 1967
5	E	4 March 1968
6	P	5 June 1969

The spacecraft were all nominally designed to carry numerous experiments, approximately 15-20, and to maintain a fixed attitude relative to the earth and sun directions by use of an active attitude control system employing gas jets. For a number of technical reasons, several of the OGO spacecraft failed to achieve this goal of attitude stabilization and in order to "save" these missions these spacecraft were placed into a spin stabilized mode. This severely compromised many of the experiments' scientific objectives, and since no provision had been made for this failure mode, the determination of the instantaneous orientation of the spinning spacecraft was made exceedingly difficult if not impossible.

Long booms, ~6 meters, were included to place magnetometer sensors at very remote distances from the main body of the spacecraft. The spacecraft also carried directional antennae for transmitting very high digital data rates, up to 64 Kilobits/second, as well as several special purpose telemetry channels for transmitting broadband analog

signals. Each spacecraft carried a pair of dual cell alkali vapor magnetometers (Rb^{85} or Rb^{87}) and a triaxial induction magnetometer. In addition the OGO 1 and 3 spacecraft each carried a triaxial fluxgate magnetometer while the OGO-5 spacecraft carried two separate triaxial fluxgate magnetometers. The high data rates of these OGO spacecraft combined with their long lifetimes has generated the largest set of magnetic field data ever obtained. For a number of reasons the major fraction of these data have not yet been analyzed.

5.2.6.1 OGO-1, 3, 5 Alkali Vapor

The magnetic field experiments on the OGO's 1, 3 and 5 included a pair of dual gas cell Rb^{87} self-oscillating magnetometers capable of operating over a wide range of field intensity. The optical axes of the two sensors were inclined at an angle of 55^{o} to each other. A spherical surface enclosed the 4 gas cell geometry and supported a triaxial set of coils for carrying a precisely known stable current and thereby converting the scalar instrument to a vector sensitive device. The sphere was located at the end of a 6 meter boom which also carried the triaxial fluxgate. In order to avoid interference between the two devices, a separation of 2 meters placed the fluxgate sensors nominally 4 meters from the spacecraft. A photograph of the last section of the magnetometer boom and the instrumentation is shown in Figure 23. The frequency signal from the Rb^{87} magnetometer was used to modulate one of the special purpose telemetry channels and the received data were processed on the ground with equipment similar to that used in the Explorer X and 18 programs.

Unfortunately, the first OGO suffered a series of technical failures which left the magnetometer boom unerected, and the attitude control system in-operative so the spacecraft was spin stabilized with a rotation period of 12 seconds. The magnitude of the spacecraft magnetic field gradient at the Rb^{87} sensor position was sufficiently large that coherent oscillation was not possible and no data was obtained. The operation of the OGO-3 and 5 alkali vapor magnetometers has been successful following the extension of the booms. The data was digitized at a standard rate of 7 samples/second with a precision of 0.1%. A preliminary survey of these data (Heppner et al., 1969) has been conducted to study the spatial distribution of small amplitude fluctuations of type PC - 1, 2, 3 and 4 in the magnetosphere.

5.2.6.2 OGO-2, 4, 6 Alkali Vapor

The magnetic field experiments on the OGO-2, 4 and 6 spacecraft included a pair of dual gas cell Rb^{85} self-oscillating magnetometers designed to operate at the high magnetic field intensities to be measured at the low satellite altitudes. The geometry of the sensors is similar to that of OGO's 1, 3 and 5 and the location is also on the end of a similar 6 meter boom. A photograph of the sensor head within the spherical thermal control surface is shown in Figure 24. However, the objective of the experiment was the precise measurement of the scalar magnetic field intensity so the spherical surface enclosing the sensors did not carry any bias coils to provide bias fields for vector measurements. The experiments on these OGO's represented the USA contribution to the IQSY World Magnetic Survey and participation in

bi-lateral space studies with the USSR. Rb^{85} was chosen over Rb^{87} because of its lower resonance frequency and the consequent ease of building a sensitive, low noise, high gain amplifier (Farthing and Folz, 1967).

Because of the close earth orbits, real time data transmissions from the satellite were not possible when the spacecraft were far from one of the receiving ground stations. An on-board tape recorder provided a means of storing data obtained under such conditions and for subsequent transmission. The data, however, were required to be in digital form and so the experiment included two digitizers to count the Larmor frequency and store it alternately for readout by the spacecraft telemetry system. The sampling rate of the experiment under these conditions was 2 Hz and the sample quantization uncertainty was $\pm 0.43\gamma$. When real time transmission was possible, the digital readout operated in the same manner but simultaneously the signal was used to modulate one of the broad band Special Purpose Telemetry channels.

The performance of these experiments has been successful even in spite of the failure of the attitude control system on OGO-2, which did not directly affect the objectives of these experiments. An analysis of the OGO-2 data as related to the objectives of the WMS has been given by Cain et al. (1967) and compared with COSMOS 26 and 49 results by Cain et al. (1968).

5.2.6.3 OGO-1, 3, 5 Fluxgates

The magnetic field experiments on the OGO-1, 3 and 5 spacecraft included triaxial fluxgate magnetometers, to provide precise vector

measurements of the magnetic fields in space. A series of three nearly identical instruments was employed by Heppner et al. (1967) and a separate triaxial fluxgate was employed by Coleman (Snare and Benjamin, 1966). All of these instruments provided analog outputs from 0-5 volts for each axis which were converted by a spacecraft subsystem to an 8 bit word representation for subsequent transmission. The spacecraft data system used a PCM telemetry format with a 128 word frame length that repeated at a rate dependent upon the transmission mode. The variable bit rates of the spacecraft were 1, 8 and 64 Kilobits/second leading to frame rates of 0.868, 6.95 and 55.5/second.

The instrumentation by Heppner on OGO's 1 and 3 used two different ranges, $\pm 30\gamma$ and $\pm 500\gamma$ which where sampled at rates of twice per frame and once per frame respectively. Thus the folding frequency for spectral aliasing considerations was 0.868, 6.95 and 55.5 Hz and 0.434, 3.48 and 27.8 Hz respectively. The bandpass of the fluxgate was fixed with the 3 db point at 12 Hz so that aliasing was possible. The digitizer yielded precisions of $\pm 0.24\gamma$ and $\pm 3.5\gamma$ for the high and low sensitivity scales respectively.

As reported in Section 5.2.6.1, the OGO-1 spacecraft failed to erect the magnetometer boom so that a large ($\sim 80\gamma$) spacecraft field was present at the detector assembly. However, the fluxgate instrument was capable of making measurements, albeit of a reduced quality, and provided the first high frequency time resolution study of the structure of the earth's bow shock wave (Heppner et al, 1967). Since there was no rubidium data to calibrate the zero levels of the

fluxgates, only the magnitude of the component transverse to the spin axis was accurately measured. In the absence of aspect information it was not possible to determine the phase angle of this field component. The later OGO's successfully achieved attitude stabilization as planned.

Both fluxgate magnetometers on OGO-5 included an automatic digital compensation capability for offset range operations. The instrument of Heppner incorporated steps of 30γ each which extended the range of each axis to ±4000γ while preserving a quantization uncertainty of ±0.12γ associated with the fundamental range of ±30γ. The instrument of Coleman used two offset scales, one of 16γ for each of 64 levels and the other of 1024γ for each of 128 levels. This leads to a total offset capability of ±65000γ while preserving the quantization uncertainty of ±0.0625γ associated with the fundamental range of ±16γ for each axis. The telemetry sampling rates of both instruments are related to the frame rate, those for the Heppner instrument being the same as OGO's 1 and 3, while those for the Coleman instrument are 0.868, 6.95 and 55.5 samples/second. The bandpass of the Heppner instrument is maintained fixed at 100 Hz while the Coleman instrument changes in response to the varying telemetry rate. The corner frequencies for the low-pass filters are 0.3, 2.5 and 20 Hz with a roll-off of 24 db/octave by use of active four pole filters. These later OGO spacecraft have yielded additional information concerning the fine structure of the earth's bow shock wave.

5.2.6.4 OGO 1-6 Induction

Every OGO has included a triaxial induction magnetometer sensitive to field fluctuations in the frequency range 0.01 to 10^3 Hz (Frandsen et al., 1969). The instruments are all identical in the mechanical geometry of their sensor units, using a coil of 10^5 turns of No. 47 copper wire wound on a core of laminated strips of high permeability nickel-iron alloy 27 cm. long with a cross section of 0.36 cm^2. The three orthogonal sensors and their associated pre-amplifiers are mounted at the end of a 6 meter boom to reduce interference from spacecraft generated fields. The natural resonance of the sensors occurs near 700 Hz and thus limits the high frequency response.

The main electronics assembly on the spacecraft processes the signal in a manner similar to that shown in Figure 6. Since the power converters in some of the SC subsystems worked at 400 Hz, there is a notch reject filter in front of the main amplifiers. The output was then applied to either a low-pass filter, whose corner frequency depended upon the telemetry sampling rate or to a series of 5 to 7 bandpass filters with center frequencies logarithmically spaced between 10 and 10^3 Hz. These later form a type of spectrum analyzer which was used to study fluctuations. Special purpose telemetry did not permit the transmission total broadband wave form except when in the real time transmission mode. Three gain levels of the main amplifiers were possible: 20, 40 and 60 db.

Four separate designs were used on the 6 OGO spacecraft, which reflected both knowledge gained concerning the occurrence of naturally produced fluctuations as well as problems associated with spacecraft interference. OGO's 1 and 3 were identical and represented an exploratory study of fluctuations in space. The Nyquist frequencies for the low frequency wave forms at the three telemetry rates were 2, 17 and 139 Hz with the time intervals between successive samples of the spectrum analyzer being 147, 18.4 and 2.31 seconds. The center frequencies of the 5 filters were 10, 32, 100, 320 and 1000 Hz. The improvements to the instrument design for the remaining OGO's was in the spirit of increasing the sampling rates of the waveform and spectrum channels as well as introducing the use of a subcarrier oscillator channel to transmit the broadband data via special purpose telemetry.

The threshold sensitivity of the sensors was originally planned to be the RMS signal equivalent to the intrinsic noise of the instrument. For OGO-1, the noise power decreased approximately as f^{-3} until the resonant frequency was approached. For OGO's 1-4, the minimum detectable signal is $10^{-8}\gamma^2/Hz$ for frequencies between 10^2-10^3 Hz, while at 1 Hz it is $10^{-2}\gamma^2/Hz$. OGO-5 had a sensitivity an order of magnitude better and OGO-6 a factor of 20 better. No calibration of the detector systems were performed in-flight. Numerous problems of interference arose due to mechanical boom oscillations (at periods of 2.4 and 4 seconds) and mutual electromagnetic coupling between various spacecraft subsystems and other experiments which raised the effective threshold sensitivity of the detector.

The analysis and interpretation of data obtained with these experiments has concentrated on the spatial distribution of fluctuations and their spectral characteristics. Noisy regions near the earth's bow shock, the geomagnetic equator and the magnetosheath have been identified (Holzer et al., 1966; Russell et al., 1969; Olson et al., 1969 and Russell et al., 1970).

5.2.7 Explorers 33 and 35: IMP Series

The two spin stabilized spacecraft Explorers 33 and 35 were part of the IMP series but modified to include a 4th stage retromotor since the objective was to place the spacecraft into lunar orbit. These spacecraft were called AIMP D and E prelaunch, the A representing Anchored. Explorer 33 was placed into a highly eccentric earth orbit on 1 July 1966 following an abortive attempt to orbit the moon. Although Explorer 35 did achieve a lunar orbit on 17 July 1967, the magnetic field instrumentation shall be discussed in this section since the magnetic field experiments were almost identical on the two spacecraft.

There were two triaxial fluxgate magnetometer experiments on each of these spacecraft with the sensors located on the ends of opposing booms transverse to the spin axis and 2.1 meters from the center of the spacecraft. The fabrication of the spacecraft was constrained to minimize magnetic field contamination and with the 90° flipper devices of both experiments, each of the three axes zero levels could be accurately checked in flight.

One experiment (Sonett et al., 1968) employed a three range sensor (±20γ, ±60γ, ±200γ) with one axis parallel to the spin axis and two transverse. The latter two sensors' outputs were synchronously demodulated on board to yield component measurements in a fixed payload coordinate system. The sampling rate was not uniform but averaged one vector sample every 6.15 seconds during the scan of the three ranges. The data were low pass filtered with a corner frequency of 0.05 Hz since the Nyquist frequency was ~0.08 Hz. The data were presented as analog signals between 0-5 Volts to the PFM telemetry system and digitization on the ground with 1% precision yielded quantization uncertainties of ±0.2γ, ±0.6γ and ±2.0γ respectively. The sensitivity of each sensor was calibrated once each day with the use of precision current sources and the zero levels checked by daily flipping (90°) of the sensor set. The stability of the zero levels was found to be 1γ during the first 30 weeks of operation for Explorer 33. An identical instrument was flown on Explorer 35.

Results from these experiments have contributed to the mapping of the geomagnetic tail and the tail magnitude gradient (Sonett et al., 1968; Mihalov et al., 1968) and the solar wind interaction with the moon (Colburn et al., 1967) and the interplanetary sector structure (Wilcox and Colburn, 1969).

The other experiment (Scearce et al., 1969) employed a single range detector of ±64γ on Explorer 33 and a dual range detector of ±24γ and ±64γ on Explorer 35 which was automatically switched in flight if necessary. The three axes were sampled essentially simultaneously

(within 15 msec) and digitized with an 8 bit digitizer within the instrument. The reconstruction of the vector field occurred subsequently on the ground during ground data processing. The sampling rate was once each 5.11 seconds with a range check occurring every 81.8 seconds on Explorer 35. The quantization uncertainty was $\pm 0.25\gamma$ for Explorer 33 and $\pm 0.094\gamma$ and $\pm 0.25\gamma$ for Explorer 35. For most of the data obtained by the Explorer 35 instrument, the range used was the more sensitive one. The bandpass of the instrument was 0-5 Hz, which permitted aliasing of signals above the Nyquist frequency of 0.1 Hz.

This has permitted the accurate measurement of sudden changes, in less than 5-10 seconds, such as shock waves in the interplanetary medium (Van Allen and Ness, 1967). A comparison of the two magnetometer results for the 15 February 1967 event is shown in Figure 25. Here the time delay and apparent slow rise time, ~25 seconds in the NASA Ames instrument are spurious instrument effects. The rapid rise time, < 5 seconds, is accurately measured by the NASA-GSFC instrument. Extending the spectral sensitivity beyond the folding frequency also permitted discovery of rapid fluctuations near the moon that otherwise would have gone undetected (Ness and Schatten, 1969). The sensitivity and accuracy of the sensors was checked daily by the addition of precisely known fields and flipping (90°) of the sensor set with a self-contained non-magnetic reorientation device. The zero levels of Explorer 33 remained constant within 0.5-1.0γ for the first 27 months of operation and those of Explorer 35 remained constant to within 0.5γ for the first 16 months of operation. The flipper device to reorient the triaxial sensor set by 90° is shown in Figure 26.

The results from these experiments have provided a mapping of the earth's bow shock and geomagnetic tail (Behannon, 1968), and contributed to the study of waves propagating upstream from the bow shock (Fairfield, 1969). The results from Explorer 35 have been analyzed to provide definitive studies of the solar wind interaction with the moon (Ness et al., 1967b; Ness et al., 1968 ; Ogilvie and Ness, 1969; Whang and Ness, 1970), the phenomenon of particle shadowing by the Moon (Van Allen and Ness, 1969) and the intrinsic magnetic properties of the moon (Behannon, 1969).

5.2.8 ATS Series

The Applications Technology Satellites have as their prime objectives the conduct of various engineering experiments at synchronous altitude. They have, in addition, included experiments to measure the physical characteristics of the space environment and under these auspices two magnetometer experiments have been carried.

The magnetic field experiment on ATS-1, launched 6 December 1966, used a multiple offset range, biaxial fluxgate magnetometer with the two sensors mounted at angles of 45° to the spacecraft spin axis (Barry and Snare, 1966). Because only two sensors were used, however, one complete spin (0.65 seconds) of the spacecraft was required to obtain the vector component transverse to the spin axis. An on-board analog data processor formed the sum and difference between the two outputs and this yielded information on the field parallel to the spin axis and transverse to the spin axis respectively. The data was transferred to a PFM telemetry system where the analog voltages, 0-5 V,

were used as input to a VCO. Subsequent ground data processing yielded a precision of $\pm 0.125\gamma$ in the quantization uncertainty for the lowest scale range of $\pm 50\gamma$. There were two more ranges possible, $\pm 100\gamma$, $\pm 200\gamma$, selected by an on-board system so as to avoid stepping through the cycle each spacecraft rotation but able to accommodate large, rapid variations which might occur.

In order to measure the steady field of approximately 125γ expected in orbit and the large ($\sim 100\gamma$) and possibly variable magnetic field of the spacecraft, an offset field generator of 64 levels of 25γ each was used to extend the range to $+925\gamma$ and -675γ. The bandpass of the instrument was basically 0-100 Hz, but was limited at the output to 0-2 Hz to avoid aliasing. The spin frequency was 1.6 Hz, rather close to the nominal ion cyclotron frequency. The sampling rates were 3.12 Hz and 6.24 Hz for the processed parallel and transverse data.

A sensitivity calibration was applied periodically to the instrument to validate the performance of the offset-field generator, the sum and difference amplifiers and the flight and ground data processing. Accurate measurements of the field component transverse to the spin axis were possible, as discussed in Section 3.3. The field component parallel to the spin axis, however, could not be accurately measured and so only variations of this quantity are determined.

The results from this experiment have been used to study the day-night asymmetry of the field at synchronous altitude due to the currents in the magnetopause (Cummings et al., 1968), fluctuations (Cummings and O'Sullivan, 1969) and the unique observation in January 1967

of the magnetopause as it was depressed to less than 6.6 R_E during a large geomagnetic storm (Cummings and Coleman, 1968).

The magnetic field experiment on ATS-5, launched 12 August 1969, is identical to the OGO-5 experiment of Heppner, with a triaxial fluxgate sensor using an offset field generator to extend the range to $\pm$4000γ with a bandpass of 0-120 Hz (Skillman, 1970). The data was transmitted both by a PCM telemetry system, in support of engineering requirements of the spacecraft, and by the PFM telemetry. The sampling rates of the vector magnetic field are 0.337 Hz and 0.196 Hz respectively. The results from the experiment have been compromised by a failure of the gravity gradient stabilization system. The large spacecraft magnetic field was partially compensated by several small permanent magnets.

5.2.9 Vela and OV Series

The magnetic field experiments on the Vela series of spacecraft, part of the USA program for the detection of nuclear weapons explosions in space, consisted of single axis induction magnetometers oriented transverse to the spin axis of the spacecraft. A total of four experiments have been performed in the two pairs of Velas, 2A and 2B and 3A and 3B, launched 17 July 1964 and 20 July 1965 respectively. The Vela 2 sensors' outputs were logarithmically extended over the dynamic range of 0-36γ while those of Vela 3 were linearly extended over the range 0-100γ. The data sampling rates were 1 Hz and 0.5 Hz respectively with the instrument bandpasses being 1.75-2.25 and 1.87-2.12 Hz. The spin rates of the spacecraft were $\sim$2.0 Hz.

The presence of a large and variable spacecraft generated field at the spin frequency of the satellites contaminated the data from the Vela 2 spacecraft. The results from the Vela 3 spacecraft have been used to study fluctuations of the magnetic field near the bow shock and the magnetosheath (Greenstadt et al., 1968).

The OV3-3 and OV5-5 spacecraft were launched as part of the US Air Force's Orbiting Vehicle program to utilize obsolete launch vehicles for placing spacecraft in orbit. A triaxial fluxgate magnetometer was included in the spin stabilized OV3-3 payload launched into a polar orbit on 4 August 1966 and provided data for all three axes with a quantization uncertainty of $\pm 30\gamma$ over the dynamic range of $\pm 60{,}000\gamma$. A biaxial fluxgate magnetometer was included in the spin stabilized OV5-5 payload launched 23 May 1969 into a moderately elliptical orbit and provided measurements over the range of $\pm 100\gamma$ with a quantization uncertainty of $\pm 1\gamma$. A boom of 1.5 meters placed the OV3-3 sensor in a position where the spacecraft field was 10γ while a mini-boom, as shown in Figure 27, placed the biaxial sensor of the OV5-5 spacecraft 0.15 meters from the body where the field was 5γ. No results have been reported from these experiments.

5.2.10 Explorers 34 and 41: IMP Series

The spin stabilized spacecraft Explorers 34 and 41 represented the last two of the initial IMP series with eccentric orbits. They have also been referenced as IMP-F and G prelaunch and IMP 4 and 5 postlaunch. Explorer 34 was launched on 24 May 1967 and performed successfully for two years until perturbations of the orbit forced

perigee to decay into the earth's atmosphere. Explorer 41 was launched 21 June 1969 and has operated successfully since then.

The magnetic field instrumentation was a triaxial fluxgate on both spacecraft. The sensor set on Explorer 34 was mounted with two axes transverse to the spin axis on one boom, diametrically opposite another boom which carried a flipper device to reorient the single sensor parallel to the spin axis by 180°. As in the previous IMP series, great care was exercised to reduce the magnetic field contamination of the spacecraft to a minimum. The placing of 3 sensors on two different booms was to attempt to balance the spacecraft, both statically and dynamically, with minimum "dead" weight. On Explorer 41, the three sensors were mounted in a triaxial set with a 90° flipper at the end of one boom. On each spacecraft a reorientation of the sensor occurred every 4 days to permit calibration of the zero levels of the individual axes. In addition a sensitivity calibration was effected once every 87.4 minutes by addition of a precisely known external field.

The dynamic range of the sensors on Explorer 34 was $\pm 32\gamma$ and $\pm 128\gamma$, switched by ground command, so that when the spacecraft was most distant from the earth the instrument operated in the lower range. When it approached closer to the earth it was placed in the higher range. The analog voltages of the three sensors were digitized by the spacecraft A/D converter with a precision of 0.5%, which corresponded to $\pm 0.16\gamma$ and $\pm 0.64\gamma$ quantization uncertainties. A vector sample was obtained every 2.56 seconds while the bandpass was

0-12 Hz. An onboard autocorrelation computer, see Section 4.2, permitted computing spectral estimates in the frequency band 0-3.125 Hz with a change of axis occurring every 40.96 seconds.

The experiment on Explorer 41 was similar to that on Explorer 34 except as noted previously in the mechanical configuration of the sensor set. The range switch was changed to an automatic in flight operation which checked the range selection once each 40.96 seconds. The ranges on Explorer 41 were $\pm 40\gamma$ and ± 200, which with the spacecraft analog-digital converter yielded precisions of $\pm 0.2\gamma$ and $\pm 1.0\gamma$. The autocorrelation computer was also changed so as to improve the precision of the readout of the accumulated lagged products. This consisted of reducing the rate at which these data were transmitted to once every 61.4 seconds.

The results of these experiments have been important in the study of low frequency waves generated at the bow shock and propagated upstream (Fairfield, 1969), the structure and physical parameters describing the Rankine-Hugoniot conditions in interplanetary shocks (Ogilvie and Burlaga, 1969) and the earth's bow shock (Burlaga and Ogilvie, 1968) and the simultaneous observation with other spacecraft of discontinuities in the interplanetary medium (Burlaga and Ness, 1969).

5.3 ESRO Instrumentation: HEOS-1

The European Space Research Organization launched the spin-stabilized Highly Eccentric Orbiting Spacecraft, HEOS-1, on 5 December 1968 with scientific objectives similar to the USA IMP series. The magnetic field experiment consisted of a triaxial fluxgate sensor mounted 2.0 meters from the spacecraft and a monoaxial fluxgate sensor mounted co-linear with spin axis sensor of the triaxial set but in board by

1.0 meters. This single axis device was used to monitor the variation of the spacecraft field and to extrapolate it to the triaxial sensor. There is no unique way to determine the zero-level stability of the triaxial sensor parallel to the spin axis and only the consistency of the data can yield an estimate. The zero level accuracy is estimated to be 0.5γ while it is $\sim$0.1γ for the 2 transverse axes.

A single linear range of $\pm$64γ with the 8 bit digitizer of the instrument provided a resolution of $\pm$0.25γ. The sampling interval of the vector field was not uniform in time, but ranged between once every 48 and 54 seconds. A complete measurement was made and transmitted during each telemetry frame (48 seconds in length) but the sampling time was determined by the relative phase of the sensor axes with respect to the satellite sun line. Each successive measurement was performed at a time which corresponded to a +90° azimuthal phase shift in the sensor position with respect to the previous sample. Thus successive measurements in four frames were made at times corresponding to the phase of the sensor position given by ϕ_{si} = 0°, 90°, 180°, 270° and 360°. Since the spin period of the spacecraft was 6 seconds, this meant that the sampling times vary from 48-0 = 48 to 48 + 6.0 = 54 seconds. The passband was 0-5 Hz so aliasing occurred except when in the memory mode.

The instrument also included a 16,384 bit memory which could store 2048 words, which correspond to either 682 three component vector or 2048 Z_p component measurements. The sampling rate for a vector measurement is once every 1/4 spin period or 1.5 seconds so that 17 minutes of data could be stored. The Z_p component sampling rate was

once every 180 milliseconds so that 7 minutes of data was stored. The memory system was continually read out in the real time telemetry but at a very low rate which required 5.5 hours for a complete transmission. The memory system was actuated by either ground command, after which readout was automatic and automatic cycling between readin and readout followed or by instrument logic which used the Z_p component sensor to determine if the field rate of change exceeded one of two selectable threshold levels. At such times, the subsequent data were stored in the memory for later transmission determined by ground command. The two levels selected for HEOS-1 were 25γ/second and 10γ/second.

The results of this experiment are being used to study the interplanetary magnetic field and the bow shock-magnetosheath-geomagnetic tail when the range of the instrument is not exceeded. The data are also being correlated with transient events in the interplanetary medium (Hedgecock, 1970).

6.0 Lunar, Planetary and Interplanetary Magnetometers

The study of the magnetic fields in interplanetary space has been accomplished not only from earth orbiting spacecraft but also from those missions to the planets and the moon as well as those few deep interplanetary space probes expressly developed for such purposes. The placing of a spacecraft in orbit about the moon or another planet represents an opportunity identical to that of an earth orbiting spacecraft to study three major phenomenon:

1) Interplanetary Medium,

2) Solar wind interaction with planet (or moon)

3) Intrinsic planetary (or lunar) magnetic field

The following sections discuss those impacting, fly-by, orbiting and purely interplanetary missions which have provided magnetic field measurements relevant to these three problems.

6.1 USSR Instrumentation

The USSR launched the first spacecraft to study the magnetic field of the moon with Luna 1 which flew by the moon at 7000 km on 3 January 1959 and Luna 2 which impacted the lunar surface on 3 September 1959.

6.1.1 Luna Series

The space probe Luna 1 was launched on 2 January 1959 carrying a triaxial fluxgate magnetometer comprised of three separate monoaxial instruments using separate drive frequencies and power supplies. The dynamic range of the sensors was $\pm 3000\gamma$, which with the traditional two channel, 5 bit equivalent digitization of the telemetry system and

the 600γ/volt sensitivity led to a quantization uncertainty of ±47γ. No results were reported by the lunar flyby portion of the trajectory and only the near earth results have been discussed (Dolginov and Pushkov, 1959).

The space probe Luna 2 was launched on 12 September 1959 and instrumented with a three component fluxgate magnetometer similar to that used on Luna 1 but with the dynamic range reduced by a factor of 4 to ±750γ so that the quantization uncertainty was ±12γ. The spacecraft spin period was 840 seconds about the major axis and there was a precession transverse to this with a period of 86 seconds. The sampling rate of the instrument was approximately once per minute.

According to Dolginov et al (1960) the errors associated with the experiments zero levels and spacecraft fields were such that the accuracy was approximately 50-100γ. The spacecraft gave similar results to those of Luna 1 in the earth's radiation belts and upon impact placed an upper limit on the lunar magnetic field at the surface of 100γ (Dolginov et al., 1961).

The Luna 10 spacecraft was launched into a lunar orbit on 2 April 1966 and measured the magnetic field in the vicinity of the moon from 220 km to 1100 km intermittently for 2 months. The instrumentation consisted of a triaxial fluxgate magnetometer, as shown in Figure 28, with a dynamic range of ±50γ. A comprehensive description of the instrument is given by Afanas'ev et al (1968). The usual two channel, 5 bit digitization of these analog outputs by the telemetry system yielded measurements with a precision of ±1.5γ. No independent

attitude determination system was employed so only the magnitude of the magnetic field, and the components parallel and perpendicular to the spin axis were determined.

The magnetometer sensor was located at the end of a boom 1.5 meters from the spacecraft surface. The sampling rate of the vector magnetic field was once every 128 seconds. The accuracy of the measurements was estimated from in-flight data to be 9γ for the component parallel to the spin axis, 2.5γ for the component perpendicular to the spin axis, yielding a residual error of 10γ for the magnitude. The data and their interpretation relative to the moon and the solar wind interaction with it have been given in Zhuzgov et al.,(1966), Dolginov et al., (1966, 1967) and Ness (1967a).

6.1.2 Venera Series

The spacecraft Venera 1 was launched on 12 February 1961 carrying a triaxial fluxgate magnetometer comprised of three separate monoaxial instruments with their axes mounted orthogonal to each other. The sensor assembly was placed at the end of a 2 meter boom. The dynamic range of each axis was ±50γ and the quantization uncertainty was ±1.5γ. Only limited results were obtained during a short transmission while enroute to the planet and no flyby results have been presented (Dolginov et al., 1962).

The spacecraft Venera 4 was launched on 12 June 1967 and the bus portion of the system was instrumented with a triaxial fluxgate magnetometer identical to that flown on Luna 10, with a dynamic range of ±50γ and a quantization uncertainty of ±1.5γ. The instrument sensor

was mounted on a boom 2 meters long. The spacecraft bus penetrated the Venusian atmosphere on 18 October 1967 and returned useful measurements on the nature of the interplanetary magnetic field in the vicinity of Venus and the solar wind interaction with the planet (Dolginov et al., 1968). Estimates of the accuracy of the measurements of 5γ were given by the investigators in their original publication. These were obtained from data during a short period when the spacecraft was rolled about the spacecraft sun line. The difficulty of accurately determining the zero levels of the three sensors is illustrated in the comparison of simultaneous data obtained by Venera 4 with that obtained by the USA space probe Mariner 5 (Dolginov et al., 1969a).

6.2 USA Instrumentation

There have been several series of highly successful USA spacecraft missions to the planets, the moon and to interplanetary space. The following sections discuss these various programs in the order of their performance chronologically and according to mission objectives. Unlike the USSR program there have been several groups which have participated in these studies and contributed to our understanding of the present state of magnetic fields in space.

6.2.1 Lunar Experiments

In addition to the early attempts in the Pioneer program to study the lunar magnetic field, there were two spacecraft in the Ranger program which carried Rubidium vapor magnetometers. These latter two missions were not successful in returning any data due to vehicle failures. The first successful experiments to study the lunar magnetic

field were those conducted on the Explorer 35 spacecraft launched into lunar orbit on July 19, 1967. These instruments and their results have already been discussed in Section 5.2.8.

The only other USA experiment has been part of the Apollo Lunar Scientific Experiment Package (ALSEP) which was set up by astronauts on the lunar surface on 18 November 1969 during the activities of the Apollo 12 mission. This triaxial fluxgate magnetometer is the first such instrument to be operated on the lunar surface.

The ALSEP-1 triaxial fluxgate magnetometer is comprised of three sensors separated from each other by 0.8 meters mounted on three separate booms 1 meter long above the lunar surface. A reorientation of the three sensors is possible in a mechanically gimballed system so that each one can be separately directed along any one of the three orthogonal axes formed by the sensor set. This permitted not only a determination of the zero levels of the sensors but also a measurement of the gradient of the magnetic field within the sensitivity limitations, which corresponds to 0.4γ/meter.

The dynamic ranges of the sensors are: ±100γ, ±200γ and ±400γ which are changed by ground command. The instrument included a 10 bit digitizer which yields a quantization uncertainty of ±0.1γ, ±0.2γ and ±0.4γ. The sampling rate of the instrument is 3.0 Hz and the instrument includes a digital filter to limit the data output bandpass to 1.5 Hz. There are no published results on this experiment.

6.2.2 Mariner Series

The Mariner series of fixed attitude spacecraft have been used to study the magnetic fields of the planets Venus and Mars and that of the interplanetary medium between 0.7 and 1.5 AU. Two types of magnetometers have been used in three successful missions. A triaxial fluxgate magnetometer was used on the Mariner II probe to Venus, which was launched on 27 October 1962 and flew past the planet, the closest approach distance being 40000 km (6.6) R_V, on 14 December 1962. A helium vapor magnetometer was employed in the Mariner IV spacecraft launched 28 November 1964 which passed by Mars at 13000 km (3.8 R_M) on 15 July 1965. A similar instrument was also flown on the Mariner V probe to Venus launched on 14 June 1967 which passed by the planet at 4000 km (0.6 R_V), on 19 October 1967.

The magnetometers in all of the Mariner programs were mounted within the spacecraft assembly itself with no special booms provided. There were no efforts made to reduce magnetic field contamination from the spacecraft in the Mariner II program although the situation improved considerably in the Mariner V program with demagnetizing of the spacecraft being conducted. Since these spacecraft are fixed attitude, the determination of the zero level accuracy and the contribution of spacecraft fields has been a continuing problem. Recently Davis et al. (1969) have suggested a technique for determining the effective zero level of the sensor from a self-consistency study of the observed discontinuities in the interplanetary medium.

The triaxial fluxgate on Mariner II was designed with two ranges, $\pm 80\gamma$ and $\pm 350\gamma$. The spacecraft digitizer of 8 bits transformed the

analog signal from 1-6 volts into a binary representation with a quantization uncertainty of $\pm 0.35\gamma$ and $\pm 1.37\gamma$. The spacecraft fields were so large at the sensor position, $\sim 100\gamma$ that it was necessary to operate the instrument in the less sensitive range for the major fraction of the flight. A comprehensive description of the instrument, the large and variable spacecraft magnetic field and data reduction procedures has been given in Coleman (1966). All published Mariner 2 data, except during the Venus flyby, was based on the low range data.

The measurementof a vector magnetic field was accomplished by the sequential sampling of the three axes in 3.84 seconds, with 1.92 seconds between each component. Thus an instantaneous vector measurement was not made and vector aliasing may have occurred. The individual component measurements were performed once every 36.96 seconds during the cruise mode of the flight data and every 20.16 seconds during the planetary encounter phase of the flight. The passband of the instrument was 0-2 Hz, so component aliasing was also possible.

A study of the magnetic field observations near Venus has been given by Smith et al. (1965a) indicating no penetration of a shock or magnetosheath. The first study of an interplanetary shock wave was conducted using Mariner II data by Sonett et al. (1962). Studies of the fluctuations of the interplanetary magnetic field have also been conducted by Coleman (1966).

The instrument on the Mariner IV spacecraft was the first space flight of a vector low-field Helium magnetometer. The dynamic range of the sensor was $\pm 360\gamma$ which with the 10 bit digitizer of the spacecraft yielded a quantization uncertainty of $\pm 0.36\gamma$. The sampling

rate of the instrument was not uniform in time, with 4 measurements made every 12.6 seconds during the first 5 weeks of the mission and every 50.4 seconds for the remainder. For the fastest sampling rate the successive vector measurements were separated in time by 1.5, 0.9, 2.4 and 7.8 seconds. For the lower rate these separations increased by a factor of 4 to be 6.0, 3.6, 9.6 and 30.2 seconds for the major fraction of the mission lifetime. Thus these data were mulitirate sampled and this may have affected the spectral estimates of the observed fluctuations. The passband of the instrument was 0-1 Hz so component aliasing was also possible.

The results from these measurements have been used to study the fluctuations and discontinuities in the solar wind (Siscoe et al. 1968) and the radial gradient and sector structure of the interplanetary magnetic field (Coleman et al., 1967 ; 1969). The flyby results have been interpreted by Smith et al. (1965b) and Dryer and Faye-Peterson (1966).

The instrument included in the Mariner V spacecraft was a similar device to that used in Mariner IV but with a reduced dynamic range of $\pm 204\gamma$. Thus the spacecraft digitizer yielded a quantization uncertainty of $\pm 0.2\gamma$. A comprehensive description of the instrument has been given by Connor (1968). There was an effort to reduce magnetic fields of the spacecraft by deperming it, and this led to a residual field of approximately 8γ, estimated both from terrestrial measurements and two axis estimates of the spacecraft field obtained during a short period of rolling of the spacecraft about the spacecraft-sun line shortly after launch. The basic method of determining the spacecraft field was

the technique described in Davis et al. (1968). The telemetry sampling rates were similar to those of Mariner V with non-uniform spacing of the successive vector samples at intervals of 1.8, 3.6 and 7.2 seconds.

The results from these measurements have been used to study the nature of the fluctuations of the interplanetary magnetic field (Belcher et al., 1969) and the fluctuations of the interplanetary magnetic field and the solar wind interaction with Venus (Bridge et al., 1967).

6.2.3 Pioneer Series

The follow-on series of Pioneer spin-stabilized spacecraft were designed to provide data on the interplanetary medium from heliocentric orbits between 0.8 and 1.2 AU. Of the 5 launches since 1965, 4 spacecraft have been successfully orbited with slightly differing orbital parameters and all carrying fluxgate magnetometers. Stringent controls on the fabrication and design of the spacecraft and its instrumentation were exercised in order to reduce the spacecraft magnetic fields at the sensor position to less than 0.5γ. The sensors were located at the extremity of booms 1.6 meters in length, and 2.1 meters from the center of the spacecraft. The spacecraft were all oriented with their spin axes normal to the ecliptic for communication, power and thermal considerations and all were rotating at approximately the same rate of 1 Hz.

The experiments on Pioneer 6, 7 and 8 were nearly identical and employed a single axis sensor oriented at an angle of $54^{\circ}\ 45'$ to the spin axis. These instruments have been described comprehensively by Scearce et al., (1968). An on-board sampling system within the

instrument used the spacecraft sun-pulse to provide a three times spin rate sampling pulse. Thus with the special orientation of the sensor, three successive measurements at 120° during the rotation of the spacecraft formed an orthogonal set of data from which the vector field was determined. The time required for a complete sample is 0.67 seconds so that these data are sensitive to vector aliasing. The pass band was 0-5 Hz so component aliasing was also possible.

An instrument digitizer of 8 bits quantized the analog voltage of 0-5 volts with an uncertainty that changed with spacecraft as the ranges were changed. For Pioneer 6, the single range was $\pm 64\gamma$, for Pioneer 7 it was $\pm 32\gamma$ and for Pioneer 8 a dual range of $\pm 32\gamma$ and $\pm 96\gamma$ was controlled by an on-board automatic range switch to maintain the sensor in its optimum range. The resultant quantization uncertainties were $\pm 0.25\gamma$, $\pm 0.125\gamma$ and $\pm 0.125\gamma$ and $\pm 0.375\gamma$ respectively.

A mechanical flipper with a finite number of 180° reversals was used on these spacecraft, the first such device flown in space, to calibrate the zero levels of fluxgate magnetometers. These units, combined with the small spacecraft field of less than 0.5γ indicated from in-flight data an uncertainty in the zero levels of $\pm 0.25\gamma$, $\pm 0.35\gamma$ and $\pm 0.15\gamma$ respectively.

The data sampling was of necessity synchronous with the spin rate of the spacecraft and thus not with the telemetry readout. A complete vector measurement was stored in a memory buffer for subsequent readout and additional data sampling inhibited until this stored data was transmitted. Since the spacecraft was capable of

operating in several modes, real time (RT) and long time memory storage, and at 5 bit rates, 512, 256, 64, 16 and 8 bit per second, the sampling rate of the instrument's stored buffer varied over a factor of 64. At the higher bit rates a sample was transmitted on average every 1.5 seconds while for the lower bit rates of 16 and 8 BPS, the interval between successive readouts was 7 and 14 seconds respectively.

The use of an on-board computer to adapt to these variable bit rates provided separate component averages for these modes and bit rates (see Section 4.2). When the spacecraft was in RT at 16 and 8 BPS., a total of 4 and 8 successive measurements were averaged by this computer. When in the data storage mode, the instrument used 64, 128 or 256 successive measurements to compute an average. This averaging of the components permitted obtaining a statistically better estimate of the vector magnetic field than if only a single value were transmitted.

The measurements from these three spacecraft have provided data for detailed studies of the interplanetary magnetic field and its fluctuations (Burlaga and Ness, 1968 ; Ness, 1969 ; Sari and Ness, 1968); the discontinuity surfaces imbedded within the magnetized medium (McCracken and Ness, 1966; Burlaga, 1968; 1969) and the collimation of cosmic rays (McCracken, Rao and Ness, 1967). Pioneer 7 data, at a distance of 1000 R_E downstream, from the earth, reported observations of geomagnetic tail related effects (Ness et al., 1967a ; Fairfield, 1968). Pioneer 8, at 500 R_E as it crossed the tail region, also reported tail related phenomenon (Mariani and Ness, 1969).

Simultaneous measurements of the plasma-magnetic field characteristics across the neutral sheet were also studied on Pioneer 7 (Lazarus et al, 1968).

The Pioneer 9 spacecraft, launched on 8 November 1968, included a triaxial fluxgate magnetometer and a 90° flipper at the end of a boom similar to that of the Pioneers 6, 7 and 8. The instrumentation included an on-board spin demodulation system similar to that employed on Explorers 33 and 35 but using digital computations rather than analog. In addition, a digital filter was incorporated to reduce the data pass band so as to strictly observe the Nyquist criteria for uniquely reconstructing the field variations in between successive samples. The sampling rate of the instrument for the 5 bit rates are: 3.5, 1.8, 0.44, 0.11 and 0.055 Hz.

The instrument has a single dynamic range of $\pm$200γ which with the instrument 10 bit digitizer leads to quantization uncertainties of $\pm$0.20γ. No results have been reported from this experiment.

7.0 Future Programs

The investigation of magnetic fields in space will continue in the early 70's, although as indicated in the introduction at a substantially reduced rate. Those ESRO, German, Italian and USA satellites for which magnetometers have already been selected (or are anticipated to be) for launch during the period 1970-1975 are shown in Table III. In keeping with the USSR past policy of not providing advance information on satellite launch schedules and instrumentation complements, no information is available about the future missions of the Soviet Union. A block diagram of a space qualified Cs^{133} self-oscillating magnetometer is shown in Figure 29.

- There are several new scientific missions included in the list which present unique instrumentation requirements. The Pioneer F and G interplanetary spacecraft, using a new spacecraft design and RTG power system, will be launched into a deep space trajectory to 5 AU and hopefully to intersect the magnetosphere of Jupiter after a flight time of several years. The instrument will be called upon to operate over an extreme range of field strengths. The very low values of the interplanetary field being approximately 0.8γ at 5 AU. In order to make accurate measurements of the direction of the field, a sensor with a resolution of at least $\pm 0.07\gamma$ is necessary to provide a sensitivity of $\pm 5^{o}$. For the Jovian field, assuming a flyby trajectory at 3 planetary radii, requires a range up to 1-5 Gauss meaning that the instrument must operate over 6 to 7 decades. Such instruments have not yet been built for space flight, and clearly present a technical challenge to the investigators. For subsequent missions to Jupiter, and especially

in the case of an orbiter, a similar wide range instrument with high reliability to operate successfully over long time intervals will be required. This increased lifetime requirement is due to the long flight time to the planet (approximately two years) and the long Jovian orbit periods, which are approximately several months for moderately eccentric orbits.

The German-USA solar probe HELIOS will pass within 0.3 AU of the sun and the instrumentation will be required to provide accurate measurements for field strengths up to several hundred γ. This will not present a problem for the investigators although the temperature control of the sensor will be a critical factor in the operation of the sensor.

The ESRO GEOS, Italian SIRIO and USA ATS F and G spacecraft are all designed to operate in synchronous (i.e., 24 hour) orbit and monitor the geomagnetosphere at different longitudes. No special requirements are envisaged beyond the present state of the art for these instruments. This is also true for the continuing IMP series, H and J being placed into nominally circular orbits at 30-40 R_E while IMP-I will be placed into the more traditional highly eccentric orbit with apogee near 40 R_E. The HEOS-A2 spacecraft will also be placed into a highly eccentric orbit but with apogee within 30^o of the north pole to explore the neutral points and nearby regions of the magnetosphere. The first Small Standardized Satellite, S^3, will be placed into a moderately eccentric earth orbit at low inclination to investigate the dynamics of the inner magnetosphere.

Additional magnetometers shall be placed on the surface of the moon and in orbit although the exact number is unknown it may be more than the several shown in Table III. There are no plans to study further the magnetic field of Mars in the USA 1971 Mariner Orbiters or the 1975 Viking Orbiters or landers. The field of Mercury and the continued study of the solar wind interaction with Venus will be studied from a single flyby trajectory of a Mariner class spacecraft.

A universal requirement of all these future missions will be for a much longer life than the usual 6 months which was needed in the decade of the 60's. Also the increased sensitivities of the instruments, the higher telemetry rates available and the need to investigate more quantitatively the rapid fluctuations of the magnetic field will demand that these spacecraft be designed and constructed to be magnetically cleaner than many of their predecessors. Since the total spacecraft weight is also increased this implies that in some of these programs, such as Pioneer F and G, extremely long booms ($\geq$ 10 m) shall be required to eliminate the effects of spacecraft generated fields. Also the experimenters shall be called upon to process, analyze and interpret much larger quantities of data than many of them have been able to, or have even attempted to, handle in the past. The essential physics of many studies will require the close collaboration of investigators on different spacecraft and with different instruments.

Continued efforts to reduce the power, weight and size of the basic magnetometers will be important as the use of special purpose computers to process the data or change the operational characteristics

of the instrument demand. The use of ground commands for deep space missions like Pioneer F and G which introduce round trip travel times of 1 hour or more for the data status-command link will require the use of sophisticated on-board logic to maintain an optimumly efficient instrument operating status. The same is true of instrumentation used in the USA Mariner Mercury-Venus flyby mission, in which the total time for crossing the solar wind wake region of Mercury is only 8-12 minutes while the round trip data status-command link time will be approximately 15 minutes. Careful instrument design will be essential to ascertain the best strategy to be employed in performing such measurements.

8.0 Acknowledgements

I appreciate the assistance given in preparing this review by several of the principal investigators listed regarding the unpublished characteristics of their instruments and performance since in many instances there exists no published description of the operation of the experiments. I appreciate the hospitality of the staff of the CNR-University of Rome, Laboratory for Space Plasmas in the preparation of this manuscript.

9.0 References

Alfanas'ev, Yu. V., V. P. Lyulik and G. D. Alekseeva, Magnetometer Instruments of Luna 10 and Venera 4 Space Stations, Cosmic Research, 6, 650-657, 1968.

Albus, J. S. and D. H. Schaefer, Satellite Attitude Determination: Digital Sensing and On-board Processing, IEEE Trans. Space Elec. Telem., SET-9, 71-77, 1963.

Aleksanyan, L. M., Ye. G. Yeroshenko, L. N. Zhuzgov and U. V. Fastovskiy, Magnetometric Equipment Aboard the "Electron 2" Space Station, Cosmic Research, 4, 278-284, 1966.

Axford, W. I., Observations of the Interplanetary Plasma, Space Sci. Revs., 8, 331-365, 1968.

Barry, J. D. and R. C. Snare, A Fluxgate Magnetometer for the Applications Technology Satellite, IEEE Trans. Nuclear Science, NS-13, 326-331, 1966.

Bauernschub, Jr., J. P., Nonmagnetic, Explosive Actuated Indexing Device, National Aeronautics and Space Administration, G-784, 1966.

Behannon, K. W., Mapping of the Earth's Bow Shock and Magnetic Tail by Explorer 33, J. Geophys. Res., 73, 907-930, 1968.

Behannon, K. W., Intrinsic Magnetic Properties of the Lunar Body, J. Geophys. Res., 73, 7257-7268, 1968.

Belcher, J. W., L. Davis, Jr., and E. J. Smith, Large Amplitude Alfven Waves in the Interplanetary Medium, J. Geophys. Res., 74, 2302-2308, 1969.

Beletskii, V. V. and Yu. V. Zonov, Rotation and Orientation of the Third Soviet Satellite, Iskusstvennyye Sputniki Zemli, 7, 32-55 (Artificial Earth Satellites, 29-52), 1961.

Bloch, F., Nuclear Induction, Phys. Rev., 70, 460-474, 1946.

Bloom, A. L., Principles of Operation of the Rubidium Vapor Magnetometer, Appl. Optics, 1, 61-67, 1962.

Bonetti, A., H. S. Bridge, A. J. Lazarus, B. Rossi and F. Scherb, Explorer 10 Plasma Measurements, J. Geophys. Res., 68, 4017-4063, 1963.

Bozorth, R. M. Ferromagnetism, D.Van Nostrand, New York 1951.

Bracken, P. A., L.R. Davis and R. W. Janetzke, A Method Used for the Determination of the Explorer XXVI Spin Axis Position, NASA-GSFC preprint X-612-69-446, 1969.

Bridge, H. S., A. J. Lazarus, C. W. Snyder, E. J. Smith, L. Davis, Jr., P. J. Coleman, Jr., and D. E. Jones, Mariner V: Plasma and Magnetic Fields Observed Near Venus, Science, 158, 1669-1673, 1967.

Burlaga, L. F., Micro-Scale Structures in the Interplanetary Medium, Solar Physics, 4, 67-92, 1968.

Burlaga, L. F., Directional Discontinuities in the Interplanetary Magnetic Field, Solar Physics, 7, 54-71, 1969.

Burlaga, L. F., and N. F. Ness, Macro and Micro Structure of the Interplanetary Magnetic Field, Canad. J. Phys. 46, S929-295, 1968.

Burlaga, L. F. and N. F. Ness, Tangential Discontinuities in the Solar Wind, Solar Physics, 9, 467-477, 1969.

Burlaga, L. F. and K. W. Ogilvie, Observations of the Magnetosheath-Solar Wind Boundary, J. Geophys. Res., 73, 6167-6178, 1968.

Cahill, L. J., Preliminary Results of Magnetic Field Measurements in the Tail of the Geomagnetic Cavity, IG Bull. 79, Trans. AGU, 45, 231-235, 1964a.

Cahill, L. J., The Geomagnetic Field, Space Physics, ed., by D. P. LeGalley and A. Rosen, pp. 301-349, 1964b.

Cahill, L. J., Inflation of the Magnetosphere Near 8 R_E in the Dark Hemisphere, Space Research 6, 662-678, 1966.

Cahill, L. J., Rocket Results, Trans. AGU, 48, 555-564, 1967.

Cahill, L. J. and P. G. Amazeen, The Boundary of the Geomagnetic Field, J. Geophys. Res., 68, 1835-1843, 1963.

Cahill, L. J. and V. L. Patel, The Boundary of the Geomagnetic Field, August to November 1961, Planet. and Space Sci., 15, 997-1033, 1967.

Cain, J. C. and S. Hendricks, Comments on the Vanguard 3 Magnetic Field Data and Analysis, J. Geophys. Res., 69, 4187-4188, 1964.

Cain, J. C. S. J. Hendricks, R. A. Langel and W. V. Hudson, A Proposed Model for the International Geomagnetic Reference Field-1965, J. Geomagnet. and Geoelec., 19, 335-355, 1967a.

Cain, J. C., R. A. Langel and S. J. Hendricks, First Magnetic Field Results from the OGO-2 Satellite, Space Research, VII, 1466-1475, 1967.

Cain, J. C., R. A. Langel and S. J. Hendricks, Magnetic Chart of the Brazilian Anomaly- A Verification, Geomagnetism and Aeronomy, 8, 84-87, 1968.

Cain, J. C., I. R. Shapiro, J. D. Stolarik and J. P. Heppner, A Note on Whistlers Observed Above the Ionosphere, J. Geophys. Res., 66, 2677-2680, 1961.

Cain, J. C., I. R. Shapiro, J. D. Stolarik and J. P. Heppner, Vanguard 3 Magnetic Field Observations, J. Geophys. Res., 67, 5055-5069, 1962.

Cantarano, S. and F. Mariani, Magnetic Field Measurements in Interplanetary Space, ESRO Scientific Report SR-4, 1966.

Cantarano, S. and G. V. Pallottino, A Correlation Technique for Power Spectrum Measurements of the Interplanetary Magnetic Field, Internal Report 195, Istituo di Fiscia G. Marconi, University of Rome, 1968.

Cloutier, P. A. and R. C. Haymes, Vector Measurement of the Midlatitude S_q Ionospheric Current System, J. Geophys. Res., 73, 1771-1787, 1968.

Colburn, D. S., R. G. Currie, J. D. Mihalov and C. P. Sonett, Diamagnetic Solar Wind Cavity Discovered Behind the Moon, Science, 158, 1040-1043, 1967.

Coleman, P. J., The Mariner 2 Magnetometer Experiment and Associated Data Reduction Procedures, UCLA-IGPP Publication No. 447, 1965.

Coleman, P. J., Variations in the Interplanetary Field: Mariner 2, 1.Observed Properties, J. Geophys. Res., 71, 5509-5531, 1966.

Coleman, P. J., L. Davis, E. J. Smith and D. E. Jones, The Polarity Pattern of the Interplanetary Magnetic Field During Solar Rotations 1798-1808, J. Geophys. Res., 72, 1637-1643, 1967.

Coleman, P. J., Jr., L. Davis, Jr., and C. P. Sonett, Steady Component of the Interplanetary Magnetic Field: Pioneer V. Phys. Rev. Letters, 5, 43-46, 1960b.

Coleman, P. J., Jr., E. J. Smith, L. Davis, Jr., and D. E. Jones, The Radial Dependence of the Interplanetary Magnetic Field: 1.0-15 AU, J. Geophys Res., 74, 2826-2850, 1969.

Connor, B. V., The Mariner V Magnetometer Experiment, IEEE Trans. Magnetics, MAG-4, 391-397, 1968.

Cummings, W. D., J. N. Barfield and P. J. Coleman, Jr., Magnetosphere Substorms Observed at the Synchronous Oribt, J. Geophys. Res., 73, 6687-6698, 1968.

Cummings, W. D. and P. J. Coleman, Jr., Magnetic Fields in the Magnetopause and Vicinity at Synchronous Altitudes, J. Geophys. Res., 73, 5699-5718, 1968.

Cummings, W. D., and R. J. O'Sullivan, Standing Alfven Waves in the Magnetosphere, J. Geophys. Res., 74, 778-793, 1969.

Davis, L., Jr., E. J. Smith and J. Belcher, The In-flight Determination of Spacecraft Magnetic Field Zeros, Trans. AGU, 49, 257, 1968.

Dehmelt, H. G., Modulation of a Light Beam by Precessing Absorbing Atoms, Phys. Rev., 105, 1924-1925, 1957.

Dessler, A. J., Solar Wind and Interplanetary Magnetic Field, Reviews of Geophysics, 5, 1-42, 1967.

Dolginov, Sh. Sh., A. N. Koslov and M. M. Chinchevoj, Magnetometers for Space Measurements (preprint). To be published in Proceedings of Paris Conference 1969b.

Dolginov, Sh. Sh., and N. V. Pushkov, Results of Measurements of Magnetic Field of the Earth with Cosmic Rockets, Doklady Akademii Nauk SSSR, 129, 77-80, 1959.

Dolginov, Sh. Sh., Ye. G. Yeroshenko and L. Davis, Jr., On the Nature of the Magnetic Field Near Venus, Kosmicheskiye Issledovaniya, 7, 747-752, 1969a.

Dolginov, Sh. Sh., Ye. G. Yeroshenko and L. N. Zhuzgov, A Survey of the Earth's Magnetosphere in the Region of the Radiation Belt (3 R_E-6 R_E) in February-April 1964 on the Electron 2 Satellite, Space Research, VI, 790-809, 1966.

Dolginov, Sh. Sh., Ye. G. Yeroshenko and L. N. Zhuzgov, Magnetic Field Investgiation with Interplanetary Station Venera 4, Cosmic Research, 6, 469-480, 1968.

Dolginov, Sh. Sh., Ye. G. Yeroshenko, L. N. Zhuzgov and N. V. Pushkov, Investigation of the Magnetic Field of the Moon, Geomagnetizm i Aeronomiya, 1, 21-29, 1961.

Dolginov, Sh. Sh., Ye. G. Yeroshenko, L. N. Zhuzgov and N. V. Pushkov, Magnetic Measurements by the Venus Automatic Interplanetary Station, Geomagnetizm i Aeronomiya, 2, 38-40 (Geomagnetism and Aeronomy, pp. 28-30), 1962.

Dolginov, Sh. Sh., Ye. G. Yeroshenko, L. N. Zhuzgov and N. V. Pushkov, Magnetic Field Measurements in the Vicinity of the Moon on the Artificial Satellite Luna-10, Doklady Akademii Nauk SSSR, 3, 574-577, 1966.

Dolginov, Sh. Sh., Ye. G. Yeroshenko, L. N. Zhuzgov, N. V. Pushkov and L. O. Tyurmina, Magnetic Measurements with the Second Cosmic Rocket, Iskusstvennyye Sputniki Zemli, 5, 16-23 (Artificial Earth Satellites, 490-502), 1960.

Dolginov, Sh. Sh., Ye. G. Yeroshenko, L. N. Zhuzgov and I. A. Zhulin, Possible Interpretation of the Results of Measurements on the Lunar Orbiter Luna 10, Geomagnetism and Aeronomy, 7, 436-451, 1967.

Dolginov, Sh. Sh., L. N. Zhuzgov and N. V. Pushkov, Preliminary Report on Geomagnetic Measurements Carried Out from the Third Soviet Artificial Earth Satellite, Artificial Earth Satellites, 2, 63-67, 1959.

Dolginov, Sh. Sh., L. N. Zhuzgov, N. V. Pushkov, L. O. Tyurmina, and I. V. Fryazinov, Some Results of Measuring the Constant Magnetic Field of the Earth with the Third Artificial Sputnik of the Earth Above the Territory of the USSR, Geomagnetizm i Aeronomiya, 1061-1075, 877-889, 1962.

Dolginov, Sh. Sh., L. N. Zhuzgov and V. A. Selyutin, Magnetometers in the Third Soviet Earth Satellite, Iskusstvennyye Sputniki Zemli, 4, 135-160 (Artificial Earth Satellites, 358-396), 1960.

Dryer, M. and G. R. Heckman, Application of the Hypersonic Analogue to the Standing Shock of Mars, Solar Physics, 2, 1112, 1967.

Fairfield, D. H., Ordered Magnetic Field of the Magnetosheath, J. Geophys. Res., 72, 5865-5877, 1967.

Fairfield, D. H., Simultaneous Measurements on Three Satellites and the Observation of the Geomagnetic Tail at 1000 R_E, J. Geophys. Res., 73, 6179-6187, 1968.

Fairfield, D. H., Bow Shock Associated Waves Observed in the Far Upstream Interplanetary Medium, J. Geophys. Res., 74, 3541-3553, 1969.

Fairfield, D. H. and N. F. Ness, Magnetic Field Measurements with the IMP-2 Satellite, J. Geophys. Res., 72, 2379-2403, 1967.

Farthing, W. H. and W. C. Folz, Rubidium Vapor Magnetometer for Near Earth Orbiting Spacecraft, Revs. Sci. Inst., 38, 1023-1030, 1967.

Fiel, O. G., The Magnetic Test Facilities at ESTEC, ELDO/ESRO Tech. Rev., 1, 59-84, 1969.

Frandsen, A. M. A., R. E. Holzer and E. J. Smith, OGO Search Coil Magnetometer Experiments, IEEE Trans. Geoscience Elec., GE-7, 61-74, 1969.

Frazier, N. A., Chapter 8, pp. 161-180, In Handbook of Soviet Space Science Research, ed. by G. E. Wukelic, Gordon and Breach, N. Y., 1968.

Fredericks, R. W., E. W. Greenstadt and C. P. Sonett, Magnetodynamically Induced Ambiguity in the Data from Tilted, Spinning Fluxgate Magnetometers: Possible Application to IMP-1, J. Geophys. Res., 72, 367-382, 1967.

Fromm, W. E., The Magnetic Airborne Detector, In Adv. in Electronics, edited by L. Marton, Academic Press, N. Y., pp. 257-299, 1952.

Geyger, W. A., Non-linear Magnetic Control Devices, Chapters 13, 14, McGraw-Hill, N. Y. 1964.

Gordon, D. I., R. H. Lundsten, R. A. Chiarodo and H. H. Helms, Jr., A Fluxgate Sensor of High Stability for Low Field Magnetometry, IEEE Trans. Magns. MAG-4, 397-401, 1968.

Greenstadt, E. W., Final Estimate of Interplanetary Field at 1 AU from Measurements Made by Pioneer V in March and April 1960, Ap. J. 145, 270-292, 1966.

Greenstadt, E. W., I. M. Green, G. T. Ionuge, A. J. Hundhausen, S. J. Bame, and I. B. Strong, Correlated Magnetic Field and Plasma Observations of the Earth's Bow Shock, J. Geophys. Res. 73, 51-60, 1968.

Grivet, P. A. and L. Malnar, Measurement of Weak Magnetic Fields by Magnetic Resonance, in Adv. in Electronics and Electron Physics, edited by L. Marton, Academic Press, N. Y., pp. 39-151, 1967.

Hedgecock, P. C. The Solar Particle Event of February 25, 1969 in Intercorrelated Satellite Observations edited by Manno and Page, pp. 591-598, D. Reidel Publishing Company, Dordrecht-Holland, 1970.

Heppner, J. P., B. G. Ledley, T. L. Skillman and M. Sugirua, A Preliminary Survey of Micropulsations in the Magnetosphere from OGO's 3 and 5, NASA-GSFC preprint X-612-69-429, 1969.

Heppner, J. P., N. F. Ness, T. L. Skillman and C. S. Scearce, Explorer 10 Magnetic Field Results, J. Geophys. Res., 68, 1-63, 1963.

Heppner, J. P., J. D. Stolarik, I. R. Shapiro and J. C. Cain, Project Vanguard Magnetic Field Instrumentation and Measurements, Space Research, I, 982-999, 1960.

Heppner, J. P., M. Sugiura, T. L. Skillman, B. G. Ledley and M. Campbell, OGO-A Magnetic Field Observations, J. Geophys. Res., 72, 5417-5472, 1967.

Hirschberg, J., A. Alksne, D. S. Colburn, S. J. Bame and A. J. Hundhausen, Observation of a Solar Flare Induced Interplanetary Shock and Helium Enriched Driver Gas, J. Geophys. Res., 75, 1-15, 1970.

Hoffman, R. A. and L. J. Cahill, Jr., Ring Current Particle Distributions Derived from Ring Current Magnetic Field Measurements, J. Geophys. Res., 73, 6711-6722, 1968.

Holzer, R. E., M. G. McLeod, and E. J. Smith, Preliminary Results from the OGO-1 Search Coil Magnetometer: Boundary Positions and Magnetic Noise Spectra, J. Geophys. Res., 71, 1481-1486, 1966.

Hundhausen, A. J., Direct Observations of Solar Wind Particles, Space Sci. Revs., 8, 690-745, 1968.

Hundhausen, A. J., S. J. Bame and N. F. Ness, Solar Wind Thermal Anisotropies: Vela-3 and IMP-3, J. Geophys. Res., 72, 5265-5274, 1967.

Inouye, G. T. and D. L. Judge, The Optimized Iron Cored Induction Magnetometer, TRW Report 9821-6001-RU00, 18 May 1964.

Judge, D. L., M. G. McLeod, A. R. Sims, The Pioneer 1, Explorer VI and Pioneer V High Sensitivity Transistorized Search Coil Magnetometer, IRE Trans. Space Elec. and Telemetry SET-6, 114-121, 1960.

Konovalova, L. V. andV. I. Nalivayko, Magnetic Chart of the Brazilian Anomaly, Geomagnetism and Aeronomy, 7, 318-320, 1967.

Lazarus, A. L., G. L. Siscoe and N. F. Ness, Plasma and Magnetic Field Observations During the Magnetosphere Passage of Pioneer 7, J. Geophys. Res., 73, 907-930, 1968.

Ludwig, G., The Orbiting Geophysical Observatories, Space Sci. Revs., 2, 175-218, 1963.

McCracken, K. G. and N. F.Ness, The Collimation of Cosmic Rays by the Interplanetary Magnetic Field, J. Geophys. Res., 71, 3315-3318, 1966.

McCracken, K.G., U. R. Rao and N. F. Ness, The Interrelationship of Cosmic Ray Anisotropies and the Interplanetary Magnetic Field, J. Geophys. Res., 73, 4159-4166, 1968.

Mansir, Dolan, Magnetometer at Work in Outer Space, Radio-Electronics 31, 38-41, 1960.

Mariani, F. W. and N. F. Ness, Observations of the Geomagnetic Tail at 500 Earth Radii by Pioneer 8, J. Geophys. Res., 74, 5633-5641, 1969.

Mihalov, J. D. and C. P. Sonett, Cislunar Geomagnetic Tail Gradient in 1967, J. Geophys. Res., 73, 6837-6842, 1968.

Ness, N. F., The Earth's Magnetic Tail, J. Geophys. Res., 70, 2989-3005, 1965.

Ness, N. F., Remarks on the Interpretation of the Lunik 10, Geomagnetism and Aeronomy, 7, 452-454, 1967a.

Ness, N. F., Remarks on Preceding Paper by E. W. Greenstadt, R. W. Fredericks and C. P. Sonett, J. Geophys. Res., 73, 3077-3080, 1968b.

Ness, N. F., The Geomagnetic Tail, Revs. Geophys. 7, 97-128, 1969a.

Ness, N. F., The Magnetic Structure of Interplanetary Space, NASA-GSFC Preprint X-616-69-334, 1969b.

Ness, N. F., Interaction of the Solar Wind with the Moon, NASA-GSFC Preprint X-692-70-141.

Ness, N. F., K. W. Behannon, H. E. Taylor and Y. C. Whang, Perturbations of the Interplanetary Magnetic Field by the Lunar Wake, J. Geophys. Res., 73, 3421-3435, 1968.

Ness, N. F. C. S. Scearce and S. C. Cantarano, Early Results from the Magnetic Field Experiment on Lunar Explorer 35, J. Geophys. Res., 72, 5769-5778, 1967

Ness, N. F., C. S. Scearce and S. Cantarano, Probable Observations of the Geomagnetic Tail at 10^3 R_E by Pioneer 7, J. Geophys. Res., 72, 3769-3776, 1967 a.

Ness, N. F. C. S. Scearce and J. B. Seek, Initial Results of the IMP-1 Magnetic Field Experiment, J. Geophys. Res., 69, 3531-3570, 1964.

Ness, N. F. and K. H. Schatten, Detection of Interplanetary Magnetic Fluctuations Stimulated by the Lunar Wake, J. Geophys. Res., 74, 6425-6438, 1969.

Ness, N. F. and J. M. Wilcox, Solar Origin of the Interplanetary Magnetic Field, Phys. Rev. Letters, 13, 461-464, 1964.

Ness, N. F. and J. M. Wilcox, Interplanetary Sector Structure, 1962-1966, Solar Physics, 2, 351-359, 1967.

Ogilvie, K. W. and L. F. Burlaga, Hydromagnetic Shocks in the Solar Wind, Solar Physics, 8, 435-450, 1969.

Ogilvie, K. W. and N. F. Ness, Dependence of the Lunar Wake on Solar Wind Plasma Characteristics, J. Geophys. Res., 74, 4123-4128, 1969.

Olson, J. V., R. E. Holzer and E. J. Smith, High Frequency Magnetic Fluctuations Associated with the Earth's Bow Shock, J. Geophys. Res., 74, 4601-4618, 1969.

Parker, E. N., Dynamical Theories of the Solar Wind, Space Sci. Reviews, 4, 666-708, 1965.

Parsons, C. L. and C. A. Harris, IMP-1 Spacecraft Magnetic Test Program, NASA TN D-3376, 1966.

Rochelle, Robert W., Satellite and Space Probe Telemetry in Aerospace Telemetry, Volume 2, ed. by H. L. Stiltz, pp. 1-59, Prentice Hall Inc., New Jersey 1966.

Ruddock, K. A., Optically Pumped Rubidium Vapor Magnetometer for Space Experiments, Space Research II, 692-700, 1961.

Russell, C. T., R. E. Holzer and E. J. Smith, OGO-3 Observations of ELF Noise in the Magnetosphere: Part 1. Spatial Extent and Frequency of Occurrence, J. Geophys. Res., 74, 766-777, 1969.

Russell, C. T., R. E. Holzer and E. J. Smith, OGO-3 Observations of ELF Noise in the Magnetosphere: Part 2. The Nature of the Equatorial Noise, J. Geophys. Res., (approved for publication-early 1970).

Sari, J. and N. F. Ness, Power Spectra of the Interplanetary Magnetic Field, Solar Physics, 8, 155-165, 1969.

Scearce, C. S., C. H. Ehrmann, S. C. Cantarano and N. F. Ness, Magnetic Field Experiment: Pioneers 6, 7 and 8, NASA-GSFC Preprint X-616-68-370, 1968.

Scearce, C. S., N. F. Ness and S. C. Cantarano, GSFC Magnetic Field Experiment: Explorers 33 and 35, NASA-GSFC Preprint X-616-69-53, 1969.

Schonstedt, E. O., Saturable Measuring Device and Magnetic Core Therefor, U. S. Patent 2916696 (December 1959) and U. S. Paten 2981885 (April 1961).

Siscoe, G. L., L. Davis, Jr., P.J. Coleman, Jr., E. J. Smith and D. E. Jones, Power Spectra and Discontinuities of the Interplanetary Magnetic Field, Mariner 4, J. Geophys. Res., 73, 61-82, 1968.

Skillman, T. L., ATS-E Magnetic Field Monitor Instrumentation, NASA-GSFC preprint X645-70-54.

Slocum, R. E., and F. N. Reilly, Low Field Helium Magnetometer for Space Applications, IEEE Trans. Nuc. Sci. NS-10, 165-171, 1963.

Smith, E. J., A Comparison of Explorer VI and Explorer X Magnetometer Data, J. Geophys. Res., 67, 2045-2049, 1962.

Smith, E. J., P. J. Coleman, D. L. Judge and C. P. Sonett, Characteristics of the Extraterrestrial Current System: Explorer VI and Pioneer V, J. Geophys. Res., 65, 1858-1861, 1960.

Smith, E. J., L. Davis, Jr., P. J. Coleman, Jr., and W. E. Jones, Magnetic Field Measurements Near Mars, Science, 149, 1241-1245, 1965b.

Smith, E. J., L. Davis, Jr., P. J. Coleman, Jr., and C. P. Sonett, Magnetic Measurements Near Venus, J. Geophys. Res., 70, 1571-1586, 1965a.

Snare, R. C., and C. R. Benjamin, A Magnetic Field Instrument for the OGO-E Spacecraft, IEEE Trans. Nuclear Science, NS-13, 333-339, 1966.

Sonett, C. P., The Distant Geomagnetic Field, 2, Modulation of a Spinning Coil EMF by Magnetic Signals, J. Geophys. Res., 68, 1229-1232, 1963a.

Sonett, C. P., The Distant Geomagnetic Field, 4, Microstructure of a Disordered Hydromagnetic Medium in the Collisionless Limit, J. Geophys. Res., 68, 1265-1293, 1963b.

Sonett, C. P., Modulation and Sampling of Hydromagnetic Radiation, Space Res., 6, 280-322, 1966.

Sonett, C. P. and I. J. Abrams, Distant Geomagnetic Field, 3, Disorder and Shocks in the Magnetopause, J. Geophys. Res., 68, 1233-1263, 1963.

Sonett, C. P., D. S. Colburn and B. R. Briggs, in the Solar Wind, ed. by R. Mackin and M. Neugebauer, p. 165-190, Pergamon Press, N.Y., 1966.

Sonett, C. P., D. S. Colburn, R. G. Currie and J. D. Mihalov, The Geomagnetic Tail: Topology, Reconnection and Interaction with the Moon, in Phys. of the Magnetosphere, ed. by R. L. Carovillano, J. F. McClay and H. R. Radoski, pp. 461-484, D. Reidel, Dordrecht, 1968.

Sonett, C. P. D. L. Judge, A. R. Sims and J. M. Kelso, A Radial Rocket Survey of the Distant Geomagnetic Field, J. Geophys. Res., 65, 55-58, 1960.

Speiser, T. W., and N. F. Ness, The Neutral Sheet in the Geomagnetic Tail: Its Motion, Equivalent Currents and Field Line Connection Through It, J. Geophys. Res., 72, 131-142, 1967.

Sudorov, I. M. and V. I. Prokhorendo, Determination of the Position Angle of an Artificial Satellite from the Data on the Magnetic Field, Cosmic Research, 6, 175-185, 1968.

Taylor, H. E., Aspect Determination in Lunar Shadow on Explorer 35, NASA Techn. Note, TN D-4544, 1968.

Taylor, H. E., Sudden Commencement Associated Discontinuities in the Interplanetary Magnetic Field Observed by IMP-3, Solar Physics, 6, 320-340, 1969.

Tyurmina, L. O., Analytical Model of the Geomagnetic Field According to COSMO 49 Data, Geomagnetism and Aeronomy, 8, 977-979, 1968.

Van Allen, J. A. and N. F. Ness, Observed Particle Effects of an Interplanetary Shock Wave on July 8, 1966, J. Geophys. Res., 72, 935-943, 1967.

Van Allen, J. A. and N. F. Ness, Particle Shadowing by the Moon, J. Geophys. Res., 74, 71-93, 1969.

Vernov, S. N., A. Ye. Chudakov, P. V. Vakulov, Ye. V. Gorchakov, Yu. I. Logachev, A. G. Nikolayev, I. A. Rubinshteyn, Ye. N. Sosovets, and M. V. Ternovskaya, Pulsations of the Magnetic Field According to the Measurements on the Satellite "Elektron 3", Trudy Vsesoyuznoy Konferentsii po Fizike Kosmicheskogo Prostranstva, Izdatel'stvo "Nauka", Moscow, June 10-16, 1965, pp. 433-434 (NASA TT F-389, pp. 587-588), 1965.

Whang, Y. C. and N. F. Ness, Observations of the Lunar Mach Cone, NASA-GSFC preprint X-692-70-60, 1970.

Wilcox, J. M., the Interplanetary Magnetic Field, Solar Origin and Terrestrial Effects, Space Sci. Rev., 8, 258-328, 1968.

Wilcox, J. M. and D. S. Colburn, Interplanetary Sector Structure in the Rising Portion of the Sunspot Cycle, J. Geophys. Res., 74, 2388-2392, 1969.

Wilcox, J. M. and N. F. Ness, Quasi-Stationary Corotating Sector Structure in the Interplanetary Medium, J. Geophys. Res., 74, 5793-5805, 1969.

Wilcox, J. M., K. H. Schatten and N. F. Ness, Influence of Interplanetary Magnetic Field and Plasma on Geomagnetic Activity During Quiet Sun Conditions, J. Geophys. Res., 72, 19-25, 1967.

Williams, F. C. and S. W. Noble, The Fundamental Limitations of the Second-Harmonic Type of Magnetic Modulator as Applied to the Amplification of Small DC Signals, Proc. IEE, 97, PartII, 445-450, 1950.

Yeroshenko, Ye., G., Investigation of the Earth's Magnetosphere at Distances 7-11·6 R_E by the Electron Satellites, Space Research, VI, 629-641, 1966.

Yeroshenko, Ye. G., Topology of the High Latitude Night Time Magnetosphere, Geomagnetism and Aeronomy, 8, 201-207, 1968.

Zhuzgov, L. N., Sh. Sh. Dolginov, and Ye. G. Yeroshenko, Investigation of the Magnetic Field from the Satellite Luna 10, Kosmicheskiye Issledovaniya, 4, 880-897, 1966.

Zmuda, A. J., J. H. Martin and F. T. Heuring, Transverse Magnetic Disturbances at 1100 km in the Auroral Oval, J. Geophys. Res., 71, 5033-5045, 1966.

Zmuda, A.J., W. E. Radford, F. T. Heuring and P. Verzariu, The Scalar Magnetic Intensity at 1100 Kilometers in Middle and Low Latitudes, J. Geophys. Res., 73, 2495-2503, 1968.

10.0 LIST OF FIGURES

Figure 11 Hyperfine energy levels for Rb^{85} isotope (a) and illustration of process of "optical pumping" (b).

Figure 12 Block diagram of system to illustrate use of optical pumping process to measure magnetic field (a) and single cell self-oscillating magnetometer (b).

Figure 13 Block diagram of dual-cell self-oscillating rubidium vapor magnetometer.

Figure 14 Zeeman diagram for ordinary ^4He, the 2^3S level of orthohelium is called metastable because it possesses a long lifetime.

Figure 15 Simplified block diagram of vector Helium magnetometer.

Figure 16 Extension of dynamic range of magnetometer by use of: (a) multiple ranges (variable sensitivity) or (b) offset ranges (fixed sensitivity).

Figure 17 Illustration of phenomenon of "aliasing" which occurs in discretely sampled data. Part (a) shows how two sine waves at different frequencies f_o and f_a possess identical values at the sampling times t_i. Part (b) illustrates how these frequencies are related for different values of the alias parameter $k_{\pm}$. Part (c) "folds" the frequency scale back on itself using breakpoints at integer multiples of the cutoff or Nyquist frequency $f_c = \frac{1}{2\Delta t}$.

Figure 18 Summary of special coordinate systems used in interpretation of magnetic field data.

Figure 19 Search coil magnetometer used on the Pioneers I, V and Explorer VI spacecraft.

Figure 20 Proton precession magnetometer used on the Vanguard III spacecraft.

Figure 21 Explorer X Dual Gas Cell Rb^{87} Self oscillating magnetometer.

Figure 22 IMP 1, 2 and 3 spacecraft.

Figure 23 EGO-1, 3 and 5 Rubidium Vapor and triaxial fluxgate sensors on special boom.

Figure 24 EGO-2, 4 and 6 Rubidium Vapor double dual-gas cell sensor on special boom.

Figure 25 Comparison of fluxgate magnetometer data for interplanetary shock wave of 15 February 1967 from the NASA Ames (Hirschberg et al. 1970) and NASA-GSFC instruments on Explorer 35.

Figure 26 Explorer 33 and 35 NASA-GSFC magnetic field instrumentation, showing flipper mechanism on left and "potted" in eccofoam triaxial sensor at right.

Figure 27 OV3-3 spacecraft (part of the TRW tetrahedral satellite series) with a biaxial fluxgate magnetometer mounted on the mini-boom.

Figure 28 Luna 10 triaxial fluxgate magnetometer (also used on Venera 4).

Figure 29 Block diagram of USSR Cesium self-oscillating magnetometer

P.I.	SPACECRAFT	LAUNCH DATE	ORBITAL ELEMENTS				DATA LIFE (DAYS)	INSTRUMENTATION	WEIGHT (KG)	POWER (WATTS)	RANGE (γ)	OUTPUT	QUANTIZATION (γ)	S/C FIELDS (γ)	BOOM LENGTH (M)	SAMPLE RATE (Hz)	BANDPASS (Hz)	SPIN PERIOD (SECS)
			APO (KM)	PERI (KM)	INCLIN (GEOG)	PERIOD (HOURS)												
Dolginov	SPUTNIK 3	15 MAY 1958	1881	226	65°	1.5	22	F(3)	>12.5	?	16,000-64,000	D/A	±80	120	NONE	?	?	ST
Sonett	PIONEER 1	11 OCT. 1958	60,000	LUNAR	PROBE	FAILURE	1	S.C. (1)	0.5	0.024	.6-1200	A	ST	ST	NONE	ST	1.5-2.5	0.55
Dolginov	LUNA 1	2 JAN. 1959	LUNAR	FLYBY	(@ 7000	KM)	1	F(3)	?	?	± 3000	A	±47	70	NONE	?	?	?
Sonett	EXPLORER 6	8 JULY 1959	42000	230	47°	12.8	61	S.C. (1) F(1)	1.0	0.024	.6-1200	A	ST	ST	NONE	ST	1.5-2.5	0.37
Dolginov	LUNA 2	2 SEPT. 1959	LUNAR	IMPACT	—	—	1.4	F(3)	?	?	± 750	A	±12	50	NONE	?	?	?
Heppner	VANGUARD 3	18 SEPT. 1959	3753	510	33.5°	2.2	85	PROTON	0.85	1	15000-68000	A	B_T	<1	0.5	ON GROUND COMMAND	N.A.	1†
Sonett	PIONEER 5	11 MARCH 1960	0.995	0.806	3.4°	*312	50	S.C. (1)	0.5	0.024	.6-1200	A	ST	ST	NONE	ST	1.5-2.5	0.5
Dolginov	VENERA 1	12 FEBR. 1961	VENUS	PROBE	NO FLYBY	RESULTS	?	F(3)	?	?	± 50	A	±1.5	?	2.0	0.032	?	?
Heppner	EXPLORER 10	25 MARCH 1961	186,000	100	32°	112	2.2	RB87 F(2)	1.0 1.6	4.2 0.2	3-10000 ±30	A	±0.05 -0.25	±1 ≤1	0.8 0.8	10 0.01	0-5	1.8
Cahill	EXPLORER 12	15 AUGUST 1961	77200	350	33°	26.5	112	F(3)	1.4	0.38	±1000	A	±12	11	0.9	3.13	0-10	0.5
Sonett	MARINER 2	27 AUGUST 1962	VENUS	FLYBY	ON 14 DEC. 62		104	F(3)	2.1	6.0	+80 ∓350	A	±0.35 ±1.35	LARGE VARIABLE	NONE	0.027	0-0.33	AS
Cahill	EXPLORER 14	2 OCT. 1962	98850	278	33°	36.6	315	F(3)	1.4	0.38	±500	A	±5	17	0.9	3.13	0-10	4.8-6.2
Dolginov	MARS 1	1 NOV. 1962	MARS	PROBE	NO FLYBY	RESULTS	?	F(1)	?	?	±50	A	±1.5	?	?	?	?	?
Cahill	EXPLORER 15	27 OCT.1962	17300	310	18°	5.2	105	F(2)	1.2	0.35	±2000	A	±20	4	0.9	3.13	0-10	6.2
Zmuda	1963-38C	28 SEPT.1963	1140	1067	90°	1.8	S.O	F(1)	0.9	0.5	±2500	A	±15	?	NONE	CONT.	S.T.	MS
Ness	EXPLORER 18	26 NOV.1963	196000	196	33°	96.0	190	RB87 F(2)	1.4 1.5	3.5 1.2	3-500 ±40	A	0.1% ±0.4	<1 <0.6	1.6 2.1	0.33 0.03	0-5	2.6
Dolginov	ELECTRON 2	30 JAN. 1964	68200	460	61°	22.7	?	F(3) F(3)	?	2.2 2.2	±120 ∓1200	A A	±2 ∓20	<2 <20	2.5 2.1	?	0-0.25	?
Dolginov	COSMOS 26	18 MARCH 1964	403	271	49°	1.5	30	2 PROTON	10	2.4	20000-80000	D	0.01%	2+	3.3	0.03	—	—
Dolginov	ELECTRON 3 " 4	11 JULY 1964 "	7040 66235	405 459	61° 61°	2.8 2.8	?	S.C. (1) 2F (3)	?	?	>25 ±240,±1200	A A	4, 20	<.4,<20	? 2.5, 2.1	? ?	1-10,3-300	?
Greenstadt	VELA 2A " 2B	17 JULY 1964 "	105000 112000	102000 95000	40° 40°	100 100	730+ 730+	S.C. (1) S.C. (1)	0.2 0.2	0.05 0.05	0-36 0-36	D D	+0.25 ∓0.25	≈30 ≈30	NONE NONF	1 1	1.5-2.5 1.5-2.5	0.43 0.43
Heppner	OGO-1	5 SEPT. 1964	149000	280	31°	64	875	RB87 F(3)	5.9 2.3	6.5 1.4	3-14000 ±30,±500	A A	0.02	75	ST	? 111,55	— 30	12
Smith	"	"	"	"	"	"	875	S.C.(3)	2.1	2.3	ST	A	ST	ST	6.1	278	10^{-2}-10^{+2}	12
Ness	EXPLORER 21	4 OCT. 1964	95500	197	33°	35	184	RB87 F(2)	1.4 1.5	3.5 1.2	3-500 ±40	A	0.1% ±0.4	<1 <0.6	1.6 2.1	0.33 0.03	0-5	4.1
Dolginov	COSMOS 49	24 OCT. 1964	490	260	49°	1.5	30	2 PROTON	10	2.4	20000-80000	D	0.01%	2+	3.3	0.03	—	?
Smith	MARINER 4	28 NOV. 1964	MARS	FLYBY	ON 15 JULY 1965		230	HELIUM	2.5	7.0	±360	A	±0.36	30	NONE	ST	0-0.8	AS
Zmuda	1964-83C	12 DEC. 1964	1089	1040	90°	1.8	90	RB85	1.1	3.5	15000-31000	D	0.01%	190±	4.9	1.67	—	MS
Cahill	EXPLORER 26	21 DEC. 1964	26198	310	20°	7.6	120	F(2)	1.2	0.35	±2000	A	±20	3	0.9	3.13	0-10	
Ness	EXPLORER 28	29 MAY 1965	270000	195	34°	149	730	RB87 F(2)	1.4 1.5	3.5 1.2	2-300 ±40	A	0.1% ±0.4	<1 <0.5	1.6 2.1	0.33 0.03	0-5	2.4
Greenstadt	VELA 3A " 3B	20 JULY 1965 "	117000 122000	106000 103000	35° 35°	110 110	S.O. S.O.	S.C. (1) S.C. (1)	0.2 0.2	0.05 0.05	0-100	D D	±1.0	60-100	NONE	0.5	1.75-2.25 1.75-2.25	0.45 0.45

TABLE I

P.I.	SPACECRAFT	LAUNCH DATE	ORBITAL ELEMENTS				DATA LIFE (DAYS)	INSTRUMENTATION	WEIGHT (KG)	POWER (WATTS)	RANGE (γ)	OUTPUT	QUANTIZATION (γ)	S/C FIELDS (γ)	BOOM LENGTH (METER)	SAMPLE RATE (Hz)	BAND PASS (Hz)	SPIN PERIOD (SECS)
			APO (KM)	PERI (KM)	INCLIN (GEOC)	PERIOD (HOURS)												
Cain	OGO-2	14 OCT. 1965	1510	413	87.4°	1.7	747	RB^{85}	7.7	7.5	15000-64000	A D	±0.2 ±0.4	< 2	6.1	7	—	AS
Smith	"	"	"	"	"	"	747	S.C.(3)	2.2	1.5	ST	A	ST	ST	6.1	332	10^{-2}-10^{+2}	AS
Ness	PIONEER 6	16 DEC. 1965	0.987	0.814	0.2°	*311	S.O.	F(1)	2.6	0.7	±64	D	±0.25	< 0.3	2	0.67	0-5	1.0
Dolginov	LUNA 10	31 MARCH 1966	1017	350	72°	3	36	F(3)	?	?	±50	A	±1.5	< 10	2	0.008	?	36±6
Heppner	OGO-3	7 JUNE 1966	122200	295	31°	50	S.O. S.O.	RB^{87} F(3)	5.9 2.3	6.5 1.4	3-14000 ±30,±500	A A	0.02 ±.25,±3.2	< 0.5 3%	6.1 4.5	7 111,55	— 30	AS
Smith	"	"	"	"	"	"	S.O	S.C.(3)	2.1	2.3	ST	A	ST	ST	6.1	278	10^{-2}-10^{+2}	AS
Ness	EXPLORER 33	1 JULY 1966	440000	16000	29°	340	820	F(3)	2.7	1.1	±64	D	±0.25	<0.2	2	0.2	0-5	2.5
Sonett	"	"	"	"	"	"	S.O.	F(3)	2.4	0.7	±20,±60 ±100	A	±0.2,±0.6 ±1.0	<0.2	2	0.16	0-0.05	2.5
Greenstadt	OV3-3	4 AUGUST 1966	4450	352	82°	2.3	226	F(3)	0.9	2	±60000	A	±30	10	1.5	CONT.	0-.5	7.5
Ness	PIONEER 7	17 AUGUST 1966	1.125	1.010	0°	*403	S.O.	F(1)	2.6	0.7	±32	D	±0.125	<0.2	2	0.67	0-5	1.0
Coleman	ATS-1	6 DEC. 1966	33500	165°W	0°	24	S.O.	F(2)	1.7	3.0	±50,±100 ±200	A	±.5,±1.0 ± 2.0	125	0.2	3.12	0-2	0.6
Ness	EXPLORER 34	24 MAY 1967	213000	244	67	104	730	F(3)	2.5	1.0	±32 ±128	D	±0.16 ±0.64	<0.3	2	0.4	0-12	0;45
Dolginov	VENERA 4	12 JUNE 1967	VENUS	IMPACT	(18 OCT. 1967)		128	F(3)	?	?	±50	A	±1.5	34	2.2	0.14	?	?
Smith	MARINER 5	14 JUNE 1967	VENUS	FLYBY	(19 OCT. 1967, 4000 KM)		180	HELIUM	2.9	7.2	±204	A	±0.2	8	NONE	ST	0-0.8	AS
Zwada	DODGE	1 JULY 1967	33800	33500	7°	22	490	F(3)	2.6	1.5	±250	A	±0.25	VARIABLE	1.7	2.0	0.5-2.0	G.C
Ness	EXPLORER 35	19 JULY 1967	7680	800	163°	11.5	S.O.	F(3)	2.7	1.1	±24 ±64	D	±0.094 ±0.25	<0.2	2	0.2	0-5	2.2
Sonett	"	"	(LUNAR ORBIT)				S.O.	F(3)	2.4	0.7	±20,±60 ±200	A	±0.2,±0.6 ±1.0	<0.2	2	0.16	0-0.05	2.2
Cain	OGO-4	28 JULY 1967	908	412	86°	1.6	820	RB^{85}	7.7	7.5	15000-64000	A D	±0.2 ±0.4	<2	6.0	7 2	—	AS
Smith	"	"	"	"	"	"	820	S.C.(3)	2.2	1.5	ST	A	ST	ST	6.1	332	10^{-2}-10^{+2}	AS
Ness	PIONEER 8	13 DEC. 1967	1.088	0.989	0°	*400	S.O.	F(1)	2.6	0.7	±32 ±96	D	±0.125 ±0.375	<0.2	2	0.67	0-5	1.0
Coleman	OGO-5	4 MARCH 1968	146700	291	31°	62	S.O.	F(3)	3.3	3.2-8	±16, to ±65000	A	±0.0625	<0.5	6	55.5	20	AS
Heppner	"	"	"	"	"	"	S.O. S.O.	RB^{87} F(3)	6.1 2.7	7.0 1.8	3-14000 ±4000	A A	0.02 ±0.12	< 0.5 < 1	6.1 4.5	7 111	120	AS
Smith	"	"	"	"	"	"	S.O.	S.C.(3)	2.3	2.2	ST	A	ST	ST	6.1	110	10^{-2}-10^{+2}	AS
Sonett	PIONEER 9	8 NOV. 1968	1.00	0.75	0°	*298	S.O.	F(3)	3.0	5.3	±200	D	±0.2	<0.5	2	3.5	1.7	1.0
Elliot	HEOS-1	5 DEC. 1968	223500	426	28.1°	113.6	S.O.	F(4)	3.3	1.4	±64	D	±0.25	0.15	2.0	ST	0-5	6
Greenstadt	OV5-5	23 MAY 1969	110000	16900	33°	52	S.O.	F(2)	0.4	0.3	±100	A	± 1	<5	0.15	0.2	0-.2	5.5
Cain	OGO-6	5 JUNE 1969	1098	396	82°	1.6	S.O.	RB	7.7	7.5	15000-64000	A	±0.2 ±0.4	<2	6.0	7 3.5	—	AS
Smith	"	"	"	"	"	"	S.O.	S.C.(3)	2.4	2.5	ST	A	ST	ST	6.1	222	10^{-2}-10^{+2}	AS
Ness	EXPLORER 41	21 JUNE 1969	177000	345	86.6	81.6	S.O.	F(3)	2.5	1.0	±40 ±200	D	±0.2 ±1.0	<0.5	2	0.4	0-5	2.2
Skillman	ATS-5	12 AUGUST 1969	37000	107°W	2.5	24	S.O.	F(3)	3.2	1.8	±500	A	0.25	10	1	0.4	120	0.78
Sonett	ALSEP-1	? NOV. 1969	ON LUNAR SURFACE				S.O.	F(3)	8.0	3.5-7.0	±100,200 400	D	±0.1,02 0.4	?	—	3.0	1.0	—

TABLE II

Principal Investigators	Spacecraft Mission	Launch Date	Instrument
Ness	IMP-I	1970	F (3)
Dyal	APOLLO 14	1970	F (3)
Hedgecock	HEOS-A2	1971	F (3)
Cahill	S^3	1971	F (3)
Ness	IMP-H	1971	F (3)
Sonett	APOLLO 15		
Dyal	APOLLO 16	1971	F (3)
Coleman	APOLLO 16 subsatellite	1971	F (2)
Smith	Pioneer F	1972	Helium Vapor
Ness	IMP-J	1972	F (3)
Coleman	APOLLO 18 subsatellite	1973	F (2)
Mariani	SIRIO	1972	F (3), SC (3)
Smith	Pioneer G	1973	Helium Vapor
To be determined	Mariner Mercury-Venus	1973	To be determined
Coleman	ATS-F	1973	F (3)
Neubauer, Mariani-Ness	HELIOS-1	1974	2F (3)
To be determined	ATS-G	1974	F (3)
Neubauer, Mariani-Ness	HELIOS-2	1974	2F (3)
To be determined	GEOS	1974	F (3), SC (2)

TABLE III

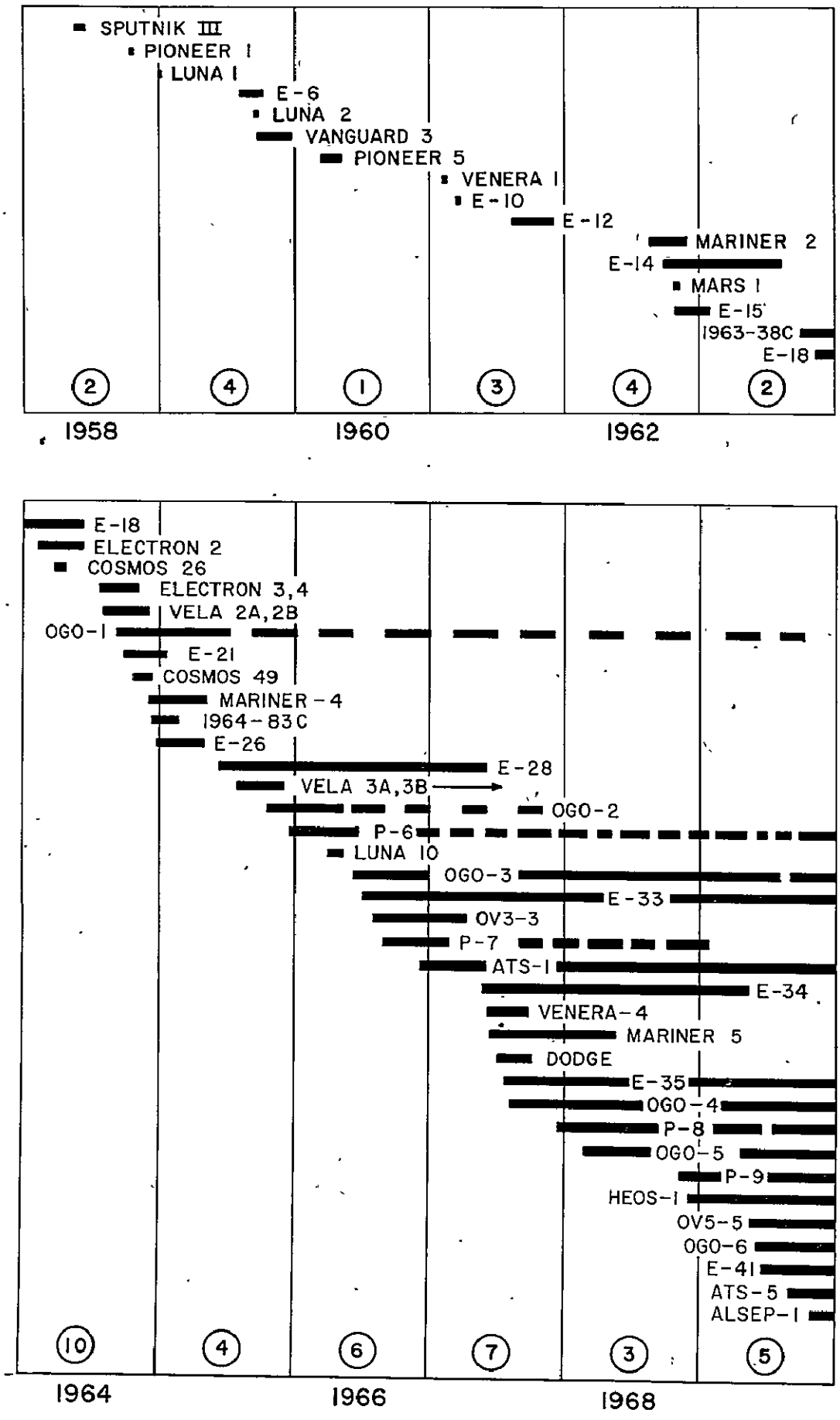
SPUTNIK III
PIONEER I
LUNA I
E-6
LUNA 2
VANGUARD 3
PIONEER 5
VENERA I
E-10
E-12
MARINER 2
E-14
MARS I
E-15
1963-38C
E-18
2
4
1
3
4
2
1958
1960
1962
E-18
ELECTRON 2
COSMOS 26
ELECTRON 3,4
VELA 2A,2B
OGO-I
E-21
COSMOS 49
MARINER-4
1964-83C
E-26
E-28
VELA 3A,3B
OGO-2
P-6
LUNA 10
OGO-3
E-33
OV3-3
P-7
ATS-I
E-34
VENERA-4
MARINER 5
DODGE
E-35
OGO-4
P-8
OGO-5
P-9
HEOS-I
OV5-5
OGO-6
E-41
ATS-5
ALSEP-I
10
4
6
7
3
5
1964
1966
1968

FIGURE 1

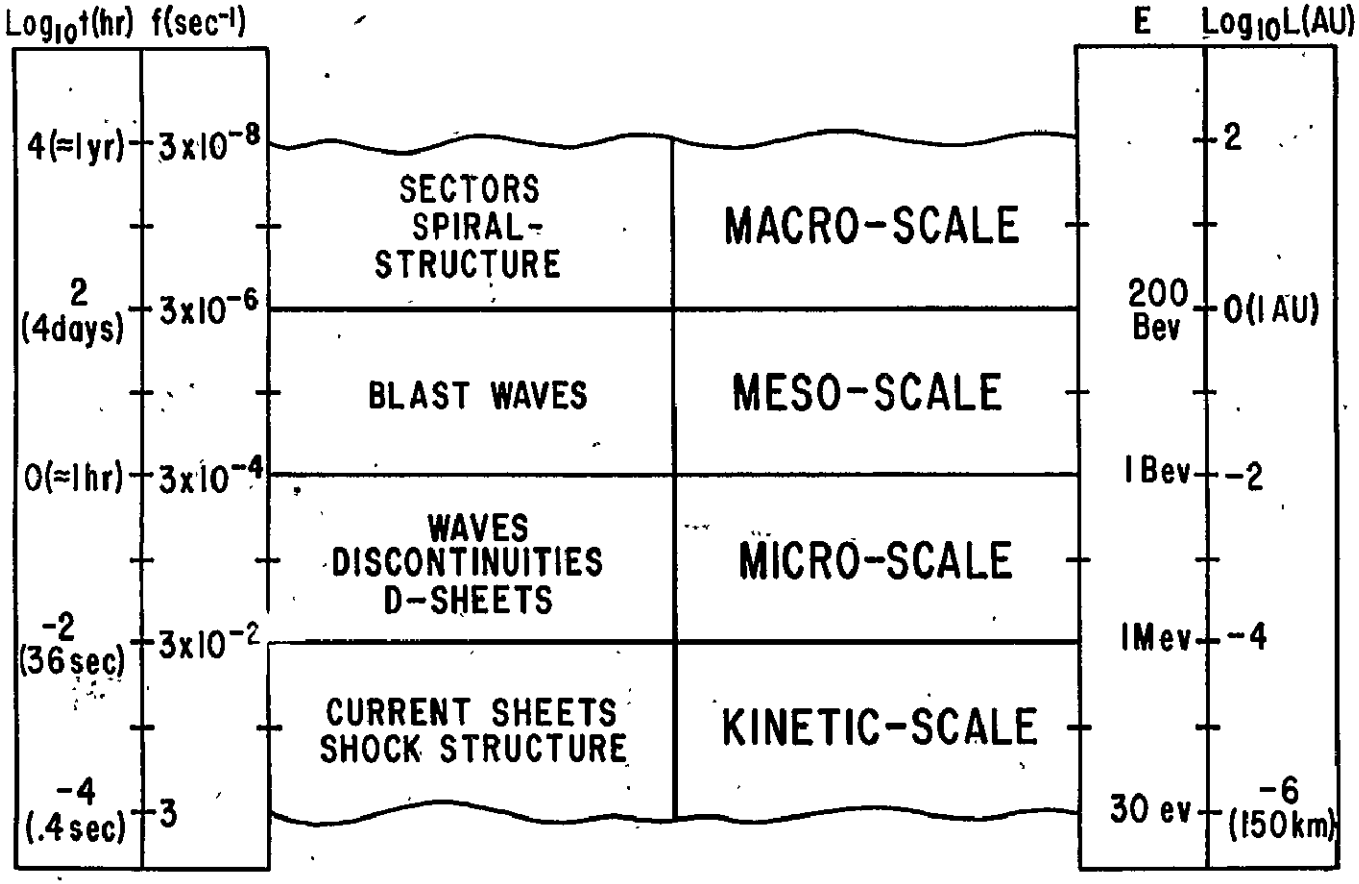
Log10t(hr)
f(sec-1)
E
Log10L(AU)
4(≈1yr)
3x10-8
2
(4days)
3x10-6
200
Bev
O(1 AU)
O(≈1hr)
3x10-4
1 Bev
-2
-2
(36sec)
3x10-2
1 Mev
-4
-4
(.4sec)
3
30 ev
-6
(150km)
SECTORS
SPIRAL-
STRUCTURE
MACRO-SCALE
BLAST WAVES
MESO-SCALE
WAVES
DISCONTINUITIES
D-SHEETS
MICRO-SCALE
CURRENT SHEETS
SHOCK STRUCTURE
KINETIC-SCALE

FIGURE 2b

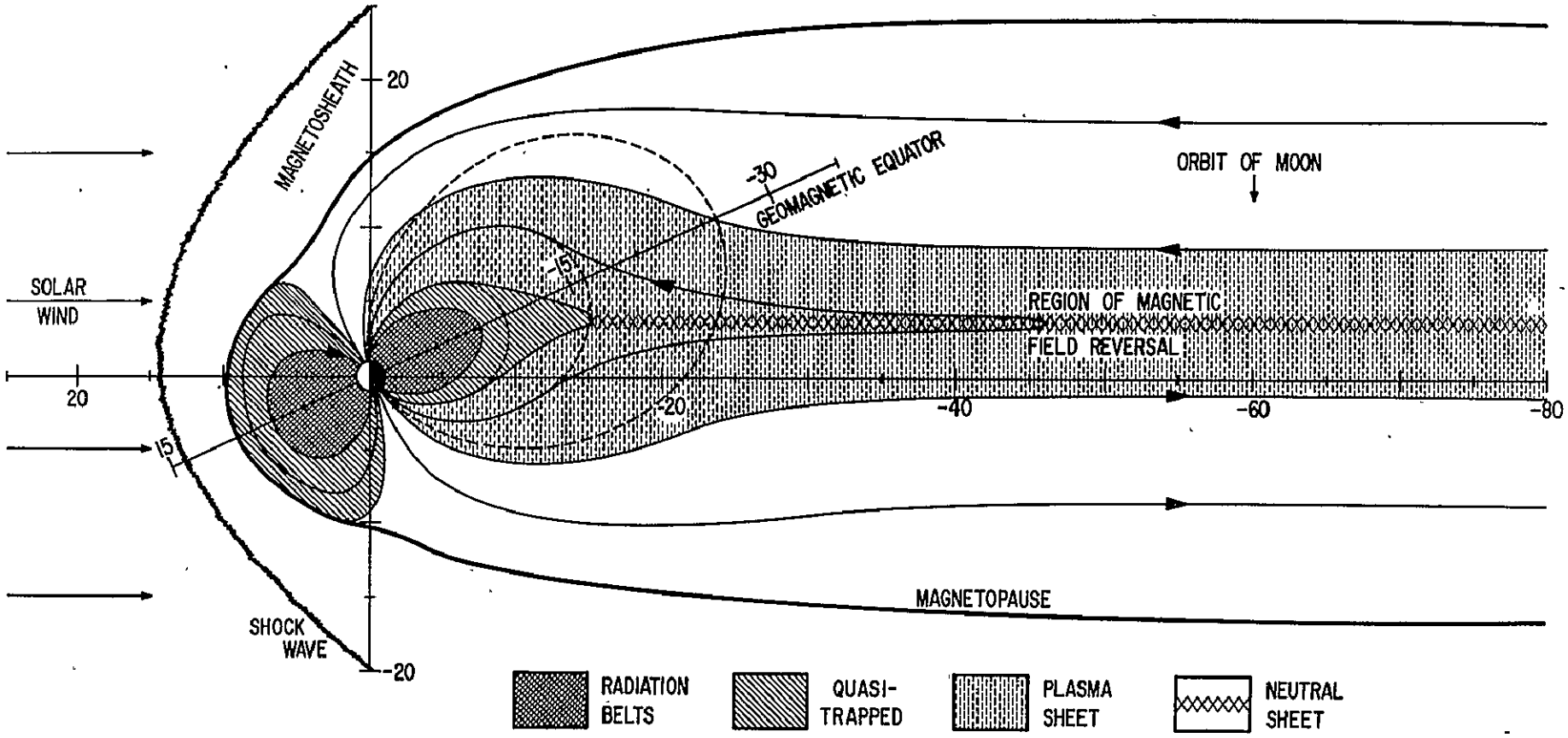

MAGNETOSPHERE AND TAIL

FIGURE 3a

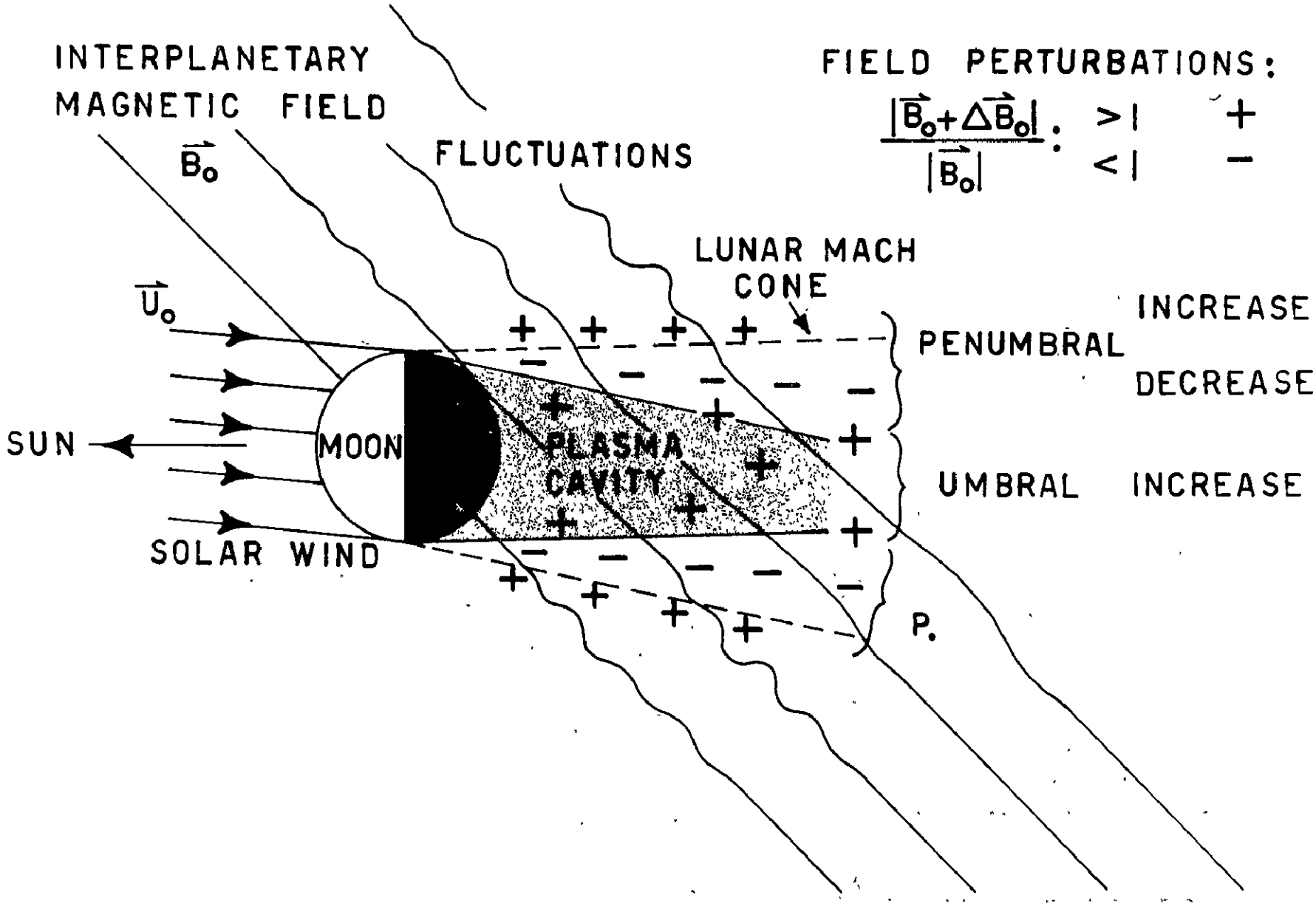
INTERPLANETARY
MAGNETIC FIELD
$\vec{B}_o$
FLUCTUATIONS
FIELD PERTURBATIONS:
$\frac{|\vec{B}_o+\Delta\vec{B}_o|}{|\vec{B}_o|}$: >1 +
<1 −
LUNAR MACH
CONE
$\vec{U}_o$
INCREASE
PENUMBRAL
DECREASE
SUN
MOON
PLASMA
CAVITY
UMBRAL INCREASE
SOLAR WIND
P.

FIGURE 3b

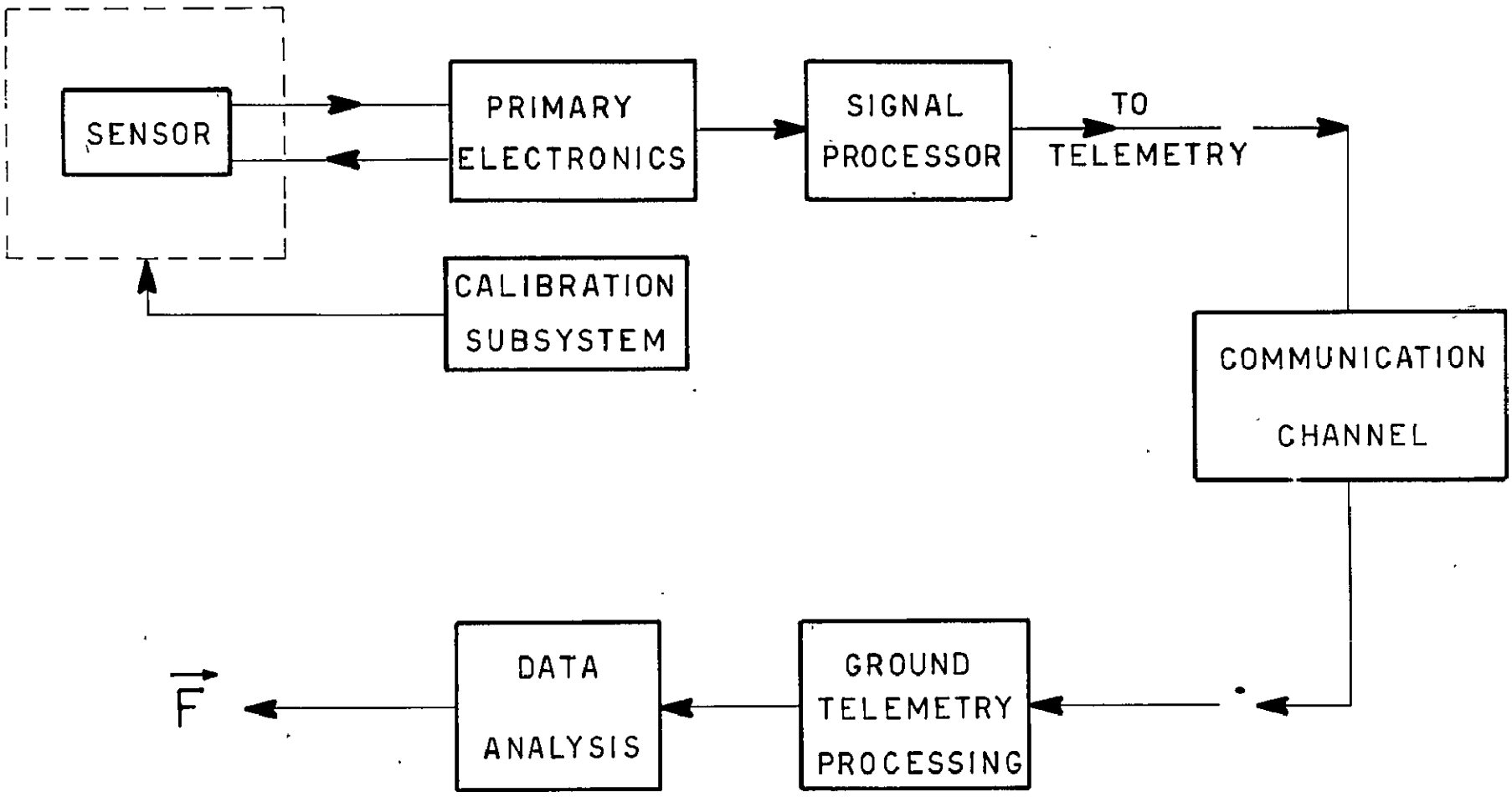

GENERALIZED MAGNETOMETER EXPERIMENT
BLOCK DIAGRAM

FIGURE

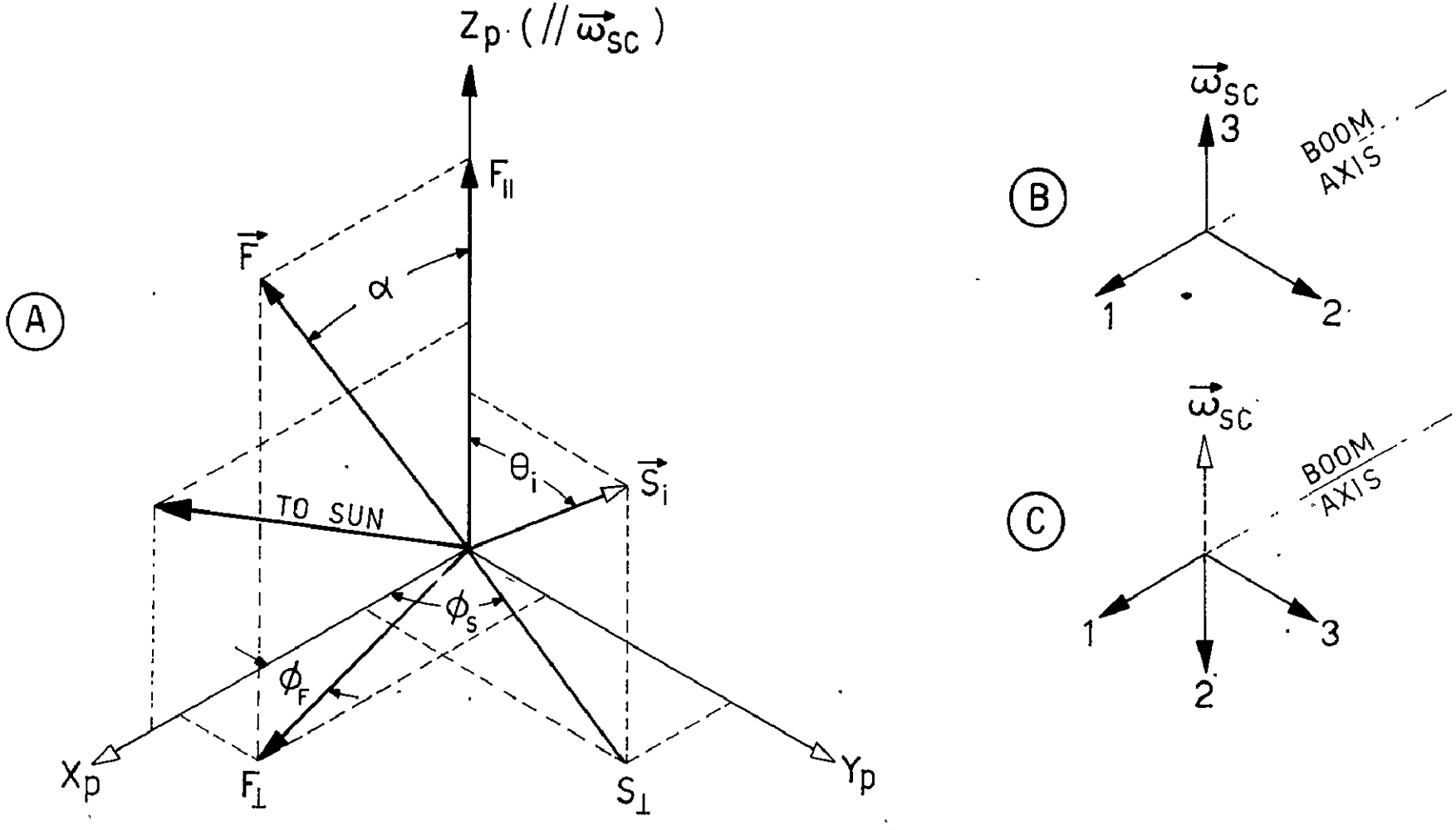
A
Z_p (// $\vec{\omega}_{SC}$)
F_{II}
$\vec{F}$
α
θ_i
$\vec{S}_i$
TO SUN
ϕ_s
ϕ_F
X_p
$F_\perp$
$S_\perp$
Y_p
B
$\vec{\omega}_{SC}$
3
BOOM AXIS
1
2
C
$\vec{\omega}_{SC}$
BOOM AXIS
1
3
2

FIGURE 5

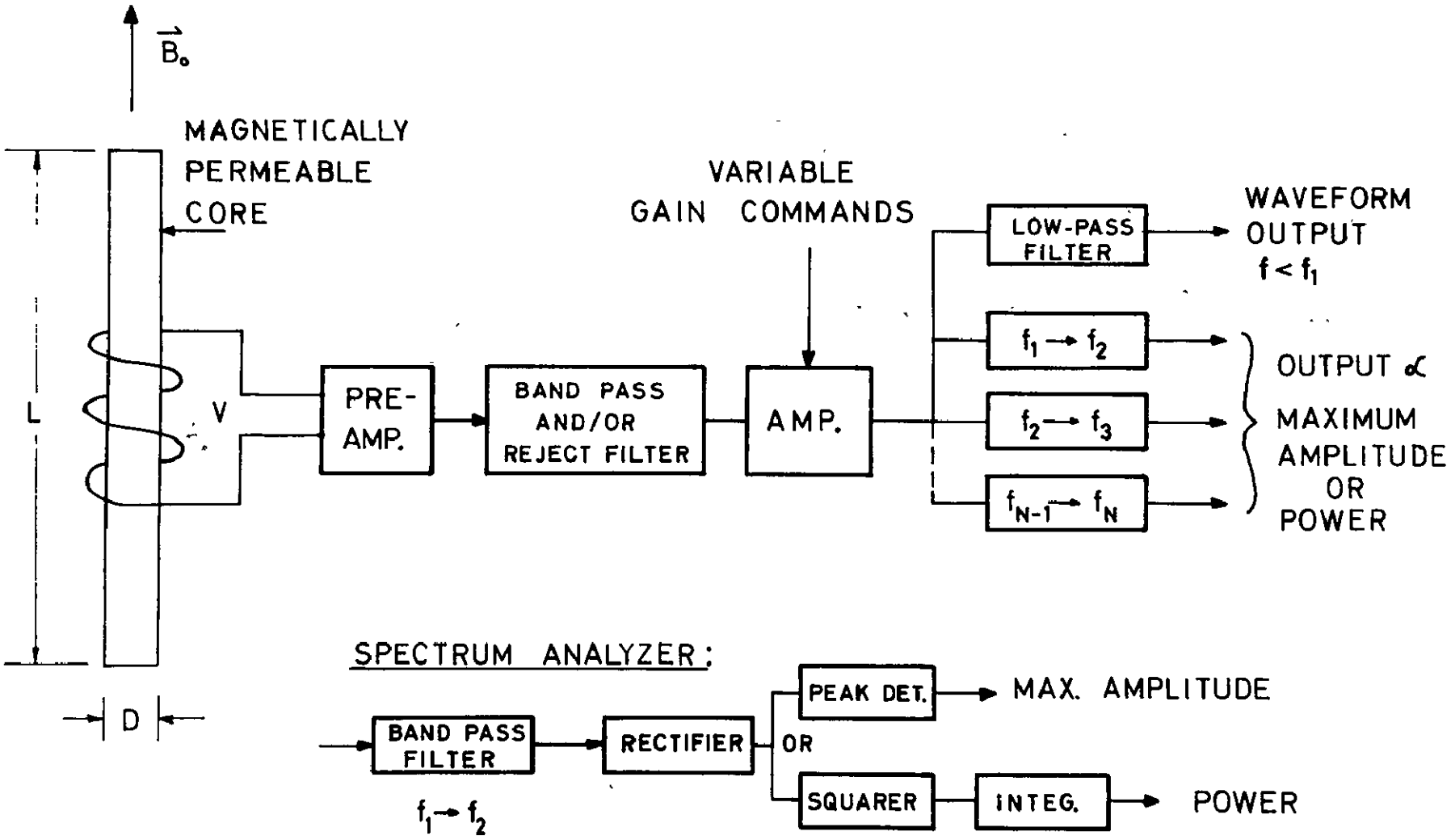
$\vec{B}_o$
MAGNETICALLY
PERMEABLE
CORE
L
D
V
PRE-
AMP.
BAND PASS
AND/OR
REJECT FILTER
VARIABLE
GAIN COMMANDS
AMP.
LOW-PASS
FILTER
WAVEFORM
OUTPUT
$f < f_1$
$f_1 \rightarrow f_2$
$f_2 \rightarrow f_3$
$f_{N-1} \rightarrow f_N$
OUTPUT $\propto$
MAXIMUM
AMPLITUDE
OR
POWER
SPECTRUM ANALYZER:
BAND PASS
FILTER
$f_1 \rightarrow f_2$
RECTIFIER
OR
PEAK DET.
MAX. AMPLITUDE
SQUARER
INTEG.
POWER

FIGURE 6

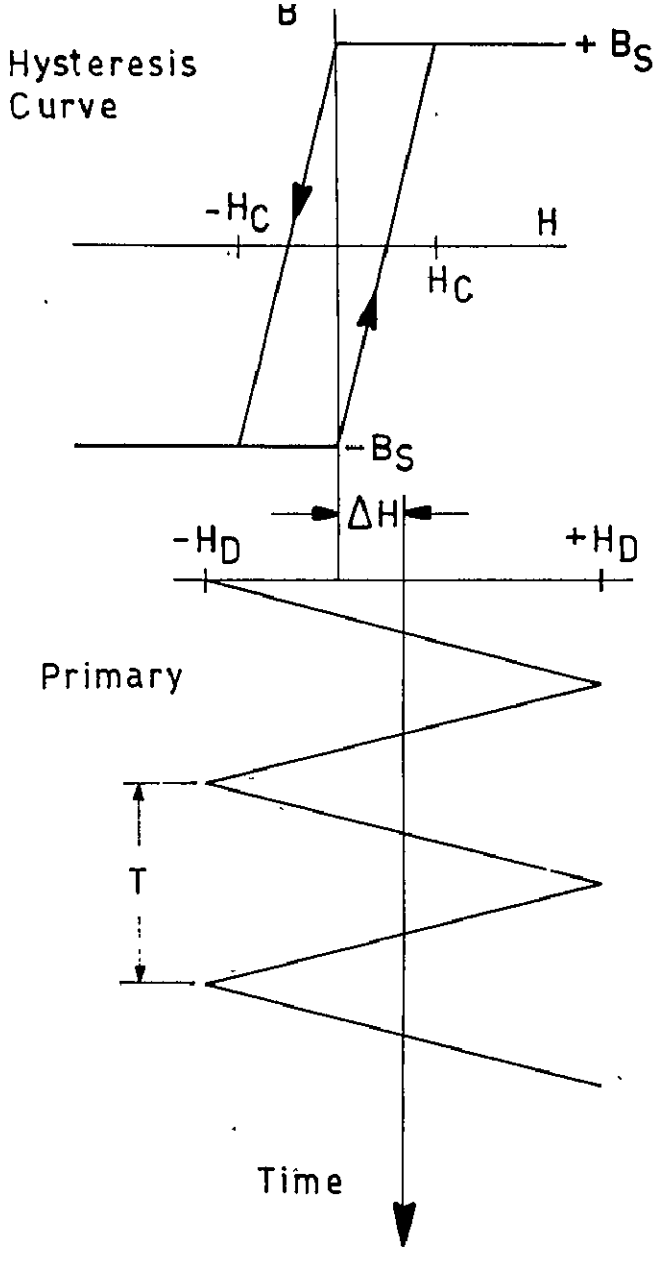

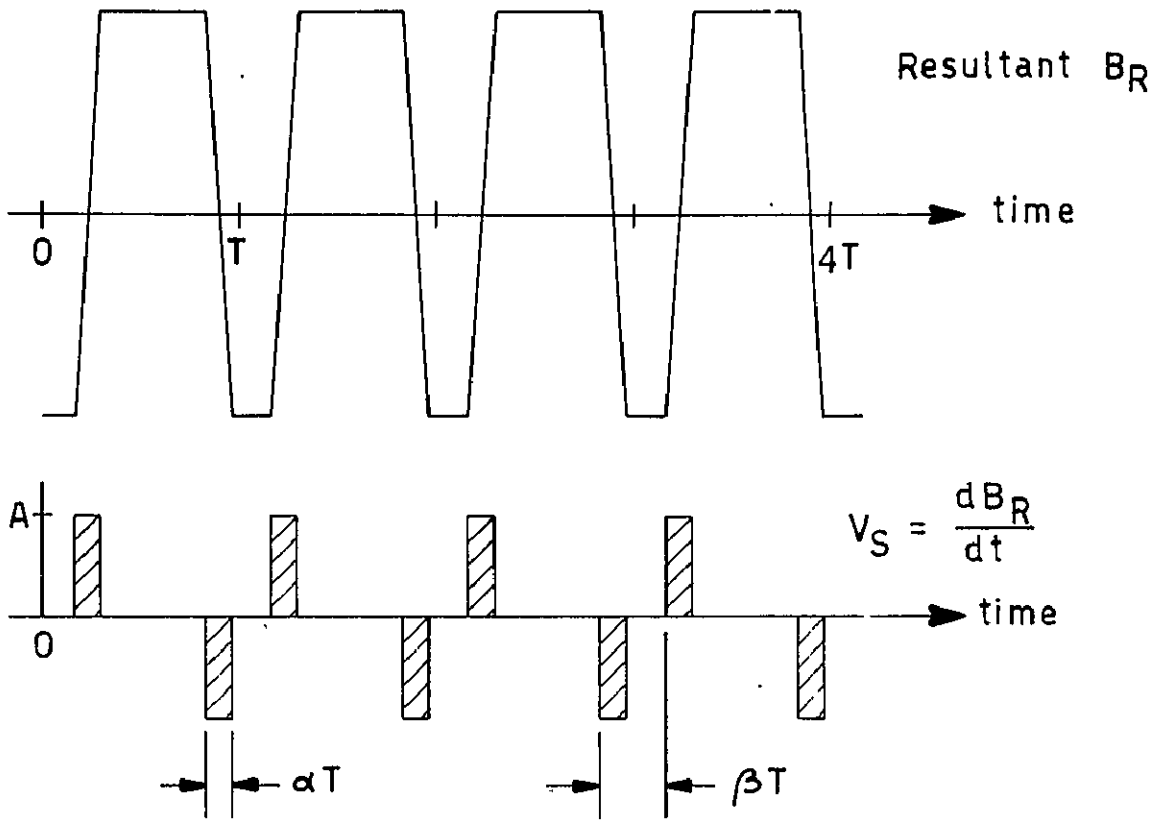

Train of +, − pulses: Fourier representation

$$V_S = A \sum_{K=1}^{\infty} \left[1 - e^{-i2\pi\beta K} \right] \frac{\sin \alpha\pi K}{K\pi} \cos\left(2\pi K \frac{t}{T}\right)$$

$$A = \frac{2B_S}{\alpha T} \qquad \alpha = \frac{1}{4}\frac{H_C}{H_D} \qquad \beta = \frac{1}{2}\left(1 - \frac{\Delta H}{H_D}\right)$$

FIGURE 7

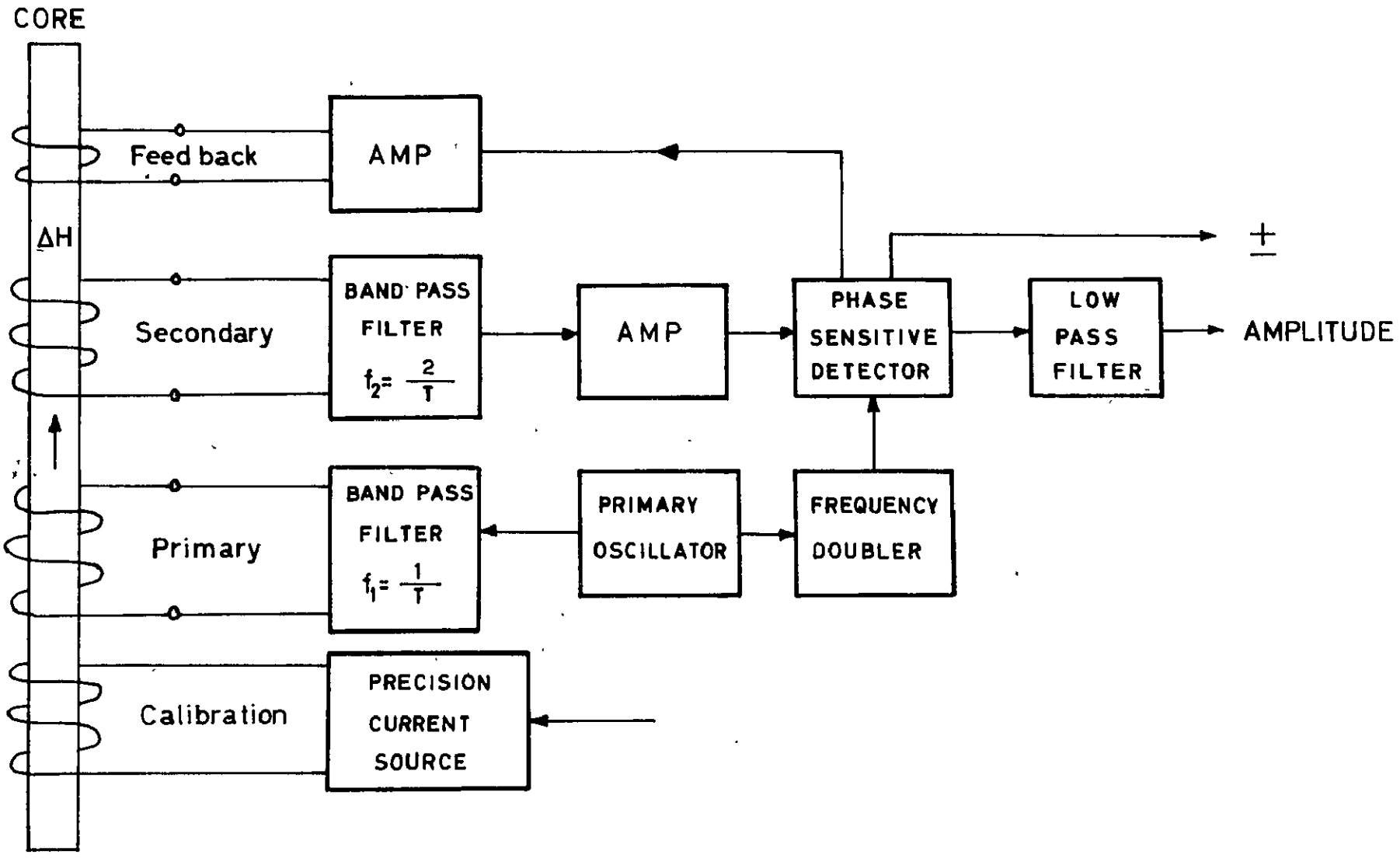
CORE
Feed back
AMP
ΔH
Secondary
BAND PASS FILTER
$f_2 = \frac{2}{T}$
AMP
PHASE SENSITIVE DETECTOR
LOW PASS FILTER
±
AMPLITUDE
Primary
BAND PASS FILTER
$f_1 = \frac{1}{T}$
PRIMARY OSCILLATOR
FREQUENCY DOUBLER
Calibration
PRECISION CURRENT SOURCE

FIGURE 8

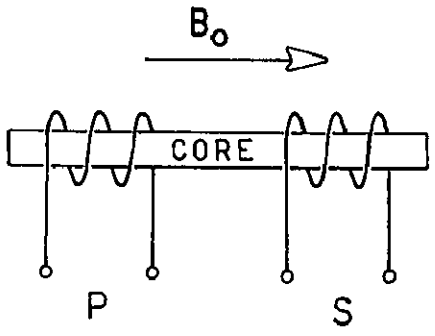

SINGLE

(a)

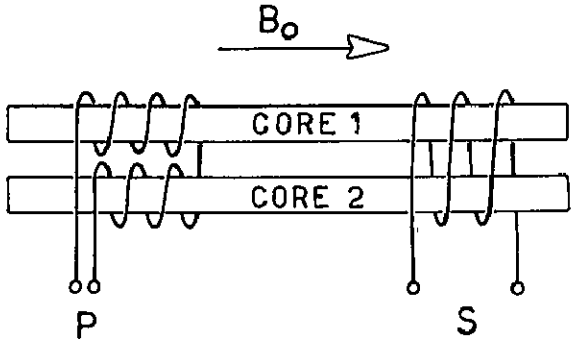

TWO-CORE

(b)

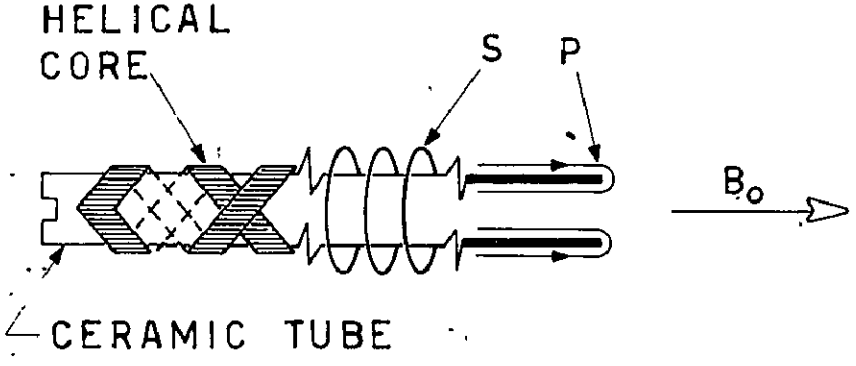

"HELIFLUX"

(c)

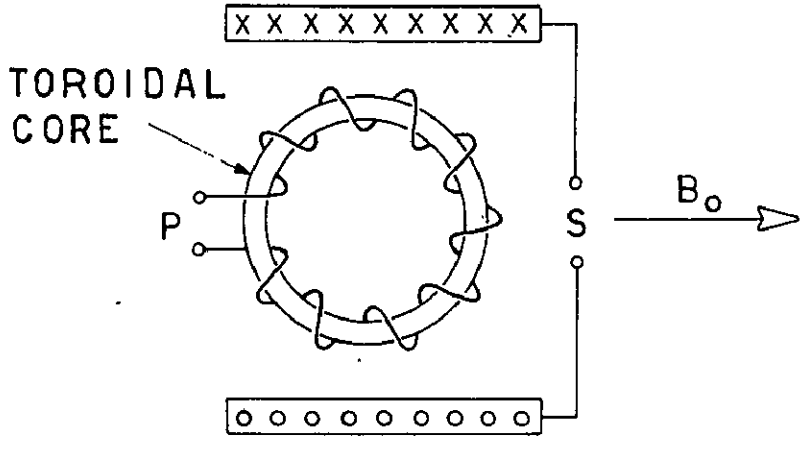

RING-CORE

(d)

FIGURE 9

(a)

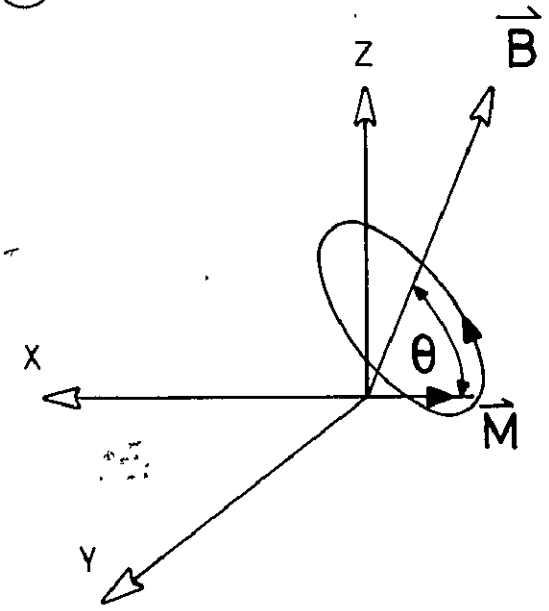

$\vec{M}$ precesses about $\vec{B}_o$
at Frequency $\omega_P = \gamma_P F$

$|\vec{M}| \propto e^{(-t/T_2)}$

(b)

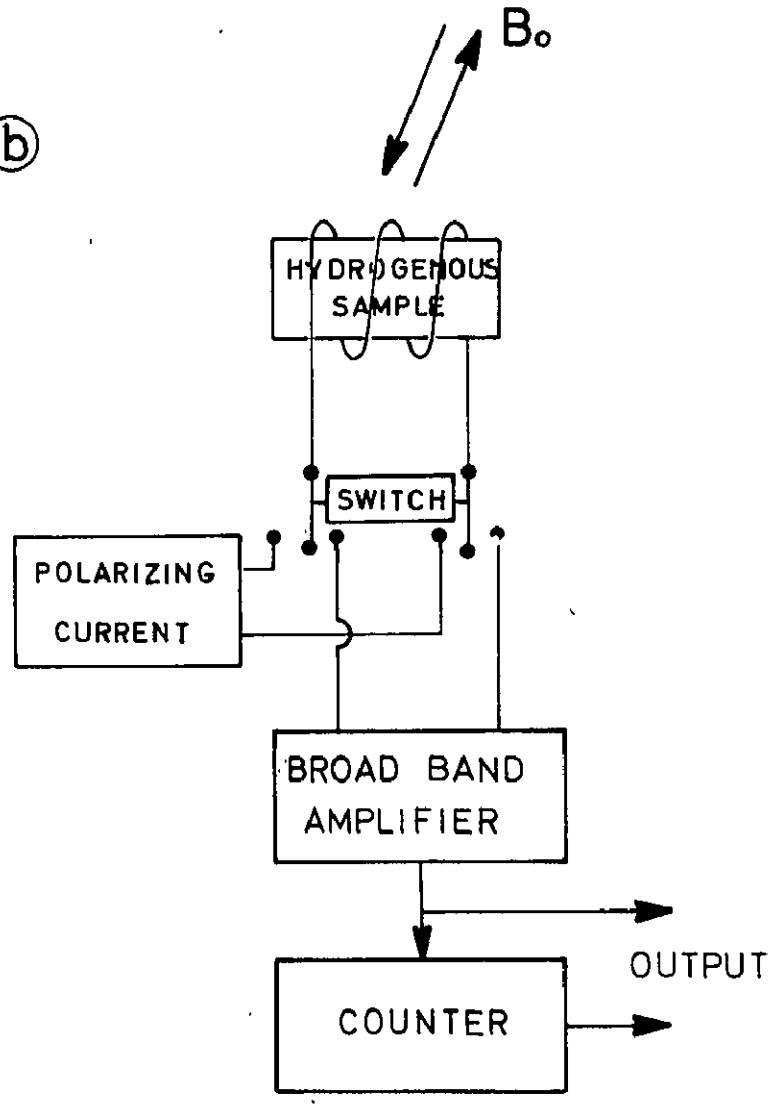

FIGURE 10

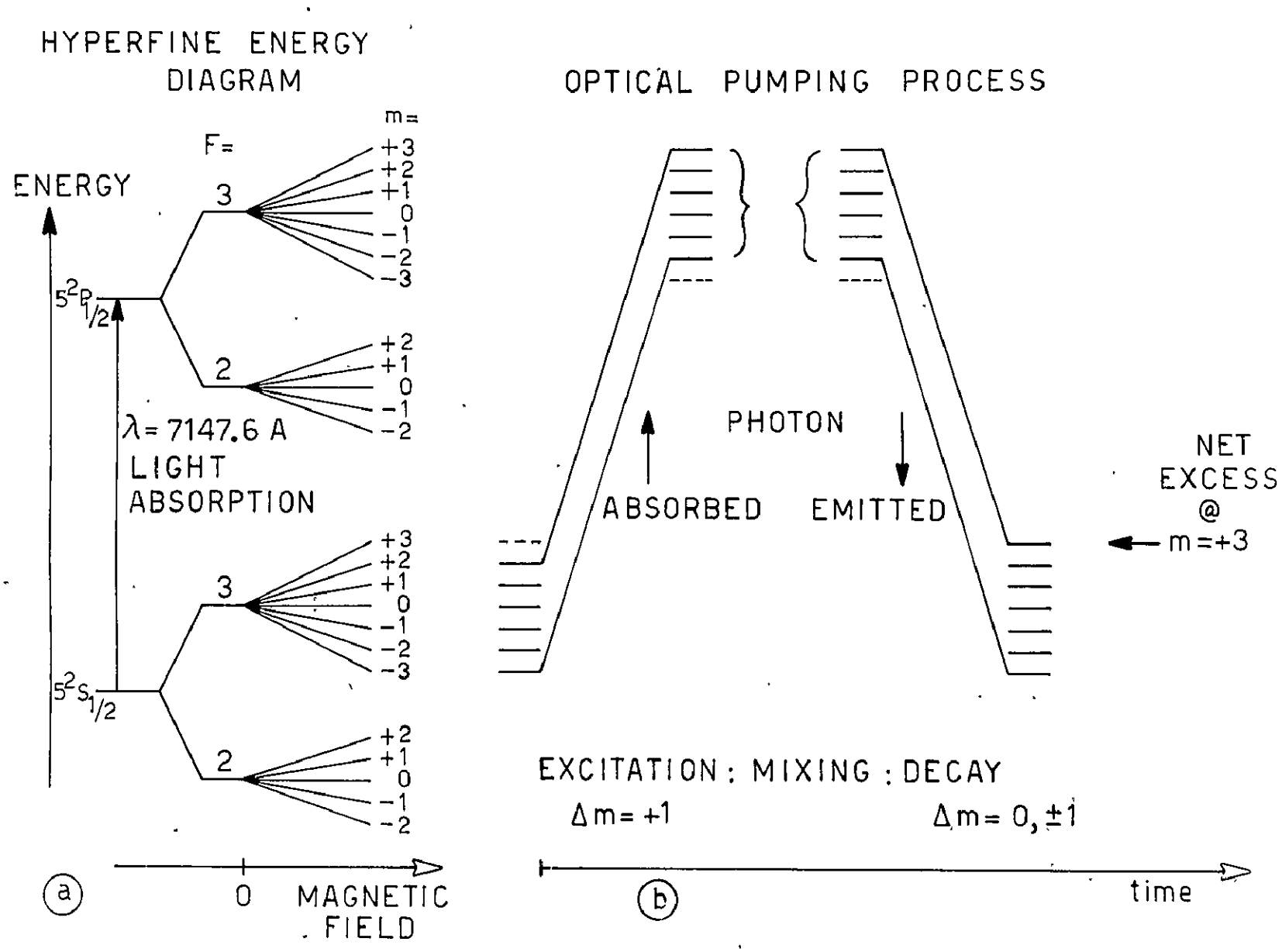
HYPERFINE ENERGY DIAGRAM
ENERGY
F=
m=
3
+3
+2
+1
0
−1
−2
−3
$5^2P_{1/2}$
2
+2
+1
0
−1
−2
λ = 7147.6 A
LIGHT
ABSORPTION
3
+3
+2
+1
0
−1
−2
−3
$5^2S_{1/2}$
2
+2
+1
0
−1
−2
a
0
MAGNETIC FIELD
OPTICAL PUMPING PROCESS
PHOTON
ABSORBED
EMITTED
NET EXCESS @ m=+3
EXCITATION : MIXING : DECAY
Δm = +1
Δm = 0, ±1
b
time

FIGURE 11

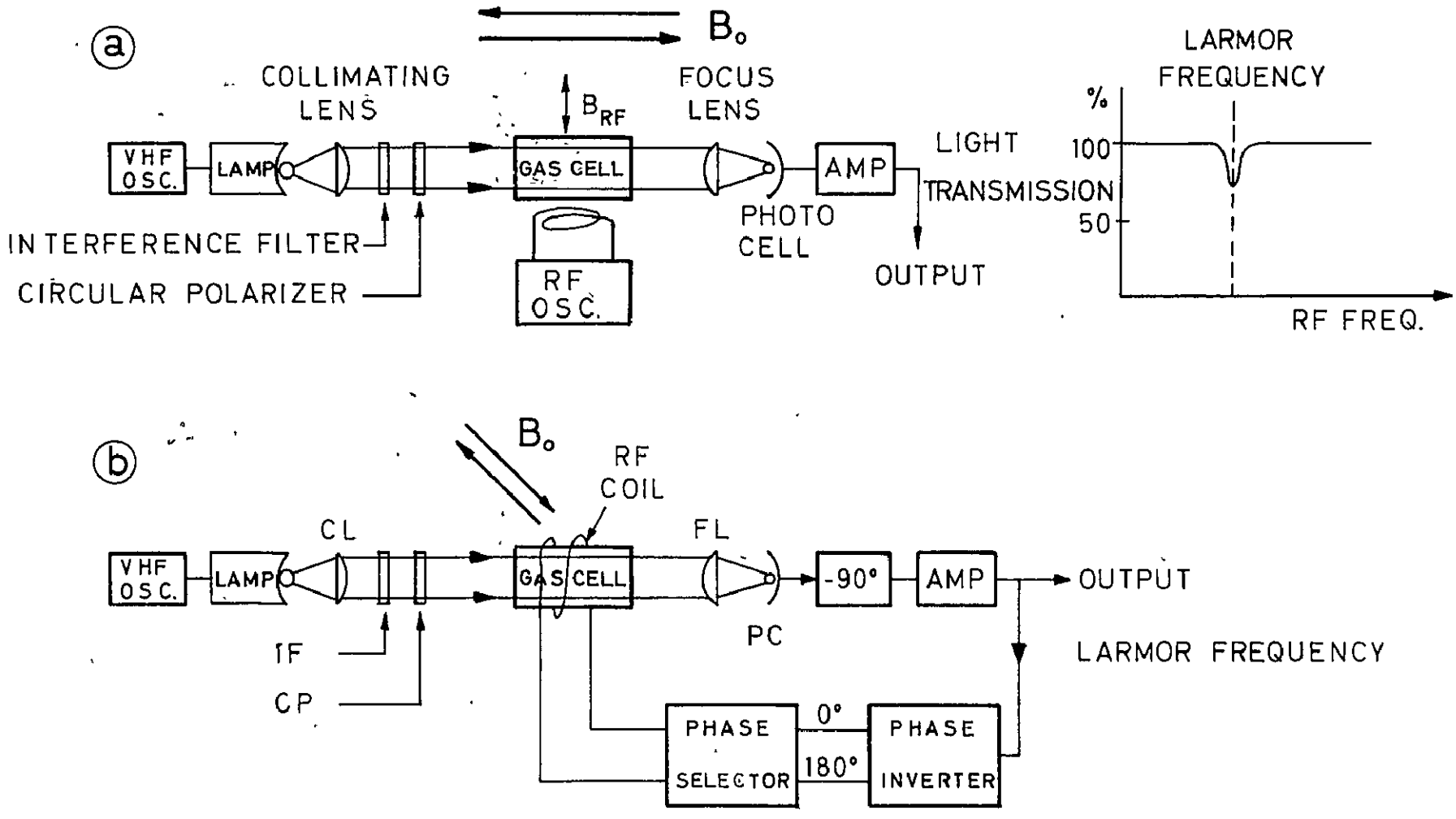

RF SELF-RESONANT LOOP

FIGURE 12

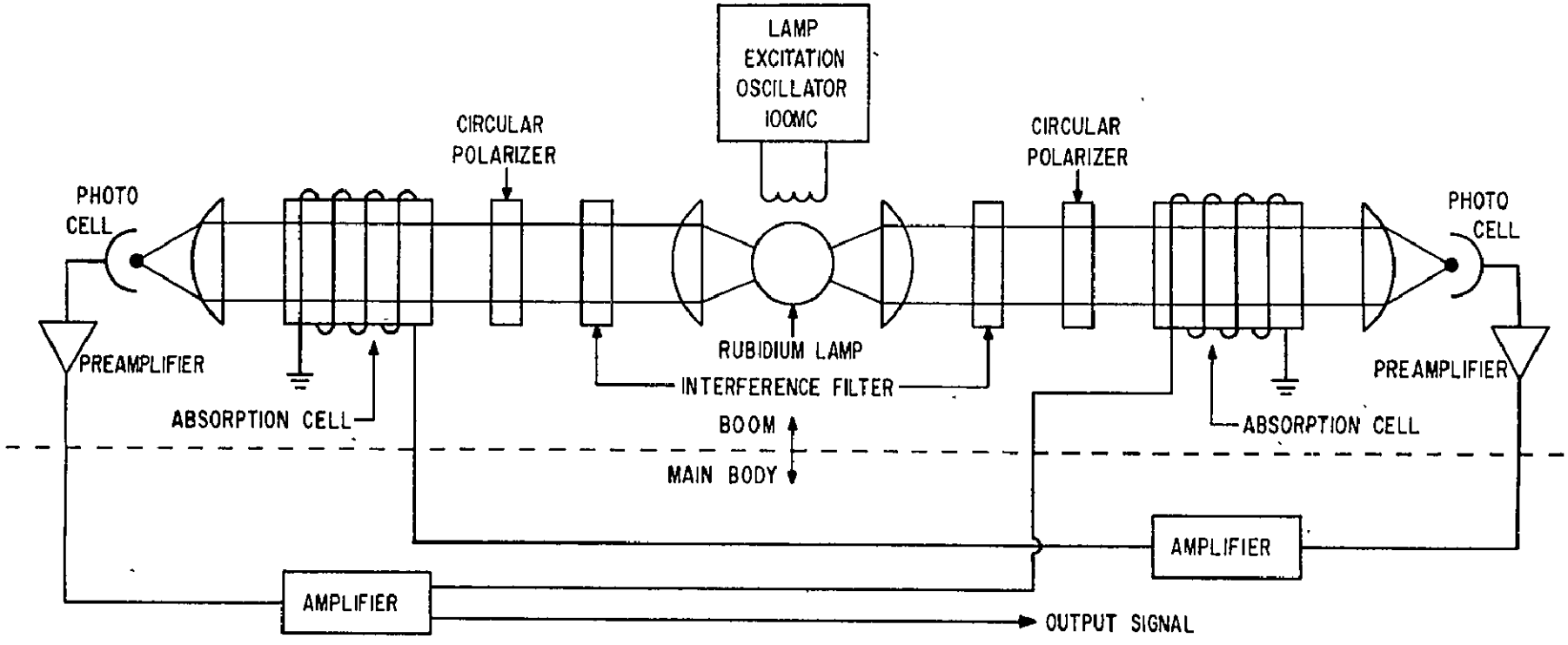
LAMP
EXCITATION
OSCILLATOR
100MC
CIRCULAR
POLARIZER
CIRCULAR
POLARIZER
PHOTO
CELL
PHOTO
CELL
PREAMPLIFIER
PREAMPLIFIER
RUBIDIUM LAMP
INTERFERENCE FILTER
ABSORPTION CELL
ABSORPTION CELL
BOOM
MAIN BODY
AMPLIFIER
AMPLIFIER
OUTPUT SIGNAL

FIGURE 13

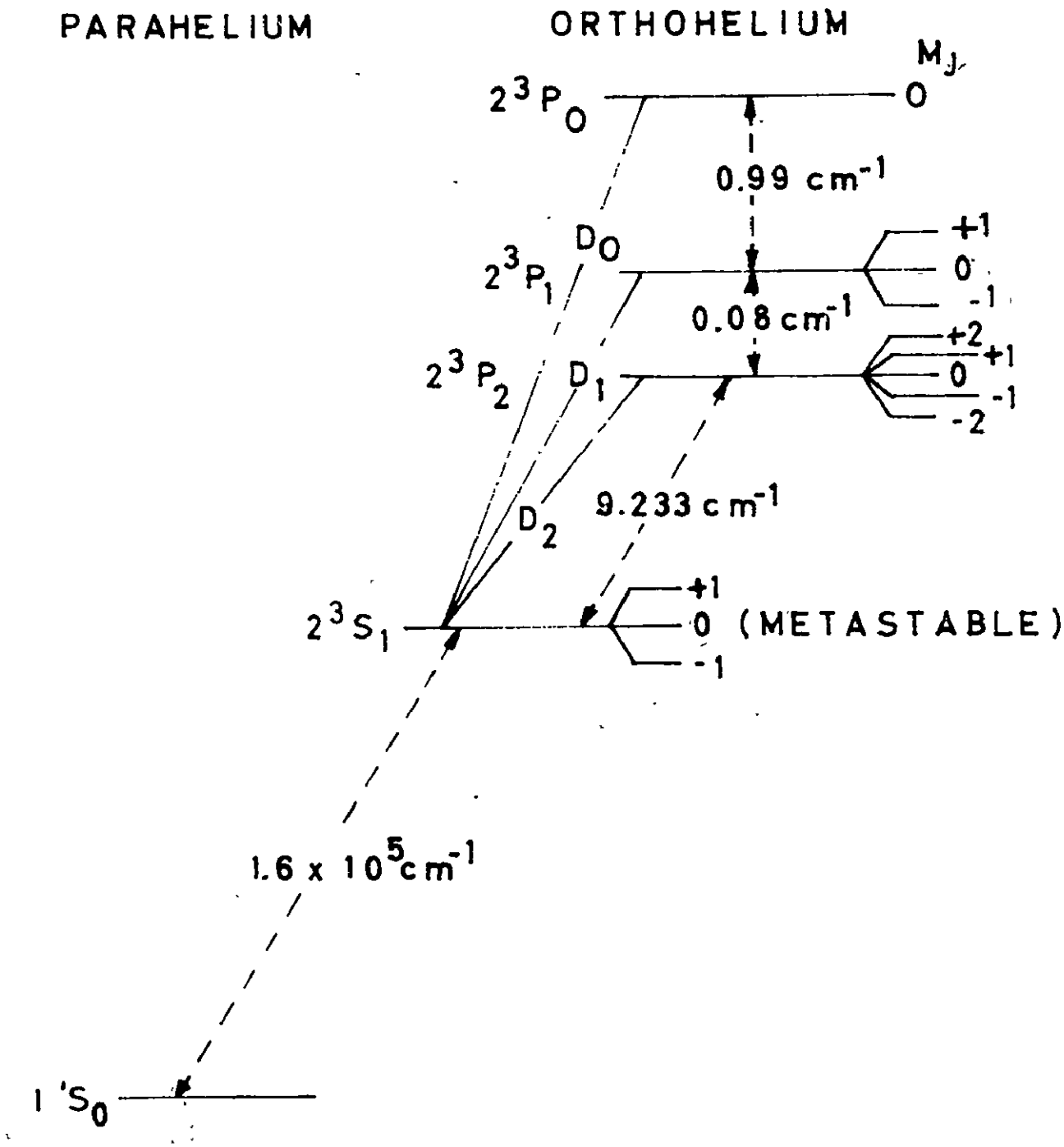
PARAHELIUM
ORTHOHELIUM
M_J
2^3P_0
0
0.99 cm^{-1}
D_0
2^3P_1
+1
0
-1
0.08 cm^{-1}
2^3P_2
D_1
+2
+1
0
-1
-2
D_2
9.233 cm^{-1}
2^3S_1
+1
0 (METASTABLE)
-1
1.6 x 10^5 cm^{-1}
1^1S_0

FIGURE 14

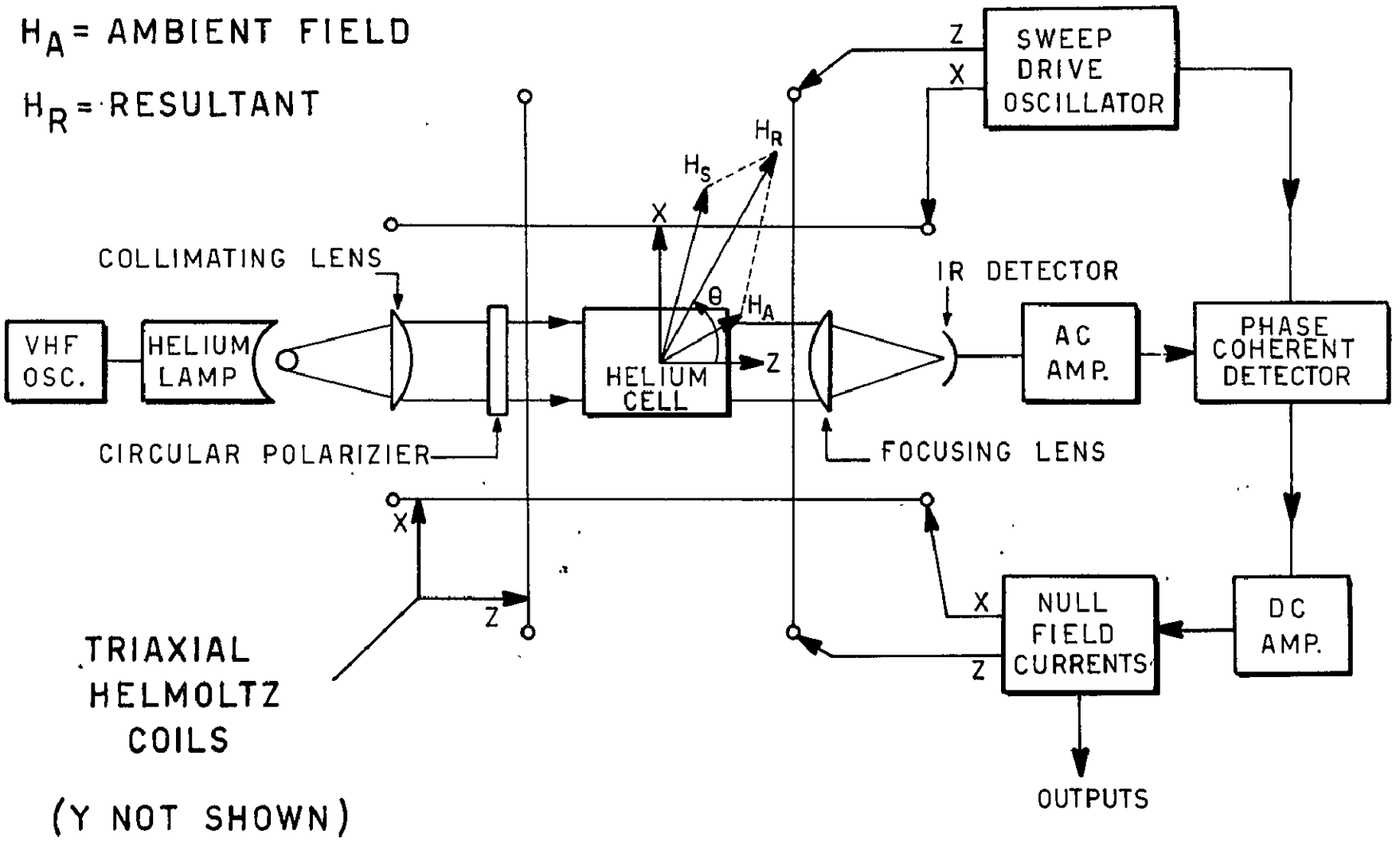
H_S = SWEEP FIELD
H_A = AMBIENT FIELD
H_R = RESULTANT
Z
X
SWEEP DRIVE OSCILLATOR
H_R
H_S
X
COLLIMATING LENS
IR DETECTOR
θ
H_A
VHF OSC.
HELIUM LAMP
HELIUM CELL
Z
AC AMP.
PHASE COHERENT DETECTOR
CIRCULAR POLARIZIER
FOCUSING LENS
X
Z
X
NULL FIELD CURRENTS
DC AMP.
Z
TRIAXIAL HELMOLTZ COILS
(Y NOT SHOWN)
OUTPUTS

FIGURE 15

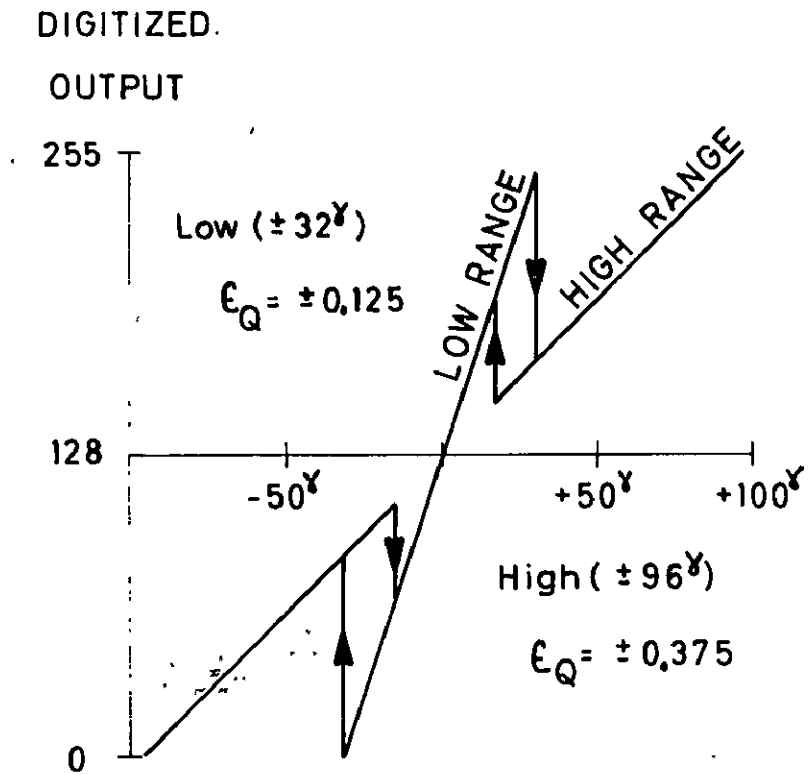

FIELD PARALLEL TO
SENSOR AXIS

MULTIPLE RANGES

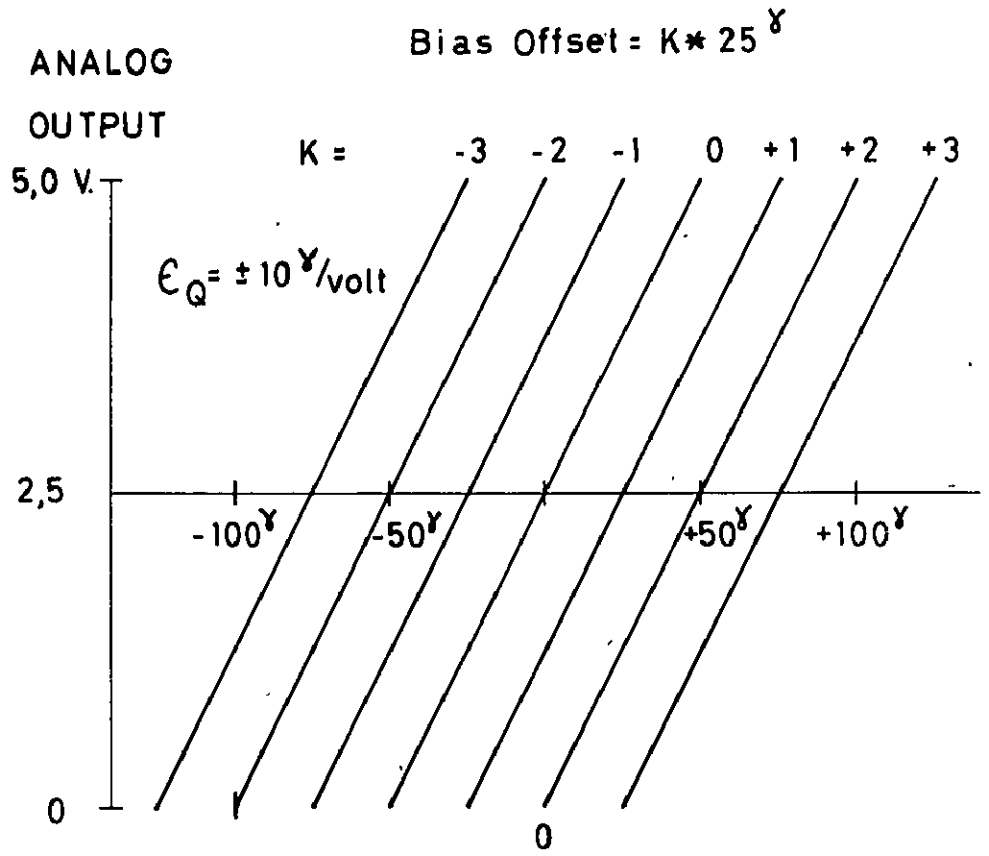

FIELD PARALLEL TO
SENSOR AXIS

OFFSET RANGES

FIGURE 16

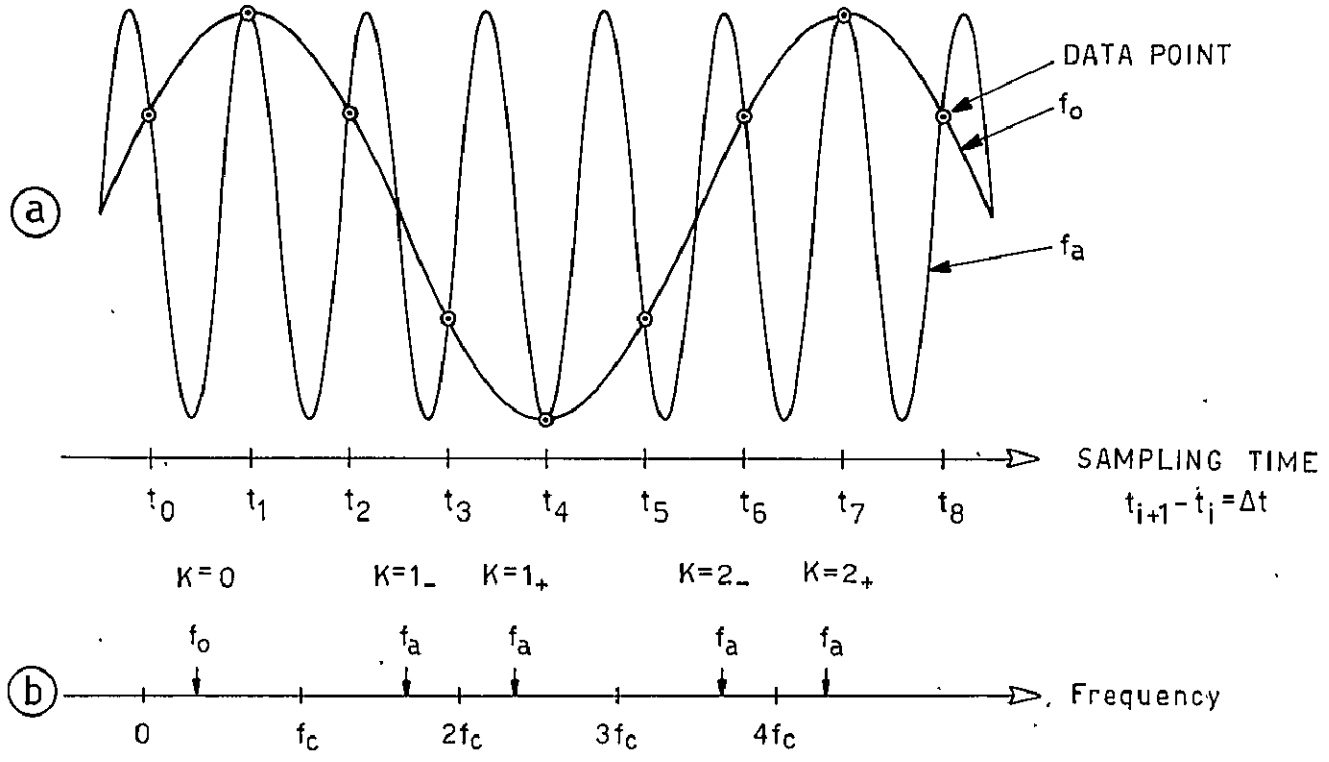

$$\text{Cut-off Frequency} = \frac{1}{2\Delta t} = f_c$$

$$\text{Aliases @ } f_a = 2Kf_c \pm f_o$$

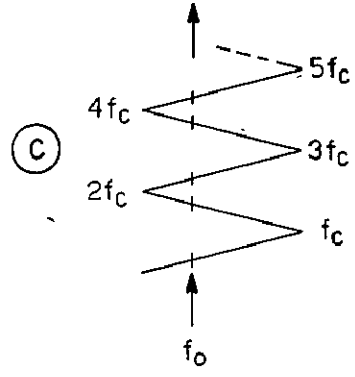

FREQUENCY AMBIGUITY =

SPECTRAL FOLDING =

ALIASING

FIGURE 17

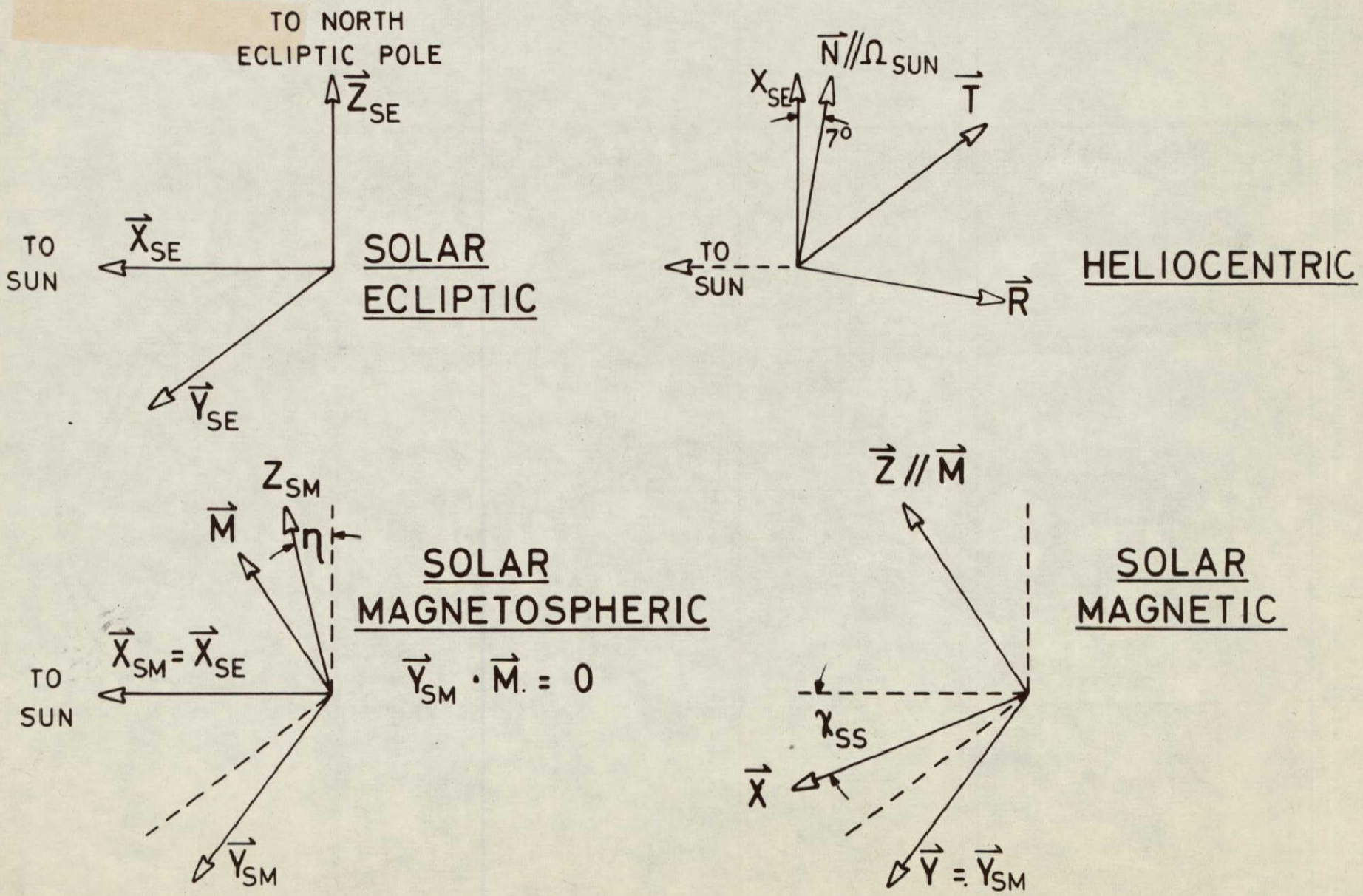
TO NORTH
ECLIPTIC POLE
$\vec{Z}_{SE}$
TO
SUN
$\vec{X}_{SE}$
SOLAR
ECLIPTIC
$\vec{Y}_{SE}$
$\vec{N}//\Omega_{SUN}$
X_{SE}
7°
$\vec{T}$
TO
SUN
$\vec{R}$
HELIOCENTRIC
Z_{SM}
$\vec{M}$
η
SOLAR
MAGNETOSPHERIC
$\vec{X}_{SM} = \vec{X}_{SE}$
$\vec{Y}_{SM} \cdot \vec{M} = 0$
TO
SUN
$\vec{Y}_{SM}$
$\vec{Z}//\vec{M}$
SOLAR
MAGNETIC
χ_{SS}
$\vec{X}$
$\vec{Y} = \vec{Y}_{SM}$

FIGURE 18

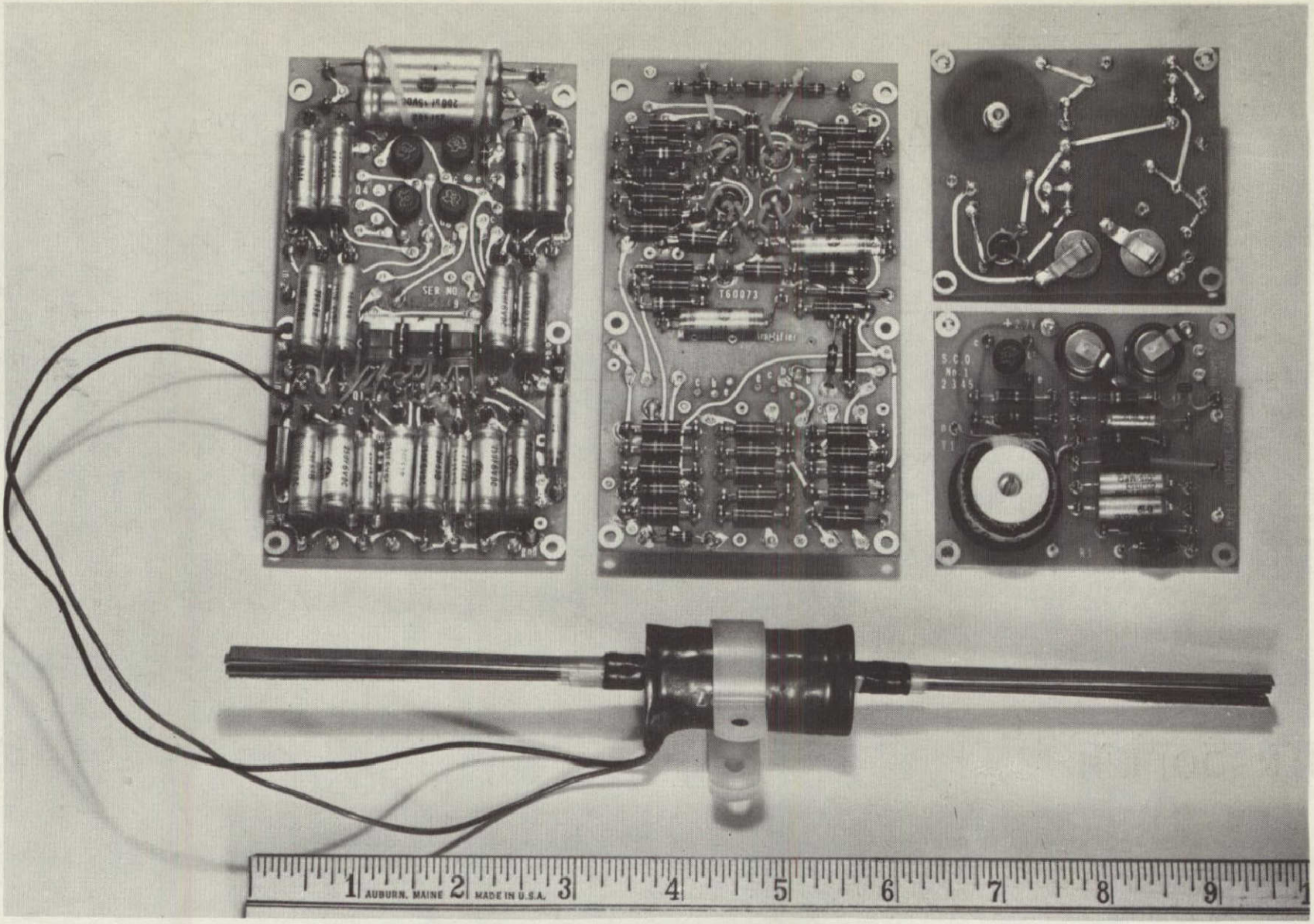

NOT REPRODUCIBLE

FIGURE 19

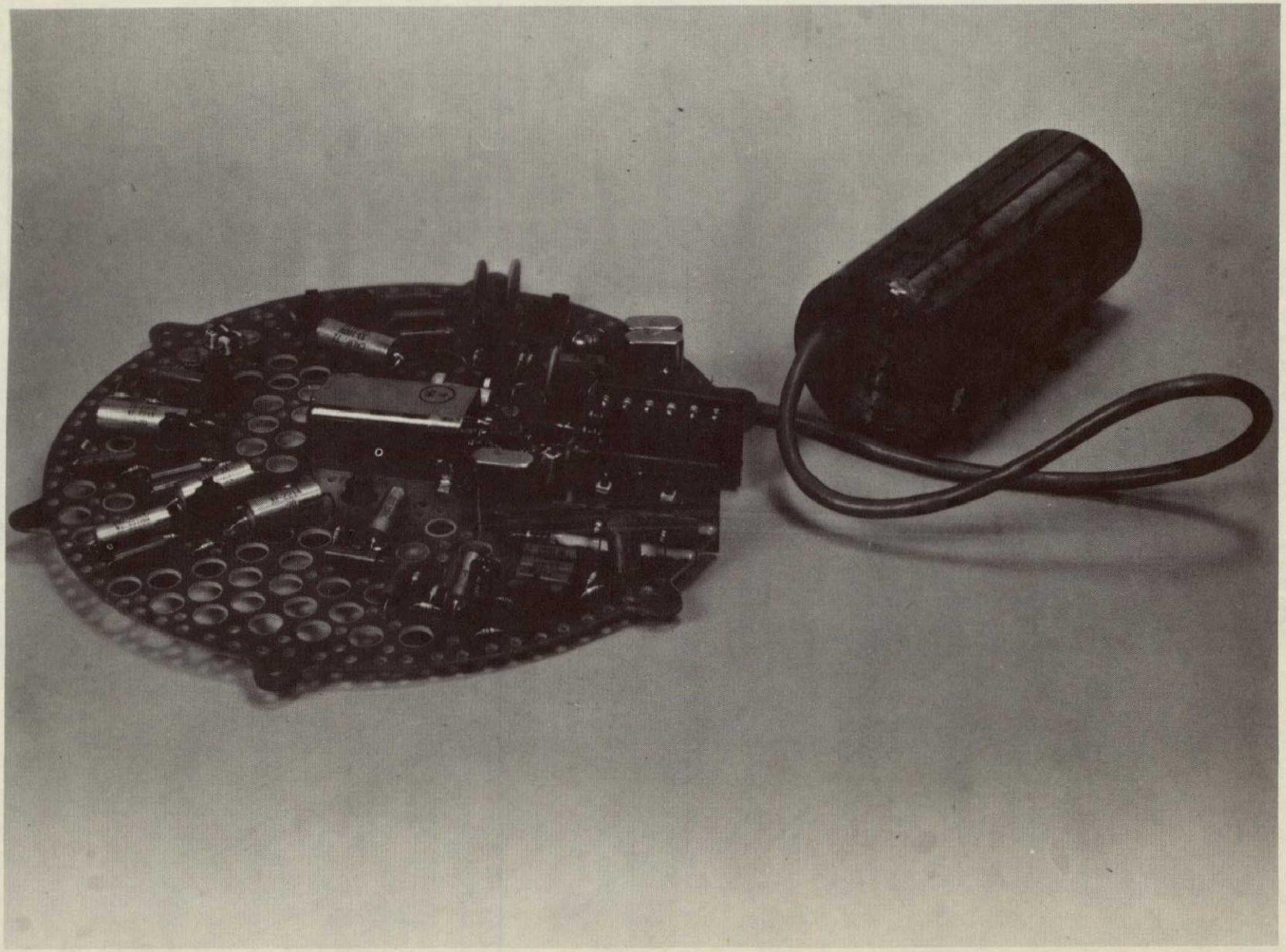

Satellite proton magnetometer that measures field with an accuracy of 1 part in 100,000

FIGURE 20

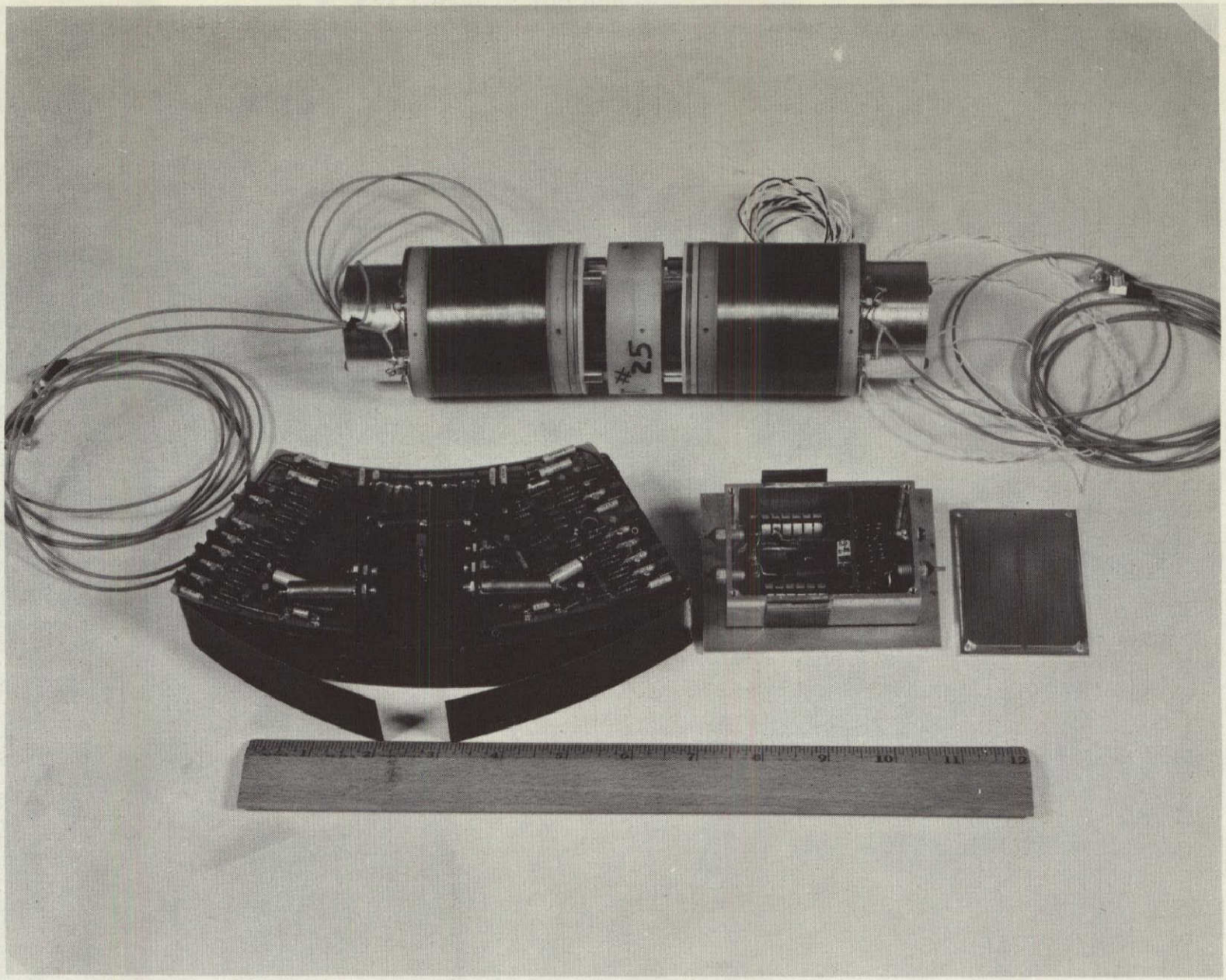

FIGURE 21

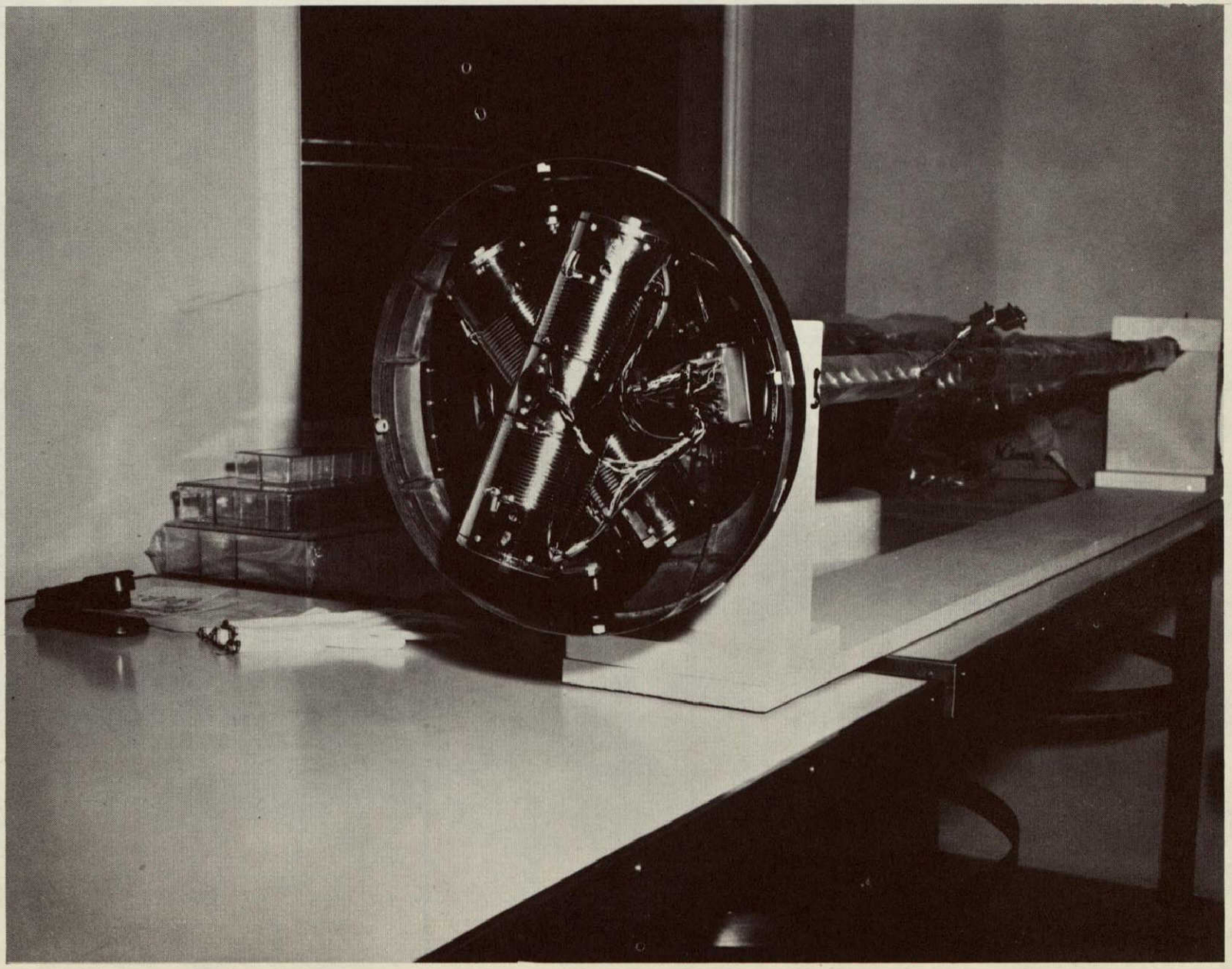

FIGURE 24

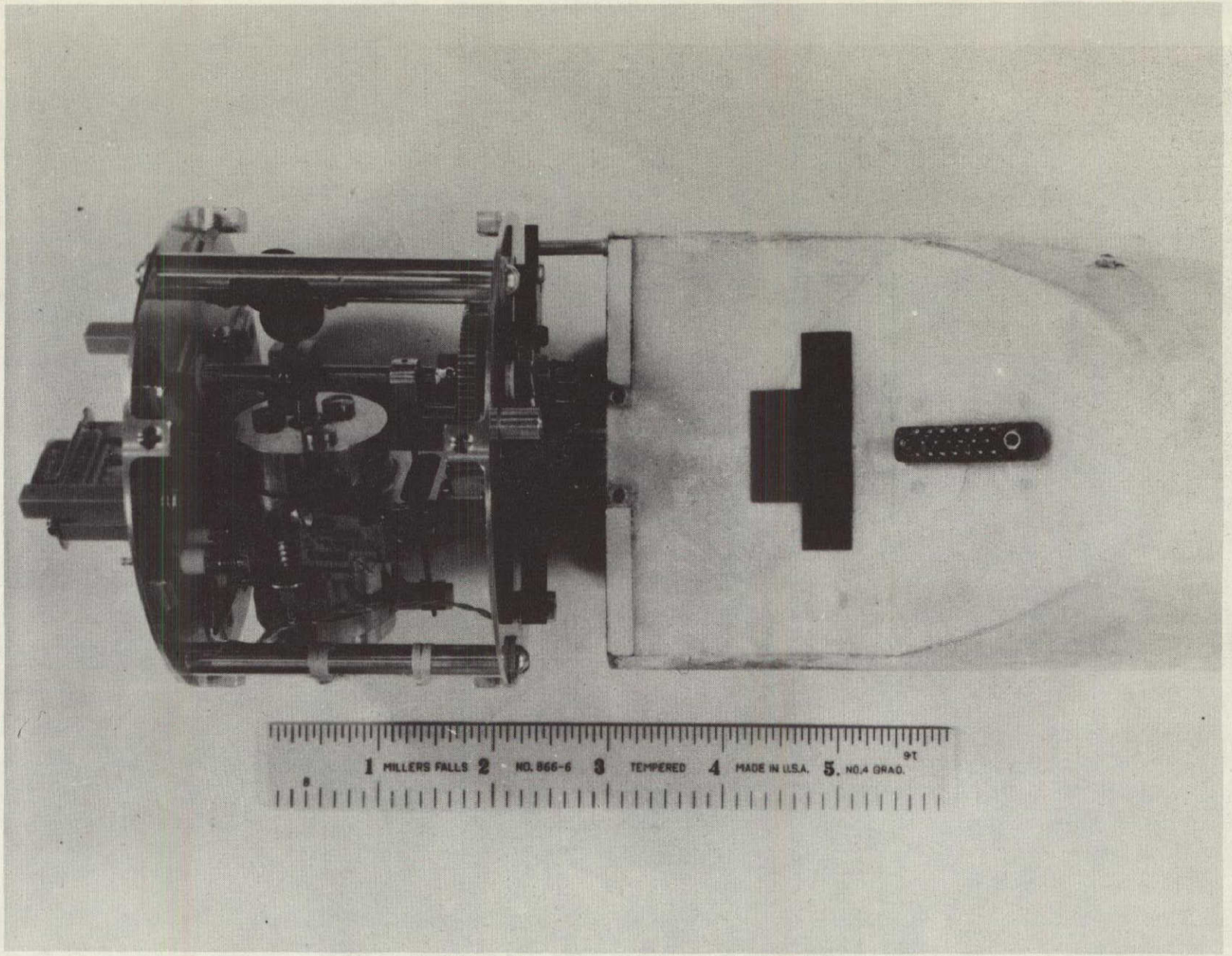

FIGURE 25

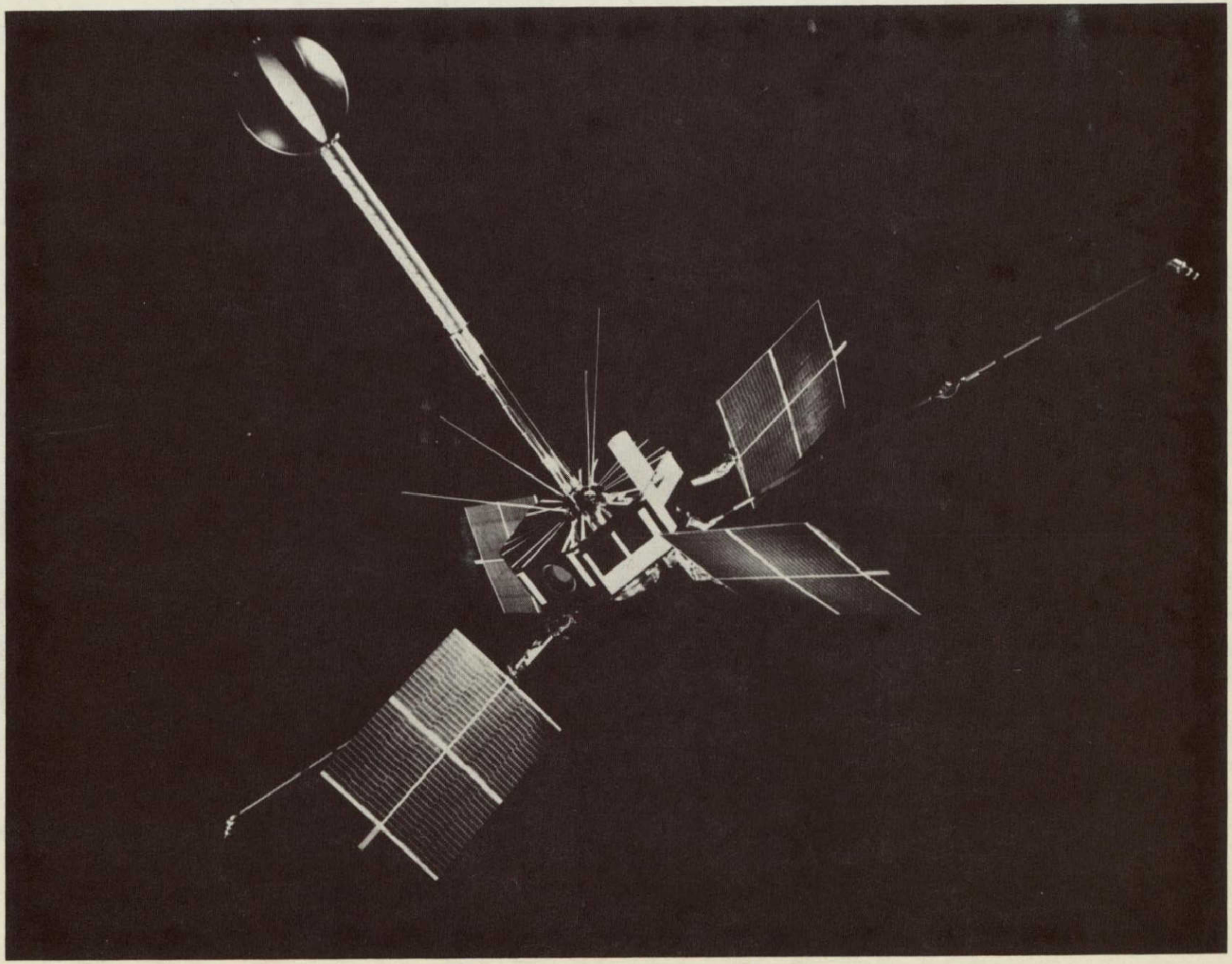

FIGURE 22

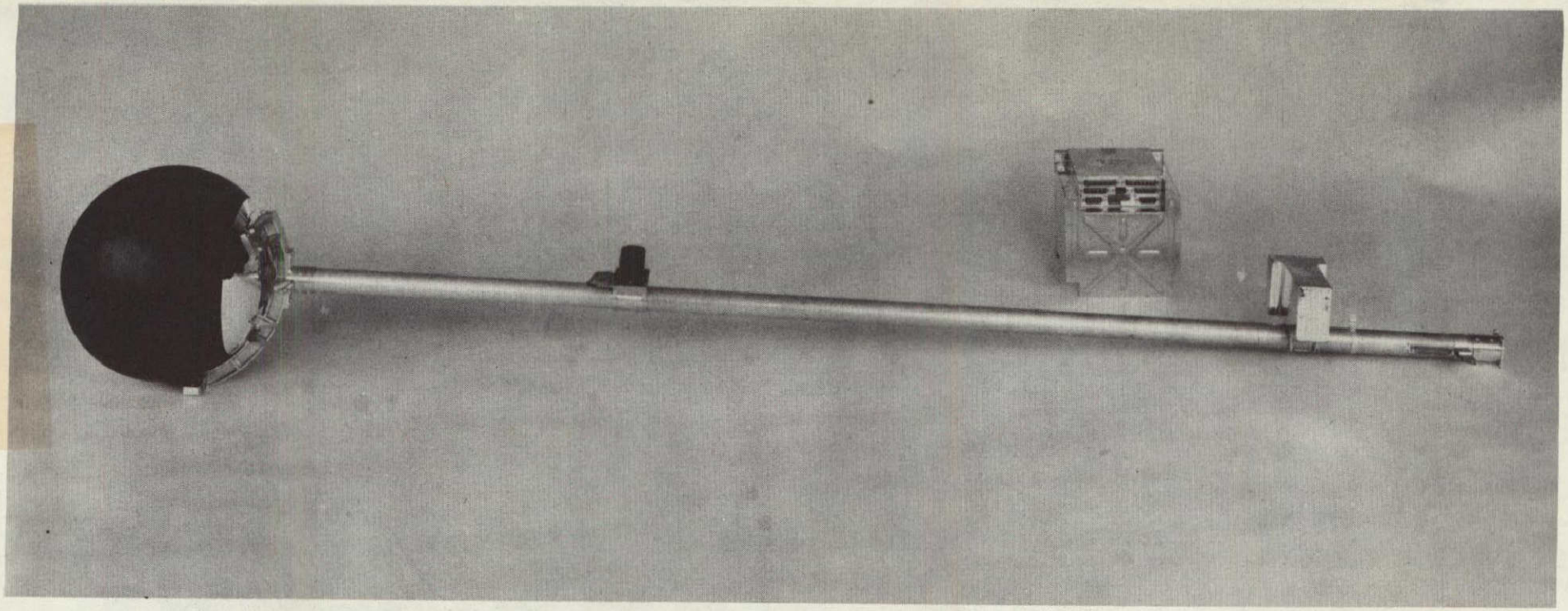

NASA G-64- 863

FIGURE 23

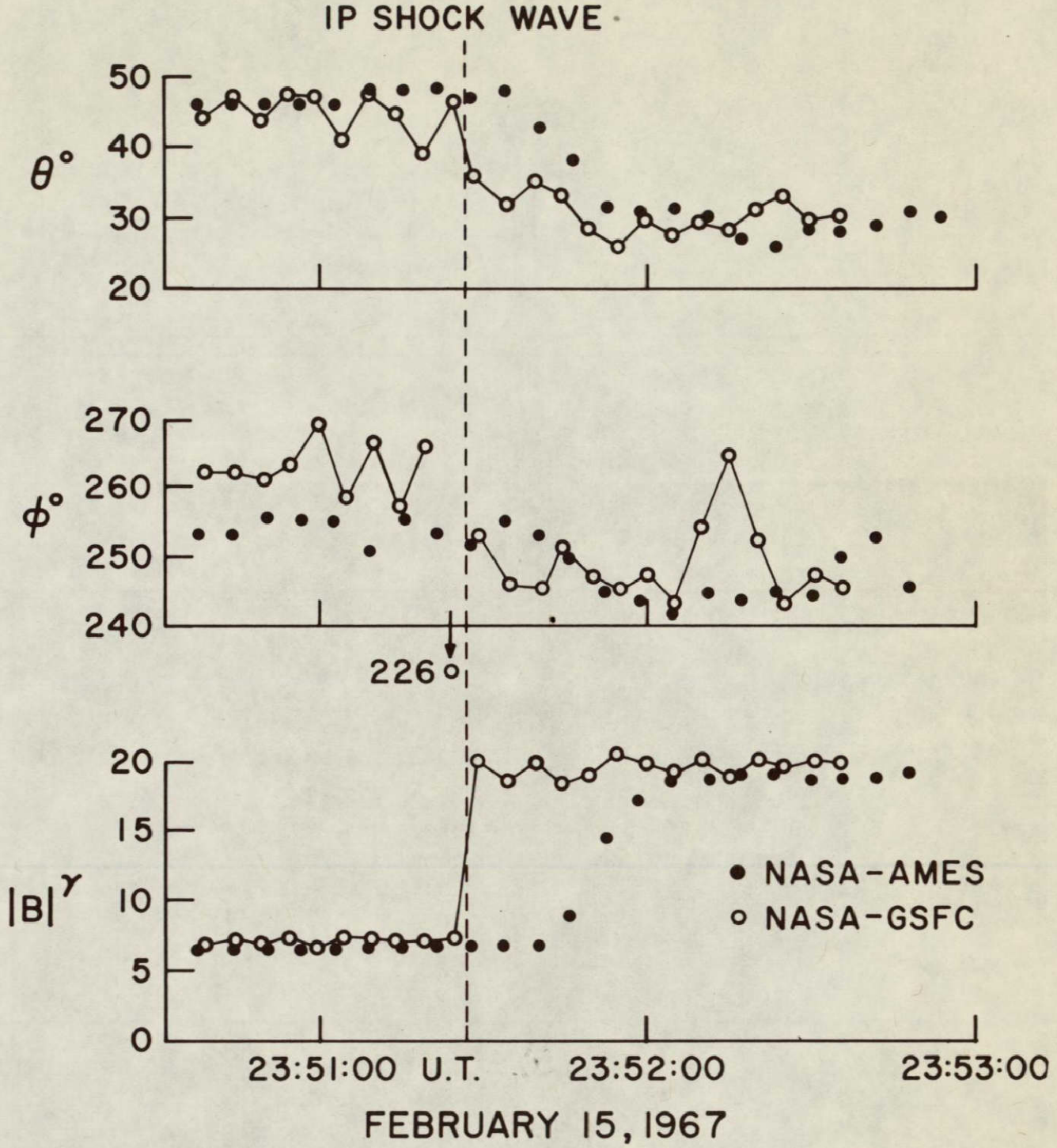
IP SHOCK WAVE
θ°
50
40
30
20
φ°
270
260
250
240
226
|B|γ
20
15
10
5
0
NASA-AMES
NASA-GSFC
23:51:00 U.T.
23:52:00
23:53:00
FEBRUARY 15, 1967

FIGURE 26

FIGURE 27

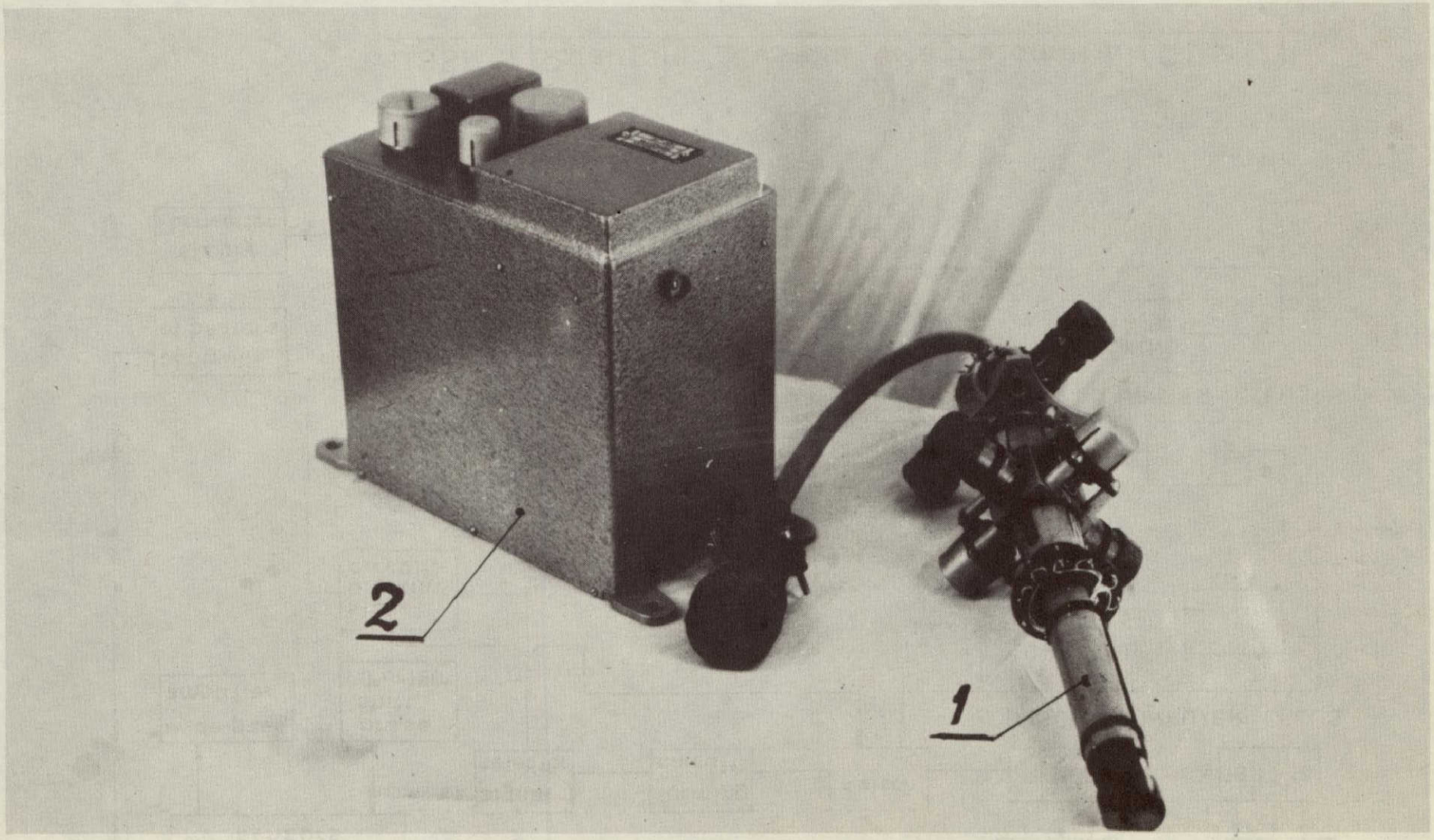

USSR TRIAXIAL FLUXGATE MAGNETOMETER (SG 50)
LUNA 1,2 ELECTRON 2,4

FIGURE 28

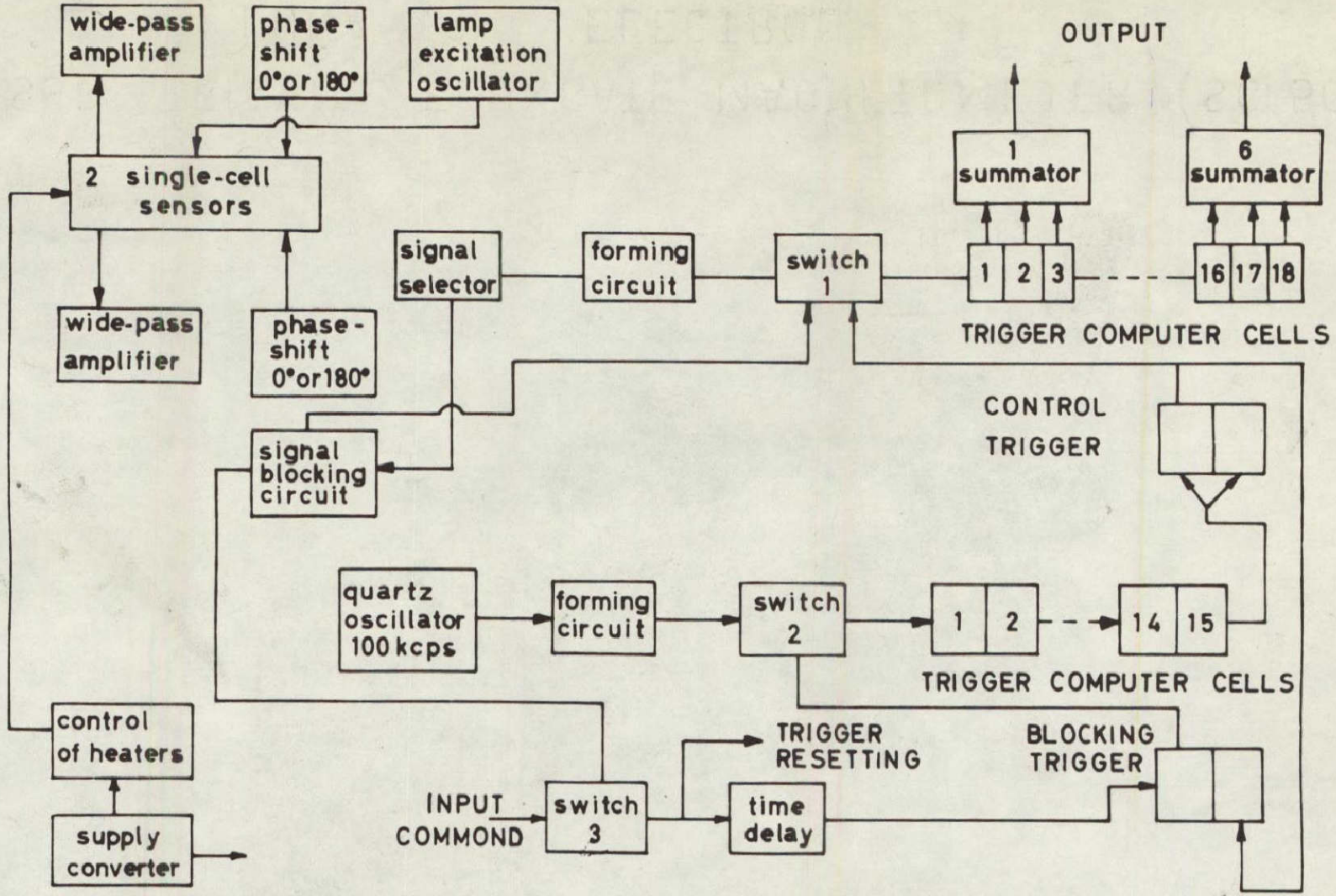

USSR Quantum Cesium Magnetometer (QCM-1)

FIGURE 29